5-2021

Characterization Of A Novel Oncogenic Mirna Inhibitor In Cancer Therapy

Iman Sahnoune

Recommended Citation

Characterization of a novel oncogenic miRNA inhibitor in cancer therapy

by

Iman Sahnoune

APPROVED:

_____
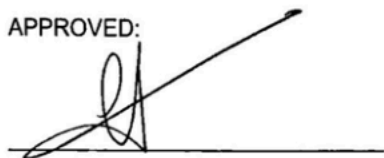
George A. Calin, M.D, Ph.D.

Advisory Professor

_____

Pratip Bhattacharya, Ph.D.

_____
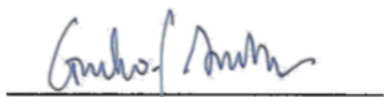
Giulio Draetta, MD., Ph.D.

_____

Cristina Ivan, Ph.D.

_____
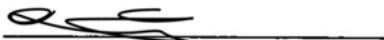
Shuxing Zhang, Ph.D.

CHARACTERIZATION OF A NOVEL ONCOGENIC MIRNA INHIBITOR IN

CANCER THERAPY

A

Dissertation

Presented to the Faculty of

The University of Texas

MD Anderson Cancer Center UTHealth

Graduate School of Biomedical Sciences

In Partial Fulfillment

of the Requirements

for the Degree of

DOCTOR OF PHILOSOPHY

by

Iman Sahnoune

Houston, Texas

May 2021

Dedication

To all who have supported me on this journey

Acknowledgements

I'm grateful to have arrived at the end of what turned out to be a transformative past few years. There are a multitude of people I'd like to thank for their support throughout this process.

I'd like to first thank my advisor Dr. George Calin for the guidance and support as we completed this project. He is a mentor that truly enjoys science and has always encouraged a collaborative and productive scientific environment. Special thanks to the members for their friendship and help as I worked through completing this project. It was a pleasure working with everyone.

I would like to thank my advisory committee for all of their invaluable advice and support over the years. Dr. Pratip Bhattacharya for being a member of my committee since the beginning, and providing important insight into the NMR and chemistry aspect of this work. To Dr. Giulio Draetta, who served as a CPRIT co-mentor on this project and for providing crucial insight into this work. To Dr. Shuxing Zhang, who provided many ideas and expertise on the direction of this project from the structural biology perspective. And to Dr. Cristina Ivan, who is not only a mentor, but has become a friend, for the many hours we've spent working through data and learning to approach datasets both mathematically and biologically.

There are several others who have been crucial to the progression of this project. I want to thank Dr. Barbara Czako from the Institute of Applied Cancer Science (IACS), for her help and support as we completed this project. To Dr. Matthew Shortridge, many thanks for his expertise in the direct binding studies. Last but not

least, thank you to Dr. Sanjay Singh, expert in cerebral organoid technology, for his mentorship and friendship the past few years.

I would like to thank the GSBS for all of their support during my time here. Getting a PhD is not easy, but it is made better by working with those who genuinely care. Special thanks to Dr. Bill Mattox, Dr. Natalie Sirisaengtaksin, Bunny Perez, Joy Lademora and to all who work to improve the experiences of the trainees. Thank you to the students and faculty of the Neuroscience program, specifically Dr. Michael Beierlein and Dr. Qingchun Tong for their leadership as program directors, and to program coordinator Amanda Williamson for her friendship and support. I'd also like to thank the CPRIT program directors Dr. Khandan Keyomarsi and Dr. Stephanie Watowich, and program managers Dr. Kari Brewer Savannah and Dr. Kara Lewis, for believing in this project and for being excellent women mentors in science.

There are several graduate school friends that I'd like to recognize. I'd like to first thank Jeanne Manalo for her friendship. From our neuroscience courses, to our leadership commitments, to everything in between, we've been through it all over the past few years and I'm grateful to have found such a wonderful friend. Thank you to Sunada Khadka. We've seen each other through difficult times professionally and personally and I'm lucky to have such a grounded and calm friend. To Merve Dede, I'm grateful for her friendship from the first day of graduate school all the way through the best and worst of times. And thank you to Ashabari Sprenger, Ileana Corsi and Alexis Mobley for their friendship and the laughs over the years. To everyone else I've crossed paths with in graduate school, thank you for the memories and I wish you all success in the years ahead.

To my friends in the real world. Thank you to Sidney Chen and Stella Wang for their support and managing to stay in touch even with distance and time. To my college best friend Maria Rahim, for a decade of friendship and support. And to Dr. Shaefali Rodgers, who was a postdoctoral fellow in the first graduate lab I worked in. I learned so much about experimental design and statistics from her that I continue to build upon and use in my work today and I'm so grateful for her mentorship and friendship all these years.

To my family, thank you for everything. To my siblings, thank you for always being there to cheer me on. To my parents, there will never be enough words. Growing up, they always instilled in us the value of education, hard work, moving forward, and always shooting for the moon. I dedicate this to them and to all who came before them.

Abstract

As cancer research continues to move towards more personalized methods, targeted inhibitors of oncogenic drivers of cancer are found to be an innovative and promising therapeutic approach. Previously thought to be undruggable regions of the genome, RNA has become an area of increasing interest in cancer due to the identification of more targetable regions and their relationship to tumor growth and progression. This work reports on the development of IACS-13743, a novel small molecule found to directly bind and inhibit microRNA-10b. Oncogenic miR-10b has been found to be overexpressed in several malignant cancer types, making it an attractive biomarker for targeted inhibitor therapy. IACS-13743 is found to impede tumor progression and proliferation in brain cancer, gastric cancer and pancreatic cancer *in vitro*. This effect is also shown in a cerebral organoid model. Using a multidisciplinary approach, this study identifies a relationship between oncogenic miR-10b and the dysregulation of the PI3K/AKT pathway in cancer, along with putting forth a compound that can mitigate these effects. These findings provide a fundamental step in moving forward a targeted therapeutic for a known oncogenic RNA driver and unique biomarker in multiple malignant cancer types.

Table of Contents

List of Figures

List of Tables

List of Abbreviations

AKT   protein kinase B

BBB   blood brain barrier

CAR   chimeric antigen receptor

CRES   CAR T-cell related encephalopathy syndrome

CCLE   Cancer Cell Line Encyclopedia

CSF   cerebrospinal fluid

CT   computed tomography

DMSO   dimethyl sulfoxide

DNA   deoxyribonucleic acid

EMT   epithelial-to-mesenchymal transition

GSC   glioma stem cells

GBM   glioblastoma multiforme

HPLC   high-performance liquid chromatography

IACS   Institute of Applied Cancer Science

iPSCs   induced pluripotent stem cells

LC/MS   liquid chromatography/mass spectrometry

mRNA   messenger RNA

miR   microRNA

MRI   magnetic resonance imaging

oncomiR   oncogenic microRNA

NMR   nuclear magnetic resonance

PDAC   pancreatic ductal adenocarcinoma

PTEN   phosphatase and tensin homolog

qRT-PCR   quantitative real time polymerase chain reaction

RNA   ribonucleic acid

SAR   structure-activity relationship

STAD   stomach adenocarcinoma

RPPA   Reverse Phase Protein Array

TCGA   The Cancer Genome Atlas

TOCSY   total correlation spectroscopy

Chapter 1. Introduction

RNA therapeutics as an emerging approach

     Cancer continues to be a leading health issue worldwide, with an estimated 1,898,160 new cancer incidences and 608,570 deaths projected in the United States in 2021[1]. As more advanced technologies and therapeutic approaches continue to be developed, these rates will decrease, although the challenges of tumor heterogeneity, metastasis and further understanding of the mechanisms of treatment resistance remain. There are several malignant cancer types through which the common modalities of surgery, radiation and chemotherapy are not sufficient in yielding anti-tumor effects, and while promising approaches such as immunotherapy are gaining traction, there is a need for more innovative methods to target tumors that are resistant to these existing modalities and for the development of more personalized approaches. Three such cancer types include brain cancer, gastric cancer, and pancreatic cancer. There will be approximately 18,600, 11,180, and 48,220 deaths from these cancers alone in the United States in 2021, with many more patients diagnosed[1]. While treatments for these tumor types exist, the life expectancy of each of these cancers is minimal, due to these increased mechanisms of therapeutic resistance and inability for early detection until the malignancies become too advanced for conventional forms of treatment.

     Targeted therapeutics are the frontrunner in the pursuit of personalized medicine. The concept involves designing drugs that are specific to oncogenic cells or to tissue microenvironments that are conducive to tumor growth and proliferation, with minimal off-target effects[2]. A large limitation of existing radiotherapies and

chemotherapies is the lack of specificity to the target of interest, along with high degrees of toxicity and potential impacts to long-term quality-of-life. Drug discovery continues to be a growing field, as advances in technology continue to allow for more avenues of therapeutic targeting. However, there are two main challenges that are consistent in creating an effective drug; the first is that the drug has to be able to arrive at the site of action, taking into consideration lipophilicity and size of the molecules as they travel throughout the body and its membranes[3]. The second is that it must be able to yield a biological effect by modulating its intended target once it reaches the site of action. This field has long focused on the therapeutic targeting of proteins, and while this strategy has shown to be effective, identifying nearly 700 therapeutically targetable proteins, only 1.5% of the human genome encodes for proteins, which leads to only approximately 0.05% of the entire human genome being successfully targeted[4, 5] (Figure 1).
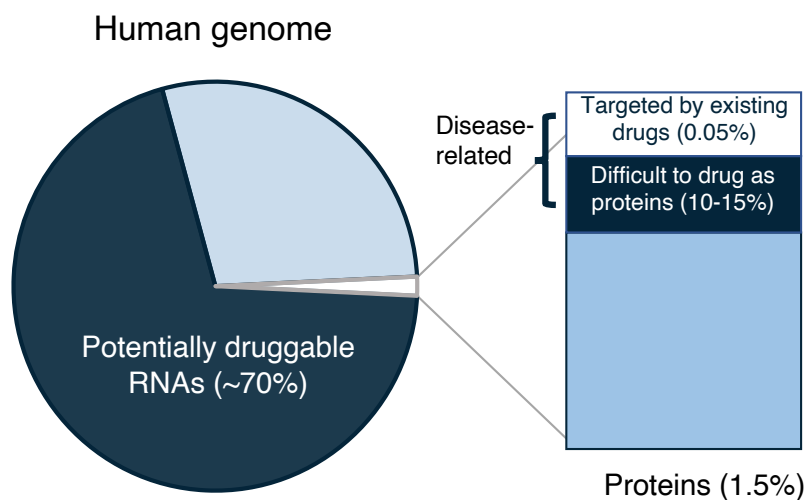
Figure 1. Diagram portraying the human genome and the potential for discovery of biomarkers and novel targeted therapeutics. Adapted from Warner K. D.; Hajdin, C. E.; Weeks, K. M., Principles for targeting RNA with drug-like small molecules. *Nat Rev Drug Discov* **2018,** *17* (8), 547-558.

While the central dogma of molecular biology has primarily focused on RNA as the intermediate transcript through which DNA is translated into proteins, it hasn't been until recent decades that the roles of RNA have been further studied and found to be much more extensive than originally thought[6,7]. There is the classical subset of RNAs that are classified as coding, where RNA transcripts are translated into messenger RNA and eventually become proteins. However, the grand majority of RNAs are classified as non-coding, which do not undergo translation. Initially thought to be non-functional because they do not translate to proteins, a multitude of studies over the years have found forms of RNAs that play significant roles in regulating gene expression at the transcriptional and post-transcriptional levels. They can either be overexpressed or repressed and thereby act as biomarkers that can then be modulated and potentially therapeutically targeted[8].

Oncogenic microRNAs, otherwise called oncomiRs, are a class of small non-coding RNAs found to be overexpressed in several tumor types and can directly target tumor suppressing genes. The overexpression of these specific miRNAs leads to the targeting of tumor suppressor genes, rendering their function limited or non-functional, thereby promoting an oncogenic outcome. By extension, the inhibition of these miRNAs via a targeted therapeutic approach, inhibiting the overexpressed oncogenic miRNAs would then allow for normal function of the tumor suppressor genes (Figure 2).
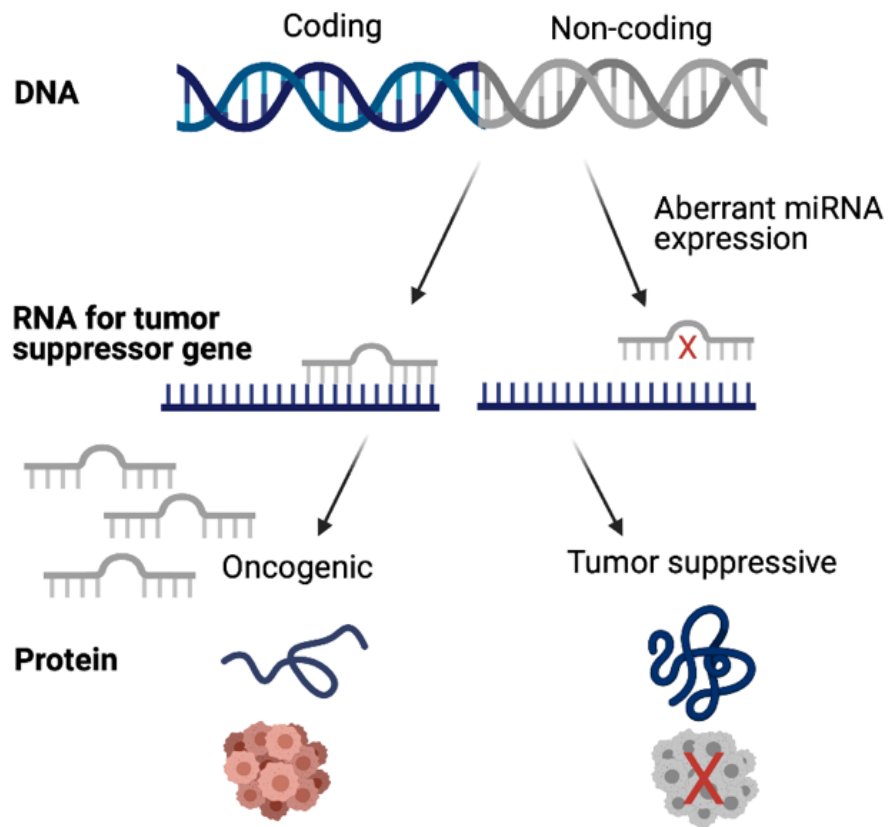
Figure 2: miRNAs can serve either oncogenic or tumor suppressive functions. Shown is a graphical depiction of both circumstances, when the miRNA is over-expressed, leading to suppression of the tumor suppressor gene, and when the miRNA is under-expressed, when there is no binding to the mRNA

There are various approaches that have been developed in the targeting of overexpressed miRNAs; ultimately the use of anti-sense oligonucleotides and small molecules have gained the most attention. Oligonucleotides work as competitive inhibitors in this mechanistic process by blocking the mature miRNA from interacting with the target mRNAs, allowing for normal functioning of the mRNA[7]. There are several limitations of such molecules in translational use, in that oligonucleotides tend to be larger and can yield off-target effects when the oligonucleotide sequence binds an RNA with a sequence similar to the target RNA[9]. Small molecules the other main group found to target miRNA. They are defined as a class of molecules with lower molecular weight and have chemical properties such that they are able to diffuse through membranes into cells much more easily. They are designed to be smaller and more specific to the target of interest, often with better cellular solubility and permeability, making it a more practical and viable approach for diffusion through tissues. Most targeted therapies are composed of small molecules.

The general concept of using small molecules to target overexpressed miRNAs as a novel therapeutic approach has gained interest in recent years[10], along with the strategies for modeling RNA providing important insights into RNA-small molecule interactions for drug development and discovery[11, 12]. Directly targeting miRNAs with small molecules allows for the functional inhibition of specific miRNAs that often cannot be achieved through targeting of proteins that are associated with these miRNAs[4]. This work will focus on the targeting of a specific oncogenic miRNA using a novel small molecule inhibitor.

Oncogenic miR-10b in cancer

Oncogenic miR-10b is a microRNA that has been reported to be involved in tumor progression by positively regulating cellular migration and invasion pathways in several cancer pathologies[13-18]. While it has long been established in cancer progression, there are several mechanistic pathways that have been theorized to yield its tumor promoting effects in multiple cancer types. The next subsections will focus on the role of this specific miRNA in our three cancer types of interest for this study.

miR-10b in brain cancer

Oncogenic miR-10b has long been established to be upregulated in a cancer context in the brain microenvironment. Interestingly, this microRNA is typically found in very low amounts in normal brain cells, but miR-10b is found to be highly overexpressed in several malignant primary brain tumor types[13, 18-21]. In a work by Gabriely et al. (2011), miR-10b expression levels in normal and tumor tissues were measured, and it was found that starting in low-grade gliomas (Grades 2 and 3), miR-10b levels were found to be significantly upregulated as compared to non-cancerous brain tissue[13]. This effect was also consistently seen in glioma stem cells in a number of other studies, where expression levels of miR-10b were as high or higher than in glioblastoma cell lines and much higher than in normal astrocytes, a common glial cell of origin for gliomas and glioblastomas[19, 20].

There are several proposed mechanisms implicated in this effect and as it is not highly detected in neuroprogenitor cells, it is proposed that it could serve as a

biomarker for the induction of gliomagenesis[20]. In a study by Lin et al., (2012), the authors investigated the impact of miR-10b as it relates to cellular growth, invasion and angiogenetic potential. While the study focused on the mesenchymal subtype of glioblastoma, the authors determined that the invasive potential of glioma cells can be modulated when silenced, and that miR-10b can play a pleiotropic role, wherein it is not limited to the mechanisms of cellular growth or apoptosis, but can also include the functions of invasion and angiogenesis[14]. In the work by Sun et al., (2019), the authors identified that miR-10b, together with miR-222, promote gliomagenesis via the gene PTEN, where both miRNAs were found to target the tumor suppressor gene and activated the p53 pathway via the suppression of MDM2, leading to cell cycle arrest and yielding an oncogenic outcome[22]. In the work by Teplyuk et al, (2016), the authors focused on establishing the role of miR-10b in glioma stem cells, and found that this miRNA was found to be implicated in cell cycle and RNA splicing functions and that its inhibition led to a sharp decrease in tumor cell viability and survival[20]. In the work by Ma et al., (2017), they established a link between the TGF-β pathway and increased rates of proliferation, migration and epithelial-to-mesenchymal transition (EMT) in glioblastoma through the suppression of a number of its target genes including PTEN, E-cadherin, and Apaf-1[23]. All of these studies provide evidence of the roles that miR-10b has been implicated in with regards to tumor progression in the brain; while the roles may be varied, it is clear there is sufficient background of establishing this miRNA as oncogenic in the brain context.

Given any number of contextual and cell-specific cues that may activate these cancer pathways, it is difficult to pin down one specific pathway that may be at play

when it comes to miR-10b and cancers of the brain, but these studies have served to provide multiple targetable avenues to therapeutically pursue.

miR-10b in gastric cancer and pancreatic cancer

Gastric cancer is one of the most common cancer malignancies worldwide generally found to occur sporadically in adults over the age of 45 years with variable survival rate according to histopathological classification[24]. While there have been several studies investigating the presence and impact of miR-10b in this microenvironment and some discussion about whether this microRNA acts as an oncogene or tumor suppressor, it is generally accepted that this miRNA contributes as a driver of cancer. In the study by Li et. al, (2010), the authors identified miR-10b as one of seven miRNAs that formed a signature correlating miRNA expression pattern with prognostic outcome. Using this miRNA signature, the study was able to differentiate between relapse-free survival and progression-free survival in a cohort of patients, along with using this signature in a predictive context to determine whether there were differential outcomes. miR-10b was specifically found to be part of the "risk" miRNAs, where expression levels of this group were correlated with shorter survival. This study supported the oncogenic role of miR-10b in gastric cancer and yields insight in stratification and treatment planning for patients with this cancer type[25]. In the work by Wang et al., (2013), authors established via RT-PCR that miR-10b was highly upregulated in primary gastric cancer tissues as compared to non-tumor gastric tissues, and found that a more severe phenotype, one that incorporates lymph node involvement and distant metastasis, was associated with a higher

expression level of miR-10b. Additionally, when investigating clinicopathological outcomes, higher expression of miR-10b correlated to poorer outcomes in Stages I-III of gastric cancer, confirming its oncogenic role[26]. In the work by Liu et al., (2012), authors established that miR-10b promoted tumorigenesis via the RhoC/AKT pathway, through the inhibition of the target tumor suppressor gene HOXD10[27]. To provide an alternate perspective where miR-10b was found to act as a tumor suppressor, in a study by Li et al. (2014), the authors found that DNA methylation yielded miR-10b acting as a tumor suppressor in gastric cancer. Using a series of *in vitro* experiments, it was established that overexpression of miR-10b led to decreased tumor progression and invasion, as mediated by the correlated CpG islands and via specific targeting of the gene T-cell lymphoma invasion and metastasis (Tiam1)[28]. This case provides more evidence of the diverse role of miR-10b in gastric cancer, though its role in an oncogenic context has been more commonly reported and has been supported by several other studies.

Pancreatic cancer has long been known to be a tumor type that is typically diagnosed at a late stage and is resistant to most common therapeutic modalities. As such, not as much is yet known about its early development. In a study by Nakata et al., (2011), the authors established miR-10b as implicated in the mechanism of invasion and correlation to a poorer outcome in patients with pancreatic cancer[29]. Cell lines and patient samples were used to qualify this effect, with miR-10b found to have higher expression in the malignant pancreatic cells versus the normal cancer cells, and yielding a higher degree of cellular invasion, as evaluated via formalin-fixed paraffin-embedded (FFPE) tissue samples. In another study by Ouyang et al., (2017),

the proposed mechanism of action of miR-10b was found to be via the suppression of TIP30 expression, yielding the promotion of EGF and TGF-β activity on the mechanisms of migration and invasion[17]. In the work by Preis et al., (2011), authors characterized a panel of miRNAs using *in situ* hybridization in resected pancreatic ductal adenocarcinoma (PDAC) to determine whether this panel could be used as a marker for diagnosis and prognosis, and concluded that miR-10b was the miRNA found to be the most frequently overexpressed, as compared with tissue from benign samples. The authors further stratified their sample size according to the therapeutic regimen received, and were able to identify subsets of patients that yielded more positive outcome to treatment than those not. The higher the levels of miR-10b that were found, the higher likelihood of disease progression and poorer overall outcome[30]. This leads credence to the established knowledge that miR-10b has been found to be a therapeutic biomarker in this cancer type and can be used for patient stratification for optimal treatment efficacy.

Assessment and treatment of brain malignancies in cancer

As the primary focus of this study is brain tumors and the therapeutic compound in this study is being modeled in cerebral organoids, this section will focus on the tumor microenvironment of the brain. When it comes to cancers of the central nervous system, one of the primary limitations to effective diagnosis and treatment is accessibility to the tumor. The brain and spinal cord are two of the most protected, yet vulnerable and critical organs of the human body. Any acute or lasting trauma carries the risk of severe, long-term effects. When it comes to cancers of the brain specifically, the gold standard for diagnosis of malignancy is histopathological confirmation. While this is a relatively confirmatory method to determine the degree of disease, it presents multiple difficulties due to the extensive nature of the invasive brain surgery needed to obtain a sample biopsy. Primarily, depending on where in the brain the lesion is located, it could be difficult to impossible to resect the tumor or obtain a biopsy without adverse effects. In addition, the average age of many Grade 4 brain tumors is in the 50s-60s, which is an older population that carries a higher likelihood of co-morbidities, making it less likely that biopsies and more aggressive treatment routes will be pursued[31]. Even when there is ability to obtain a biopsy sample, brain tumors are typically composed of multiple molecular subgroups. In Grade 4 anaplastic astrocytoma, otherwise known as glioblastoma multiforme, there have been at least three molecular subgroups that have been characterized transcriptionally and immunologically; these are the classical, proneural, and mesenchymal groups. All three subgroups have been found to express varying mutations, along with evidence for differentially response to existing therapeutic

modalities, which complicates the ability to determine an effective course of treatment when a tumor may compose more than one of these subgroups[32, 33]. Therefore, access to a biopsy may be misleading due sampling error or due to the heterogeneous nature of the biopsy sample. Furthermore, the microenvironment of the brain has long been known to be unique due to the presence of the blood-brain barrier (BBB). The BBB is a highly selective, semi-permeable membrane composed of a network of blood vessels and endothelial cells that tightly regulate the entry and exit of molecules and cells and work to maintain overall brain homeostasis. This barrier works in conjunction with immune, glial and neural cells to ensure that the brain is protected from the external world, via inflammation, pathogens, toxins, injury and disease[34, 35]. The BBB is often the rate limiting factor for drug development and discovery efforts to treat pathologies in the central nervous system. This is due to its propensity to hinder the majority of existing therapeutics from reaching the microenvironment of the brain, adding a level of complexity to the administration of many chemotherapies, targeted agents and immunotherapies[35, 36]. Advanced forms of primary brain tumors, along with brain metastases, have been reported to significantly compromise the blood-brain barrier[37]. This effect is demonstrated by the diffusion of gadolinium-based contrast agents in magnetic resonance imaging (MRI), which delineate the general area and structure of malignant brain tumors and can indicate whether there is BBB leakage. Under normal circumstances these molecules are not able to cross the BBB to begin with, and are not supposed to show enhancement[38]. This is a double-edged sword, because while this leakage typically indicates advanced or progressive disease, it means that there is a possibility for

therapeutics to surpass the compromised blood-brain barrier, and for certain molecules to directly reach and impact the tumor. Lastly, there is a known a lack of reliable biomarkers that help monitor the response to tumors in the brain to therapy; the introduction of a methodology that could detect biomarker modulation in the bloodstream via miRNA levels would add immeasurable insight due to the ease of access and ability for longitudinal assessment[39]. The development of non-invasive detection methods of cancer would supplement the existing therapeutic toolbox.

One such method that could potentially be applicable to the use of RNA therapeutics is imaging. Imaging in cancer is a powerful tool used to visualize morphological as well as functional information such as angiogenesis, mutation status, cellular invasion, and the presence of specific tumor metabolites. Identifying and characterizing these imaging biomarkers is key to better understanding tumor composition, subgroup classification and the building of robust predictive models that can confer therapeutic benefit. While magnetic resonance imaging (MRI) is the standard tool used to assess disease status, it has yet to lead to a reliable method to distinguish between treatment response and progression of cancer in the context of therapeutic regimens such as radiotherapy and immunotherapy. Imaging features thought to be associated with progressive disease, as characterized by variations in contrast enhancement in MRI, may be conflated with pseudo-progression - a subacute treatment-related effect with features that mirror those of tumor progression. Another treatment effect is radiation necrosis, a late effect resulting from stereotactic radiosurgery at the tumor site and surrounding regions. This emphasizes

the need for enhanced techniques to discriminate between these outcomes in order to better tailor treatments to patients.

In my past work, several forms of imaging studies were conducted to develop non-invasive methodologies to evaluate treatment response as a result of immunotherapeutic agents. In the first study, the aim was to evaluate the impact of anti-PD-1 and anti-CTLA-4 immunotherapy, both separately and together, on treatment response of brain metastases using standard-of-care MRI scans in a retrospective clinical study. Identification of an imaging signature that differentiates between responders and non-responders to immunotherapy in a model of brain metastasis would allow for better stratification of patients in clinical trials, and to increase the likelihood of patients receiving more accurate and effective treatments and not treatments that maybe confer toxicity with no benefit. The second aim of this work was to identify imaging biomarkers that could be predictive of response in brain metastatic disease to these two forms of immunotherapy. Metastases in the brain are unique in that they involve a high degree of immune response activation, given that the blood-brain barrier (BBB) is often significantly compromised due to the nature of the tumor, and they become immunologically "hot" tumors, as compared to primary brain tumors, which are "cold" tumors, due to the relative lack of immune cell involvement. Treatment-related effects such as pseudo-progression and radiation necrosis have also been found to activate the immune system, and are theorized to

yield differential signals via imaging. An example of an axial T1 imaging sequence is shown (Figure 3). Metastatic lesions to the brain are also often unique due to their degree of infiltration and fluidity. Contrast enhancement, shown in yellow, is an indicator of active, proliferating tumor best reflected on T1-post weighted images; edema is a marker of fluid content in the tumor lesion and is associated with high levels of aggressiveness and invasion. This signal is typically
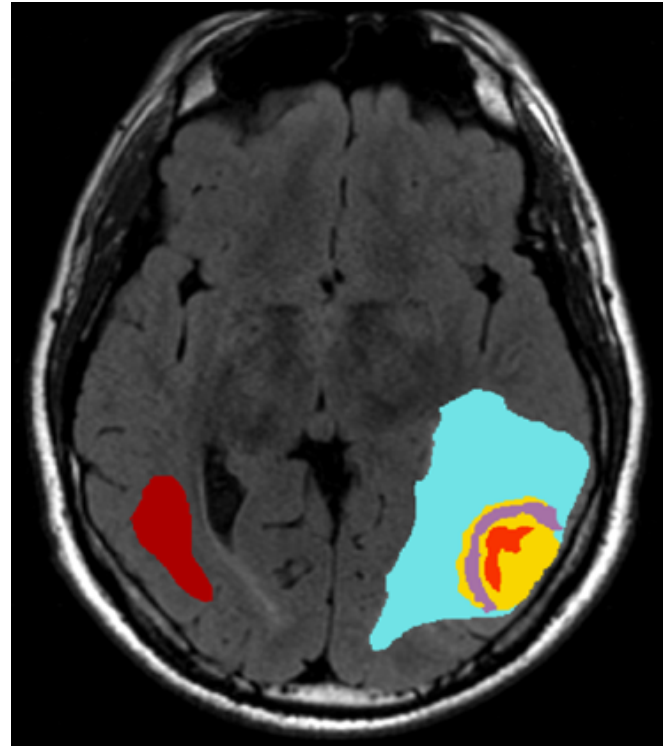
Figure 3. Segmentation of imaging phenotypes. Axial T1 MRI scan of a metastatic lesion to the brain annotated with imaging phenotypes, labeled below: <u>Yellow:</u> active tumor enhancement; <u>Light Red:</u> necrosis; <u>Purple:</u> hemorrhage; <u>Blue:</u> edema; <u>Red:</u> contralateral white matter

found on T2 FLAIR sequences (blue); and necrosis is a signal that is indicative of hypoxia and dead tissue, or necrosis, found on T1 images (light red). Hemorrhage/blood products (purple) are a common finding in certain tumors such as melanoma brain metastases, as these tumors are characterized with more vascularization and blood throughout the tumor, as well as having melanin content. These unique factors are found to be associated with poorer long-term outcomes as compared to other cancer types and can be captured via imaging with both T1 and T1 post scans[40]. Tumor-infiltrating edge was segmented within the enhancement region on T1 post-contrast weighted images and incorporates an immunologically

active region around the border of the lesion, a region called the "ring of fire", where immune cells begin to infiltrate into the tumor. Contralateral white matter, shown in dark red, was segmented as normalization for calculation purposes.

Nearly 500 scans of patients who underwent anti-PD-1 and anti-CTLA-4 therapy at MD Anderson Cancer Center were retrospectively reviewed for this study, with standard-of-care magnetic resonance images semi-automatically segmented and electronic medical records evaluated for clinical and demographic information. In addition, imaging characteristics such as volume and morphology of any tumors and metastatic lesions were collected using the 3D Slicer image analysis software (www.slicer.org)[41] to investigate potential relationships between these factors with the eventual goal to build predictive models for the clinic. While the analyses of this specific work have been on hold, the approach and methodology through which this study was pursued was extensively tested and can easily be applied to similar studies that incorporate imaging.

In the second study, the aims were to evaluate the association between CAR T-cell related neurotoxicities and clinical features in a cohort of patients in a clinical trial at MD Anderson Cancer Center, along with evaluating the association between the occurrence of these neurotoxicities and the survival of patients. Chimeric antigen receptor (CAR) T-cell therapy has been found to be a promising intervention for various malignancies, but is associated with severe toxicities throughout the body. With reference to the brain, CAR T-cell-related encephalopathy (CRES) involves confusion, delirium, brain swelling and seizures that can be fatal and impacts a large

range of patients that undergo CAR T-cell therapy, with the majority sustaining a Grade 3 or above[42-44].

Using the FSL 6.0: FMRIB Software Library[45-47], an established neuroimaging tool for analysis of MRI brain imaging data, all major components of implicated neuroanatomical sites of neurotoxicity were able to be identified and reconstructed using standard-of-care baseline MRI scans. The areas of focus were mainly the volume and distribution of gray and white matter, and the volumes of subcortical structures in the limbic system, the region theorized to be impacted the most after this form of therapy. This semi-automatic segmentation of various structures is shown in Figure 4.

The innovation of this work comes in the form of imaging and clinical data collection before the administration of the CAR-T cell therapy, where there is a baseline assessment of the brain microenvironment taken before any evidence of CRES neurotoxicity occurs. In this way, it can be assessed whether there are "imaging biomarkers" that can be detected, and later compared to the scan after the CAR-T cell therapy is administered, in order to evaluate any treatment effects and aid in the determination of whether there is any correlation or pathology that can be used to predict or investigate further.
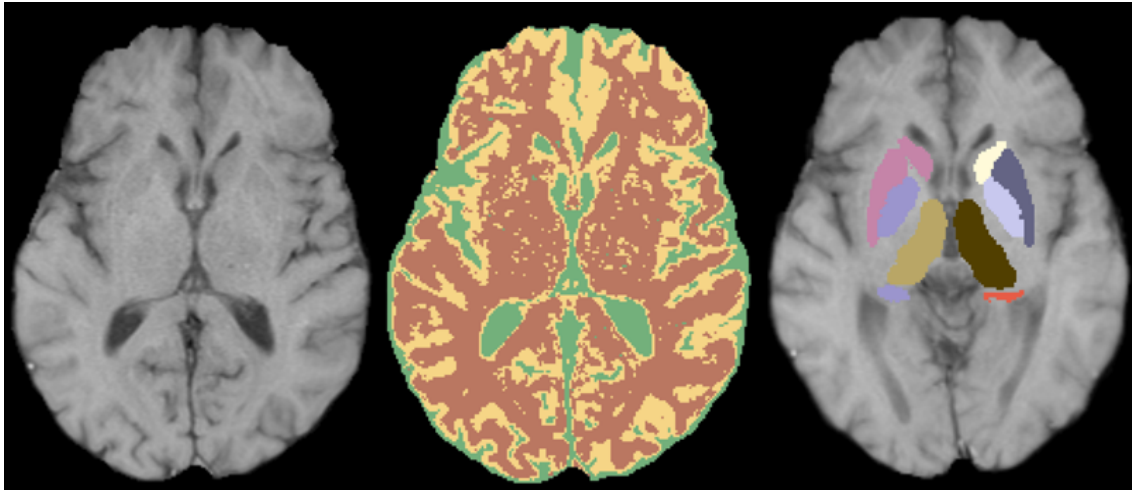
Figure 4. Imaging phenotypes for evaluation of neurotoxicity. Axial T1 MRI scans displaying the segmentation of gray matter (yellow), white matter (orange), and cerebrospinal fluid (green). Shown on the panel on the right are the segmentation of left and right subcortical regions implicated in the limbic system, which is thought to contribute to CRES, or neurotoxicity after CAR T-cell therapy

While both of these studies have remained on hold, they have yielded significant insight into methodologies to non-invasively and qualitatively assess malignancies and treatment response in the brain. This experience has since been introduced in the world of miRNA research in the laboratory, where the imaging techniques applied to scans from the brain have been used in a preliminary study on targeting an oncogenic miRNA called miR-155, which has been associated with metastatic lesions in the lungs. This methodology was used to reconstruct these tumors using thoracic CT scans in a translational therapeutic model and the morphology of tumors was evaluated (Figure 5).

With the rise in RNA therapeutics, including with the novel compound proposed in this study, this provides an interesting avenue for further study, wherein non-

invasive detection of tumor progression, coupled with targeted therapeutics, can lead

to the development of improved and more specific approaches.
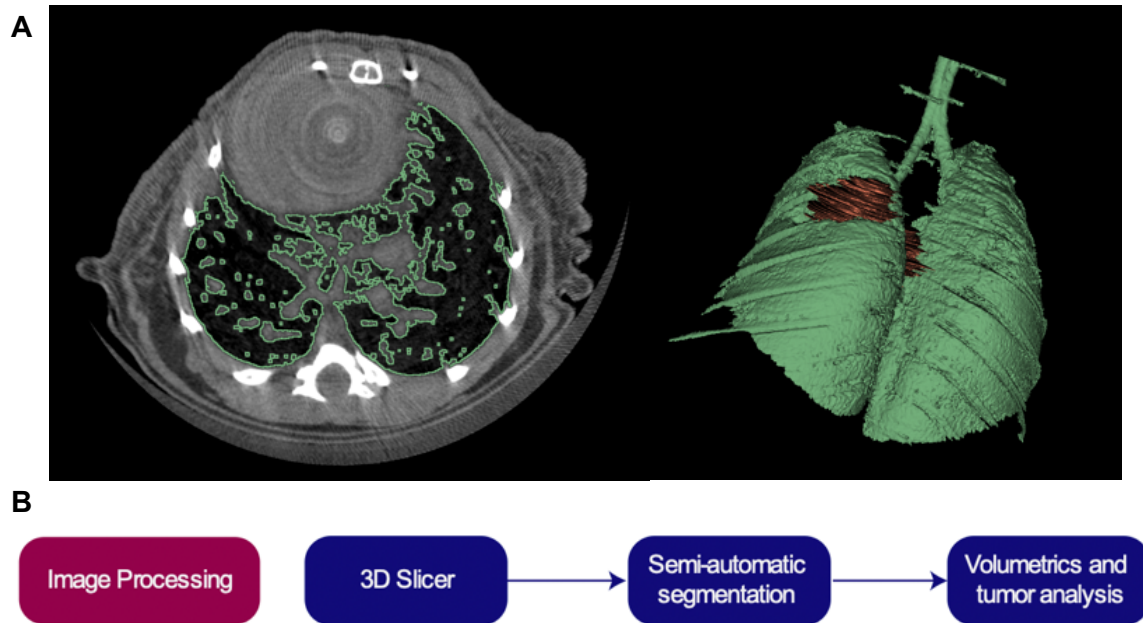
Figure 5. 3D reconstruction of lung metastases. A. Axial CT scan of the thoracic cavity at the region of the lung. The area has many small lesions and areas of enhancement, indicating the presence of lesions. The largest one is outlined in the 3D reconstruction of the lungs on the right panel. B. Workflow for the preliminary study

As previously mentioned, several limitations currently exist in the study of cancer, particularly in the translation of biological findings from bench to bedside. While cancer cell lines, PDX models and *in vivo* studies continue to provide valuable mechanistic insight into the progression of cancer, these models have an inherent difficulty in mimicking the microenvironment in which tumors are initiated and proliferate in humans, and thus have multiple limitations in their ultimate translation and generalizability of novel drugs that are designed and developed[38, 48].

This study is the first known of its kind to investigate small molecule inhibitors of miRNAs in cerebral organoids. By definition, organoids are 3D cultures of human-derived cells that are able to develop into tissues that are structurally and phenotypically similar to the organ of interest. Importantly, they are able to represent cellular heterogeneity of an organ and can be used to model a number of disease conditions, along with their treatment responses. When cultivated and stably grown, they can be used in cancer research to bridge the gaps between *in vitro* and *in vivo* studies and clinical trials in humans and more authentically represent the tissue microenvironment in which tumors are growing and proliferating[49-52].

There are several methodologies that have been described in the generation of organoids in multiple cancer types. In the work by Krieger et. al (2020), authors described a brain tumor organoid model, validating that glioblastoma cells invade into the cerebral organoids via similar mechanisms as they do *in vivo*, and using single-cell RNA sequencing techniques, were able to distinguish consistent transcriptional changes across varying patient samples[53]. In the work by Linkous et al., (2019), a cerebral organoid glioma model was developed, derived from human embryonic stem

cells and co-cultured with glioma stem cells. This work established a robust model where the tumors developed were phenotypically similar to those found to develop in humans, and allowed for a technique that could model growth and also be used for drug screening[54]. The benefit of using similar models is the ability to conduct drug screening in a more cost-effective, experimentally controlled setting, where organoids are a closer representation of human tissue response than those found in *in vitro* or *in vivo* contexts. As they are patient-derived, organoids can serve to design and develop treatments in a personalized medicine approach[49]. This work incorporates the use of cerebral organoids derived from human-induced pluripotent stem cells (iPSCs), which have been an established model in recent years[49, 52, 55]. The cerebral organoid model used in this study was initially developed by Dr. Sanjay K. Singh in the Department of Neurosurgery at MD Anderson Cancer Center, wherein adult fibroblasts are isolated, grown and expanded. Using specialized neural growth media, along with additional nutrients specific to brain development, the mechanism of neural differentiation is induced, with the development of ectoderm and epithelial cells. When stably grown, these organoids become anatomically representative 3D cultures with all major brain cell types expressed, namely the multiple forms of neuronal and glial cells. This provides a powerful and applicable model through which invasion of brain cancer cells into tissue can be demonstrated and the potency of the novel small molecule inhibitor can be tested.

Rationale for the study

In the lab's previous work[56], a robust methodology was established to screen a primary library of small molecule compounds, with the goal to increase the generalizability of already FDA-approved and clinically tested agents and expedite the process of drug development and discovery. This library was screened against a panel of miRNAs that were determined via comprehensive literature search to be oncogenic. The previous study identified the small molecule linifanib (ABT-869), a multi-tyrosine kinase inhibitor targeting VEGF and PDGF to have anti-tumor and anti-proliferative effects[57-59], as an inhibitor of miR-10b expression in several cancer types. Previously, linifanib was advanced to the clinic for clinical trials, as it was found to be effective in anti-tumor effects; however, it failed to meet survival endpoints when tested against its competing inhibitor sorafenib in advanced hepatocellular carcinoma[60]. However, in the screening that was published by the laboratory, this particular compound was found to potently inhibit this oncogenic miRNA as compared to other miRNAs.

Small molecule therapeutics provide a unique approach and opportunity for treatment, as they are generally of a molecular weight conducive to permeate through membranes, such as the blood brain barrier under normal conditions, and with a compromised barrier in the cases of malignancy, are more likely to be able to target and impact the tumor directly. In addition, they possess more optimal characteristics of solubility and permeability to be able to pervade through membranes and tissues that may have previously have been impermeable or challenging to diffuse through. Chemical derivations of small molecule compounds that have been FDA-approved

and have gone through all of the experimentation and validation of the bench-to-bedside pipeline allows for easier application of these agents to novel contexts, in this case in the targeting of overexpressed and oncogenic miRNAs. This allows for the generation of new hypotheses and derivations of compounds that have a high potential of specificity and efficacy and ultimately success in human application.

The goal of this work is to characterize a novel small molecule inhibitor derivative of linifanib, designed to increase the selectivity and specificity of the small molecule compound to the nucleotide sequence of oncomiR-10b. Via medicinal chemistry, structural biology and cancer therapeutics approaches, this novel compound, IACS-13743, was identified from a number of chemically derived compounds, with primary objectives to prove direct binding to miR-10b and validate anti-tumor effects in a screening of multiple malignant cancer types, namely brain cancer, gastric cancer, pancreatic cancer both in an *in vitro* and cerebral organoid context.

Hypothesis and Aims

The hypothesis of this work is that IACS-13743 can directly bind to oncogenic miR-10b, inhibiting molecular pathways that promote tumor progression and malignancy. To address this hypothesis, the following aims were pursued:

Aim 1: To conduct mechanistic in vitro studies and validate direct binding of IACS-13743 to the miR-10b transcript

Aim 2: To validate findings in cerebral organoid studies

Aim 3: To identify oncogenic pathways implicated in the effects of IACS-13743

Chapter 2. Methods

Compound generation: Approximately 42 small molecule compounds derived from linifanib (ABT-869) were synthetized by the Institute of Applied Cancer Science (IACS) at the MD Anderson Cancer Center. After *in vitro* screening in multiple cell lines of interest, IACS-13743 was determined to be the primary compound of interest in this study to be further analyzed.

Microsomal stability assay: This assay, along synthesis and solubility analyses, were conducted in collaboration with the Institute of Applied Cancer Science (IACS), with the methodology described by Dr. Barbara Czako. The assay was conducted on a Beckmann Biomek FXp automation system. The liver microsomal incubation mixture was composed of liver microsomes (with a concentration of 0.5 mg microsomal protein/ml), the test compound (1 μM), MgCl2 (3 mM), EDTA (1 mM) in potassium phosphate buffer (100 mM, pH 7.4). The control substrates used for the assay were Midazolam and Ketanserin. The reaction was initiated with the addition of an NADPH regeneration solution (1.3 mM NADPH) and maintained at 37 °C with shaking. At five sequential time points ranging from 0 to 45 minutes, aliquots of the mixture (50 μL) were removed and quenched with acetonitrile (100 µL) containing an internal standard control (imipramine). After vortexing and centrifugation, samples were analyzed by liquid chromatography-mass spectrometry (LC-MS/MS). The *in vitro* T1/2 was then calculated and clearance followed literature[61].

Synthesis of inhibitors: The inhibitors provided in this study were developed via standard chemical transformations. All reagents and materials were obtained from suppliers such as Sigma-Aldrich, Alfa Aesar, TCI, or Acros. Anhydrous solvents (e.g.,

THF, DMF, DMA, DMSO, MeOH, DCM, toluene) were purchased from Sigma-Aldrich and directly used as manufactured without further purifications. Other inhibitors were purified by preparative high-performance liquid chromatography (HPLC). The identity and purity of all compounds with reported biological activity was confirmed by NMR spectroscopy, low-resolution mass spectrometry and HPLC. NMR spectra were recorded on Bruker instruments operating at 300, 500, or 600 MHz. NMR spectra were obtained as $CDCl_3$, CD_3OD, D_2O, $(CD_3)_2SO$, $(CD_3)_2CO$, C_6D_6, or CD_3CN solutions (reported in ppm), using tetramethylsilane (0.00 ppm) or residual solvent ($CDCl_3$, 7.26 ppm; CD_3OD, 3.31 ppm; $D2O$, 4.79 ppm; $CD_3)_2SO$, 2.50 ppm; $(CD_3)_2CO$, 2.05 ppm; C_6D_6, 7.16 ppm; CD_3CN, 1.94 ppm) as the reference standard. Low-resolution mass spectra were collected on either a Waters H class UPLC with a Waters Acquity UPLC BEH C18 1.7 µm, 2.1 mm × 50 mm column, UV detection between 200 and 400 nm, evaporating light scattering detection, and a SQ detector mass spectrometer with ESI ionization or a Water I class UPLC with a Waters Acquity UPLC CSH C18 1.7 µm, 2.1 mm × 50 mm column, UV detection at 254 and 290 nm, evaporating light scattering detection, and a SQ detector 2 mass spectrometer with ESI ionization.

Solubility assay: Solubility of the IACS-13743 compound and linifanib were assessed using the FeSSIF method, which stands for "fasted state simulated intestinal fluid", to simulate the microenvironment through which these compounds could dissolve. The compounds were measured at two different pH levels, normal: 7.4, and slightly acidic: 5.8. The metrics for determination of solubility were classified as 0-10µM as low to no

solubility, 10μM-80μM as moderate solubility, and values of 80μM and above as compounds with high solubility.

Detection of compound binding to miRNA: This experiment was conducted in collaboration with the University of Washington and methodology described by Dr. Matthew Shortridge. The human pre-miR-10b RNA hairpin sequence (nucleotides 40-75, per miRbase) was transcribed enzymatically (T7) and purified using methods previously described[62-67]. Ligand detected NMR experiments were conducted on a Bruker Avance III 600 MHz spectrometer equipped with TCI cryoprobe. The NMR screening buffer consisted of 20 mM d19-Bis-Tris at pH 6.5, 10 mM sodium chloride, 0.2% tween-20, and 11.1 µM DSA as chemical shift reference (integrates to 100 µM)[65, 68], prepared in 99.99% D_2O or 95%H_2O/5%D_2O. Each ligand was first dissolved in DMSO to a 10 mM stock concentration. Free ligand screening samples were prepared at a final DMSO concentration of 10% at a concentration of 100 µM in NMR screening buffer. This concentration was used as the safe upper limit beyond which the structure of the RNA would be affected. For RNA target detected experiments, the lyophilized RNA pellets were dissolved in DMSO-free NMR screening buffer and heated for 4 min at 90 °C, then snap-cooled for 5 min at −20°C. 1D-1H experiments for both ligand and RNA were collected using the Bruker "zgesgp" excitation sculpting pulse sequence to suppress background water signal. Data was collected with 64 scans and 16K data points. Data was processed using 16K zero points, then Fourier transformed followed by manual phase and baseline correction. 2D-1H TOCSY experiments were collected using the Bruker "mlevesgpph" pulse sequence with excitation sculpting water suppression, data collected with 32 scans,

2K × 512 data points, a recycle delay of 1.2 s, and spin-lock mixing time of 80 ms. A reference, ligand free RNA ([pre-miR-10b] =50μM) TOCSY spectrum was collected prior to adding 4x of IACS-13743 ([IACS-13743] = 200μM). Concentrations were lower than typically used in order to help prevent aggregation and precipitation of the small molecule. All data was processed using NMRPipe and visualized using SPARKY. Peak assignments and secondary structure mapping were completed using methods described previously[65-67].

In vitro experiments: *Cell line selection and maintenance:* Using the Cancer Cell Line Encyclopedia (CCLE)[69], in-house cancer cell lines were screened to identify cancer and tissue types with significant levels of miR-10b expression level (Figure 6). Initial screening experiments were conducted using the MCF7 and MDA-MB-231 cancer cell lines, but as experimentation was conducted with various other cancer cell types, this was shifted to more representative cell lines for the second phase of this experiment, due to better characterization and compound treatment response in these cancer types. For the purposes of *in vitro* experiments, cell lines were selected with varying high expression levels of this microRNA, and were also validated to be highly overexpressed, as substantiated by additional clinical and survival data in The Cancer Genome Atlas (TCGA).

All experiments were performed using the human-derived cell lines U251 and LN229 (brain cancer), AGS and SNU-1 (gastric cancer), and AsPC-1 and PANC-1 (pancreatic cancer). The two cell lines chosen for brain cancer analysis accounted for PTEN mutation status; PTEN is a tumor suppressor gene found to have the most

frequent mutation (35-40%) in glioblastoma and its dysregulation is found to potentially lead to differential treatment response[32, 70]; U251 has a two base pair duplication at PTEN, yielding a frameshift mutation, whereas the LN229 cell line is wildtype for this gene.
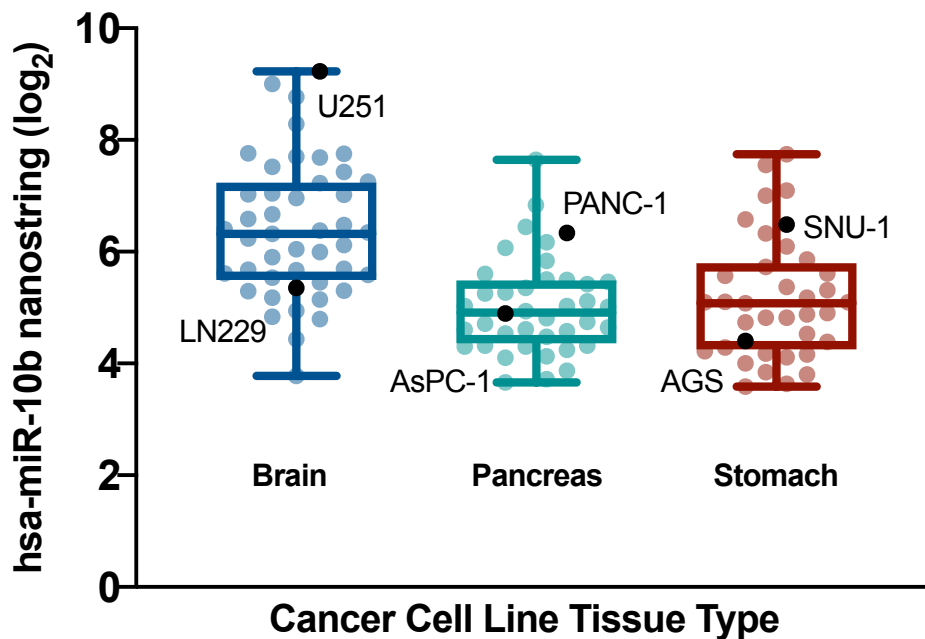
Figure 6. Expression level miR-10b in cancer cell lines according to tissue type.

Cell lines were obtained from the American Type Culture Collection and grown and maintained per instructions from the supplier. U251 and PANC-1 cell lines were cultured in DMEM supplemented with 10% fetal bovine serum (FBS) and LN229 was cultured in DMEM with 5% FBS. AGS was cultured in F12K medium supplemented with 10% FBS. Both SNU-1 and AsPC-1 cell lines were cultured in RPMI, with 10%

FBS added. All cells were kept at 37°C in a humidified atmosphere of 5% CO_2, and underwent regular mycoplasma testing. All *in vitro* experiments were conducted when cells were 70-80% confluent.

Dose-response curves: IC_{50} dose-response curves were determined using the MTS assay system. 5,000 cells of each cell line were plated in 96-well microculture plates in replicates of 6. When cells became adherent, 10 sequentially decreasing doses of IACS-13743 were diluted into new media and added to 10 wells. Control wells were included for comparison. After 48 hours, MTS reagent was added to each well at the same time of day as treatment and incubated for 2 hours at 37°C. The optical density (OD) was read at 490nm on a microplate spectrophotometer and data analyzed to determine the IC50 via the dose-response curve method in GraphPad Prism.

Proliferation assay: The impact of the compound on cellular proliferation was assessed, with 5,000 cells in each cell line seeded in replicates of 6 in a 96 well plate and treated with DMSO or IACS-13743. After 48 hours, cells were treated with the MTS reagent and optical density read, in a method similar to the dose-response curves. Data was analyzed via GraphPad Prism.

Quantitative real time PCR analysis: RNA was isolated utilizing Trizol (Invitrogen) and the Direct-zol RNA Miniprep kit (Zymo Research). RNA concentration was assessed with the NanoDrop ND-1000 spectrophotometer (ThermoFisher Scientific). miR-10b expression was tested using qRT-PCR. Cells were seeded in 6 well plates 24 hours before treatment, at a cell confluency of 50-60%. Each cell line was treated with 10μM of compound or the control compound dimethyl sulfoxide (DMSO), the solvent for the compound. RNA was collected after the 48-hour time point. Expression of miR-10b

was assessed utilizing the TaqMan microRNA assay (Applied Biosystems). The complementary DNA (cDNA) was synthesized using the TaqMan Reverse Transcription Reagents kit (Applied Biosystems) and was used with the TaqMan probes and Supermix (BioRad) for qRT-PCR analysis. The primers of interest were hsa-miR-10b and the normalizers U6 or U48, used as internal controls. All experiments were performed in triplicate, with all samples normalized to the internal controls and relative expression levels calculated using the $2^{-\Delta\Delta Ct}$ method.

Clonogenic assay: In vitro clonogenic assays were conducted with adherent lines seeded in 12-well plates, treated for two weeks, and stained with crystal violet. Images were analyzed via the software ImageJ where colonies were semi-automatically counted and compared across groups.

Flow cytometry: Apoptosis and cell cycle assay: In 6-well plates, 1 x 10^5 cells/mL were added into each well. After 24 hours, sequential concentrations of DMSO and IACS-13743 were administered and the plates were incubated for 48 hours. The supernatant and adherent cells were collected and centrifugated. Each dose was done in triplicate, with each sample composing two wells. For apoptosis analysis, the supernatant was discarded after centrifugation and the pellet washed with PBS twice. Then, BD Annexin V-FITC/PI was used to stain the cells for analysis via flow cytometry on a Gallios machine. For cell cycle analysis, after washing with PBS, cells were fixed with ethanol and incubated. They were then treated with RNase enzyme and counts analyzed across groups.

Cell sorting: For co-culturing with cerebral organoids, the brain cancer cell lines U251 and LN229 were transduced with an RFP lentiviral vector expressing MCherry and

luciferase, and sorted twice via an Aria Influx Cell Sorter. Cell lines were expanded to at least 1 x 10^6 cells/mL and properly grown, maintained and stored until experiments began.

Western blot analysis: Western blot analysis was conducted according to standard established protocols, as outlined in the laboratory's previous work[56]. Briefly, proteins were extracted and collected from lysed cells from all screened cell lines of interest. The Bradford assay was used to measure and normalize protein concentrations. Quantification of protein expression after the experiment was conducted using the image analysis software ImageJ[71].

Cerebral organoids: Human induced pluripotent stem cell (iPSC) derived cerebral organoids were obtained, courtesy of Dr. Sanjay Singh and Dr. Frederick Lang in the Department of Neurosurgery at MD Anderson Cancer Center. Organoids were maintained in a specialized neural based media on a continuous running shaker inside a 37°C incubator. After maturation, organoids were moved to 24-well ultra-low attachment plates, and individually co-cultured with 5 x 10^5 – 1 x 10^6 cells from RFP cell sorted brain cancer cell lines until RFP signal on individual cells was clear on the surface of the organoid, approximately 48-72 hours, indicating cell adherence and attachment. Organoids were then moved to 6 well plates and grouped into triplicates within each of the wells. The treatment regimen of control, and the group treated with the compound IACS-13743 was started, at an analogous schedule to *in vitro* experiments. For fixation and embedding for *in situ* hybridization, the organoids were processed using 4% PFA and placed in optimal cutting temperature (OCT) compound in -80°C for sectioning.

Reverse Phase Protein Array (RPPA): Proteomics analysis was conducted at the Reverse Phase Protein Array Core facility at MD Anderson Cancer Center, the methods of which are described in detail in the referenced publication[72]. Briefly, controls and treated samples were analyzed in triplicate for 486 unique antibodies. The outputs were then normalized for protein loading and transformed to the linear value, and the normalized data was $\log_2$ transformed ($\log2(x+1)$) and sorted by FDR-adjusted p-values with a significance level of $p < 0.05$. Differentially expressed proteins between the groups were identified using the moderated t-test from the LIMMA package[73]. The results of the differential expression analysis (fold changes and p-values) were displayed in a volcano plot, highlighting proteins of interest. Analyses and graphical representations were carried out in R (http:///www.r-project.org/). The clusterProfiler package was used for data visualization and analysis.[74] Differentially expressed genes were $\log_2$ normalized. For pathway analysis, the Hallmark gene set[75] and Gene Ontology[76, 77] datasets were used.

Statistical analysis: All statistical analyses were performed in GraphPad Prism Version 8 or 9. All tests were two-sided and considered statistically significant at the $p < 0.05$ level. Graphs with error bars represent mean ± SEM.

Chapter 3. Results

Aim 1: To conduct mechanistic in vitro studies and validate direct binding of IACS-13743 to the miR-10b transcript

Screening of compounds in the secondary library: In the past work, a library of small molecules was screened for miRNA specificity and linifanib (ABT-869) was identified as a viable drug candidate to specifically target a dysregulated microRNA in cancer - microRNA-10b[56]. While this effect was shown in an *in vitro* context, due to the insolubility of the parent molecule, direct molecular binding between the sequence of miR-10b and linifanib was not able to be confirmed. The generation of a secondary small molecule library allowed for the ability to evaluate molecules that were modified and found to yield greater levels of solubility and specificity to the sequence of this miRNA. In this aim, a panel of cell lines derived from multiple cancer types with significant levels of miR-10b was used to validate the function of this molecule *in vitro*, to provide a broader perspective as to its mechanistic function.

IACS-13743 is an inhibitor of oncogenic miR-10b: To identify a novel small molecule compound candidate, 42 small molecules were developed via structure-based design from the parent compound linifanib, and after a rigorous screening process, IACS-13743 was identified as the candidate for further *in vitro* studies (Figure 7). Based on the structure of linifanib, a 2-dimensional structure-activity

relationship (SAR) study was performed by making structural modifications in the 1H-indazol-3-amine and the 2-fluoro-5-methylphenyl region of the molecule.
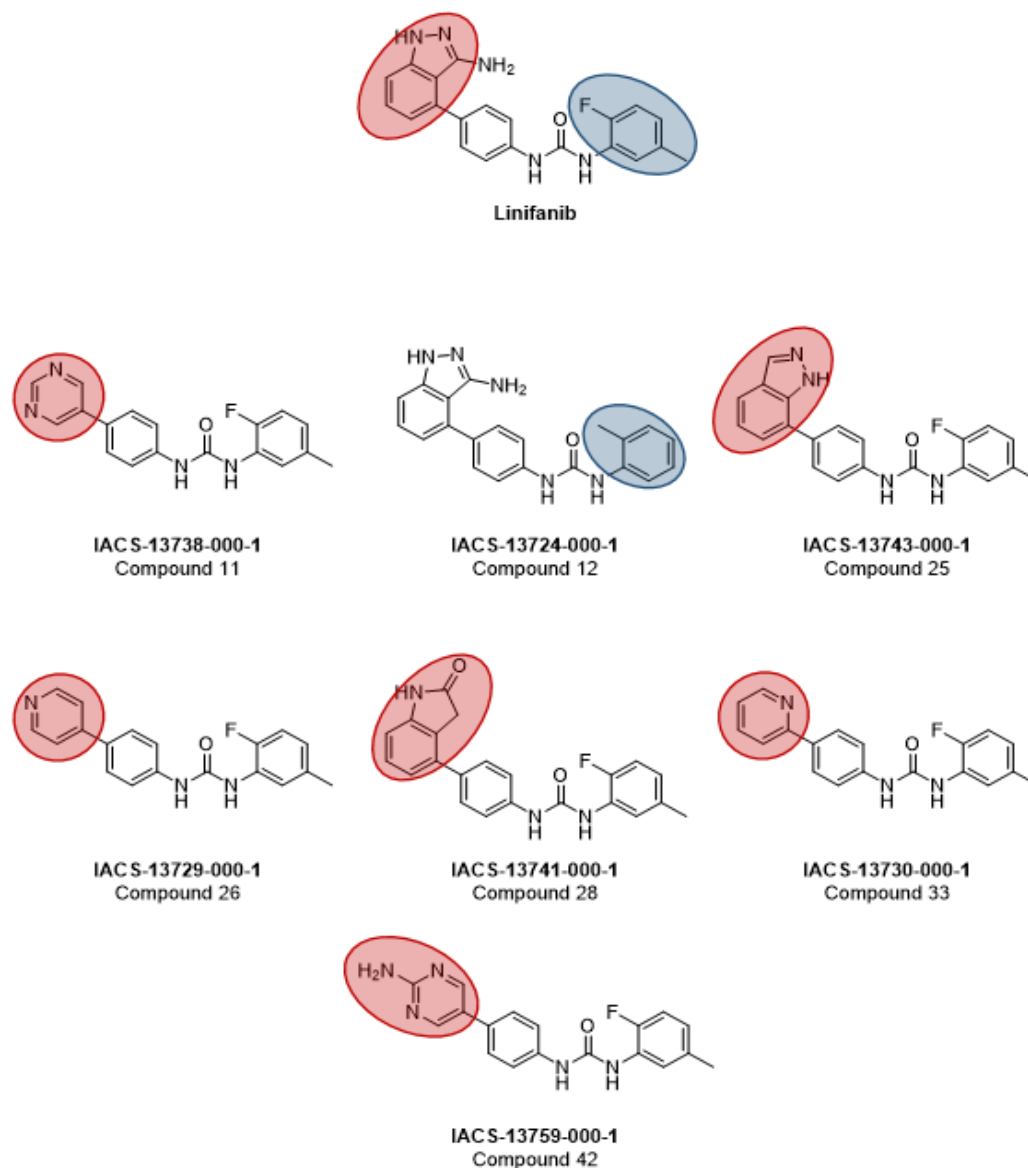
Figure 7. Structure-activity relationship (SAR) studies of microRNA-10b inhibitors based on the structure of linifanib. The development of derivative compounds initially yielded 42 compounds and was further filtered to 8 compounds via luciferase assay. Compounds 25 emerged as the candidate for further *in vitro* analyses

As an early study identified miR-10b identified as an oncogenic marker in breast cancer[78, 79], the screening of the secondary library derived from linifanib was conducted in the MCF-7 cell line using a luciferase assay, using DMSO as the negative control and the parent compound linifanib as the positive control. Briefly, the luciferase assay is a rapid screening methodology utilized to detect miRNA expression levels. When a molecule or inhibitor targets the miRNA of interest, the mature sequence of the microRNA is decreased due to the inability to be processed from the premature form, and the luciferase gene is expressed. If the compound is not found to be specific to the sequence of miRNA and by extension doesn't bind or impact the activity in any way, the miRNA binds to the target sequence and inhibits the expression of the luciferase gene, decreasing its effect. As shown in Figure 8, based on activity in the primary cell assay, 8 compounds yielded a fold change greater > 2 in the MCF-7 cell line and were prioritized for further screening in the MDA-MB-231 cell line. Compounds 11 and 25 were two of the top hits from both screenings, and were utilized for further *in vitro* assays in the selected panel of cancer cell lines.

MCF-7

MDA-MB-231
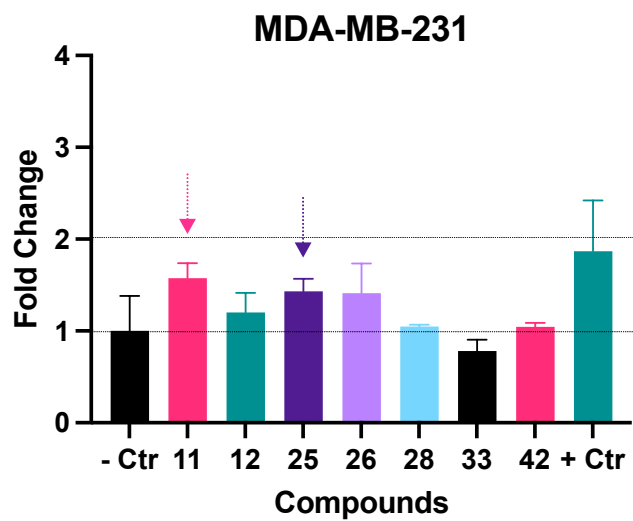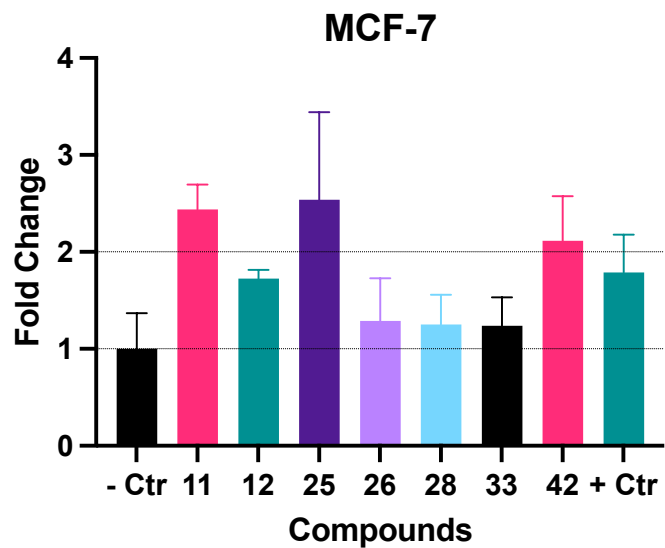
Figure 8. Luciferase screening of secondary candidate compounds in the first part of this study. This experiment narrowed down compounds from secondary library generation to Compound 11 and Compound 25 and later focused on Compound 25

These SAR studies revealed that the 1H-indazol-3-amine moiety is not required for activity, and can be replaced by a variety of heterocycles as depicted on Figure 8. Small variations in the substituent pattern on the phenyl ring were also tolerated, as shown by IACS-13724. As a result of this study, IACS-13743 (Compound 25) emerged as a leading compound. IACS-13743, or Compound 25, has acceptable calculated properties and is Rule-of-Five[80] compliant, with a cLogP of 4.75, TPSA of 69, 3 H-bond donors of 2 H-bond acceptors. The compound has low kinetic solubility of 0.71 μM in PBS (pH 7.4) but excellent solubility in buffer that simulates fed state (FeSSIF) (pH 5.8) with a solubility of 51 μM. The compound was also found to exhibit favorable microsomal liver stability in human, rat and mouse microsomes with a clearance level of 14.9 mL/min/kg, 41 mL/min/kg and 58 mL/min/kg, respectively, and a half-life of 116 min, 60 min and 92 min, respectively (Table 1). Clearance level (CL_{int}) is a measure of the amount of drug being cleared from the liver or hepatic system. Therefore, the higher the clearance level, the more favorable the effect of the drug can be, as it has a longer duration in the system. While the clearance levels for the derivative compound IACS-13743 fall under the "medium clearance" classification, their values do not significantly vary from the parent compound linifanib. Based on the activity of the compound, as well as the calculated and *in vitro* pharmaceutical properties, the compound was further evaluated.

Compound	Species	Half-life (min)	CLint(mL/min/kg)
	MLM	92.8	58.9
IACS-13743	RLM	60.4	41.1
	HLM	116	14.9
	MLM	63.1	86.5
Linifanib	RLM	122	20.4
	HLM	197	8.8

Table 1: Microsomal stability assay evaluating the half-life and clearance levels of IACS-13743 and the parent compound linifanib. Mouse liver microsome (MLM), rat liver microsome (RLM), human liver microsome (HLM)

In preliminary experiments evaluating the candidate compounds for the second phase this study, several cancer types were evaluated and considered for inclusion. Initial studies in hepatocellular carcinoma and triple negative breast cancer were conducted for Compounds 11 and 25, but yielded data that was not consistent between the compounds, indicating that the mechanisms of tumor impact in this context may not have been miR-10b mediated or the tissue tumor type was not receptive to the compound. Brain cancer, gastric cancer, and pancreatic cancer have long been studied in the context of miR-10b[13, 14, 16, 17, 29] and had supporting data of its significant expression and impact in these cancers, so they were chosen for further screenings.

The antitumor efficacy of IACS-13743 was evaluated in the six cell lines of interest. Half-maximal inhibitory concentration (IC_{50}) was determined for each cell line at 24 hours and 48 hours post-treatment. The time point at 48 hours was found to be the time point that yielded the lowest IC_{50} value for the majority of cell lines, indicating

the most potent effect[81], and was thereby chosen as the time point for further *in vitro* experiments (Figure 9, Figure 10).
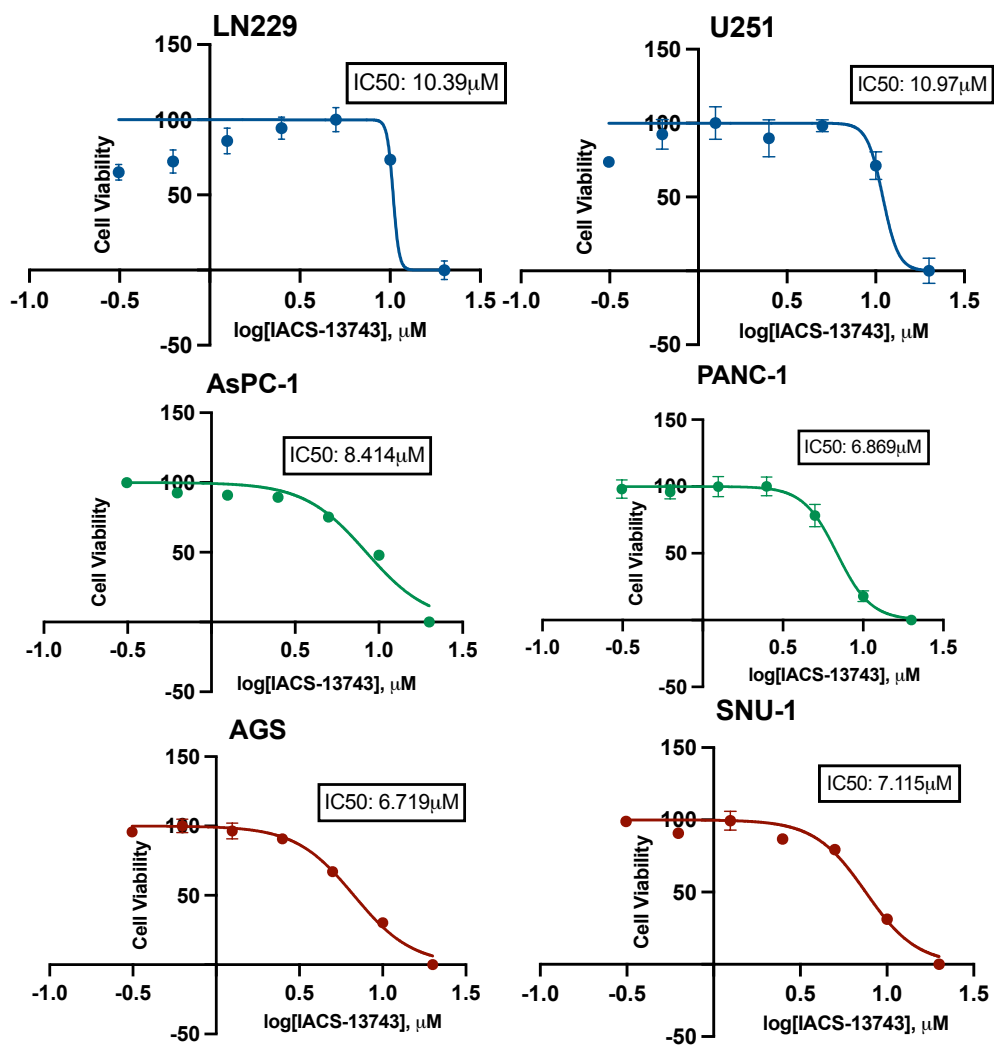
Figure 9: IC$_{50}$ values of each cell line at 24 hours after treatment with IACS-13743
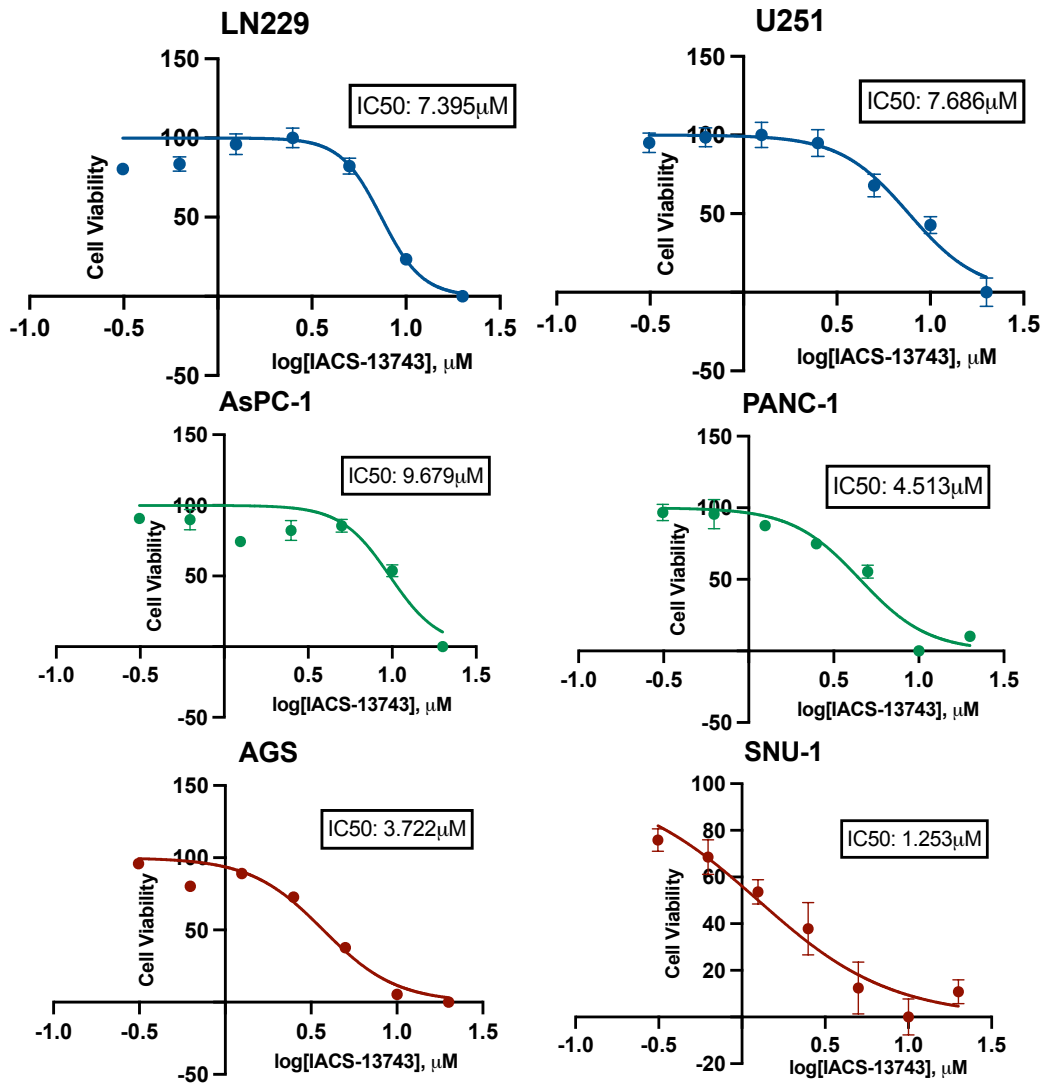
Figure 10: IC$_{50}$ values of each cell line at 48 hours after treatment with IACS-13743

Using expression data gathered from the Cancer Cell Line Encyclopedia (CCLE)[69], a Pearson's correlation was conducted to evaluate whether there was a relationship between the expression level of miR-10b in the six cell lines that were screened and their IC_{50} value. As shown, a significant correlation between all lines was not found,
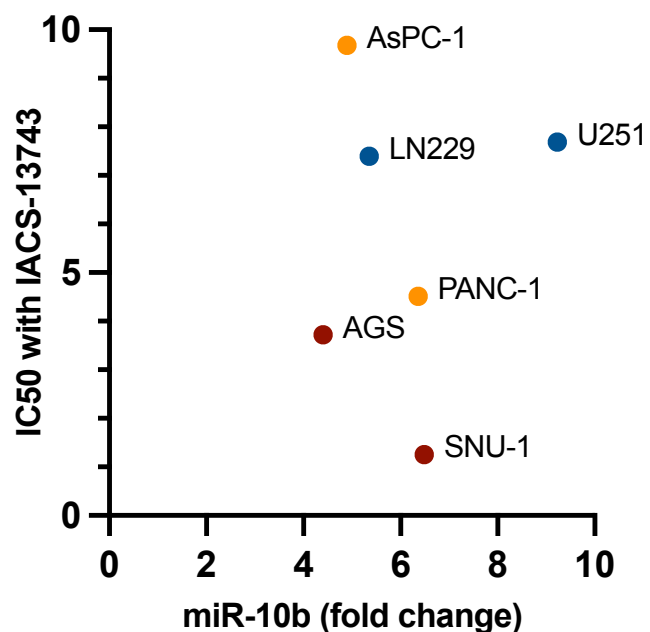
Figure 11. Correlation between miR-10b expression level and IC_{50} values

however this graph shows that tissue type may play an important role in each cancer cell type sensitivity to the compound.

The two primary brain cancer cell lines (U251 and LN229) were shown to have comparable IC_{50} levels and relatively higher miRNA expression level. In fact, from the data gathered in the Cancer Cell Line Encyclopedia (CCLE), the U251 cell line was found to have the highest expression of miR-10b of all analyzed brain cancer cell lines, which is consistent with this data and is the rationale for its primary use in this study. Both gastric cancer cell lines had IC_{50} values under 5μM, with AGS being a primary cancer cell line and SNU-1 a metastatic cell line. For the two pancreatic cell lines, AsPC-1 is a metastatic pancreatic ductal adenocarcinoma line and showed a higher IC_{50} value than PANC-1, a primary PDAC line, indicating a varying level of efficacy of the drug. While all IC_{50} values were found to be under 10μM, which is

promising in terms of its potential mechanism of action in a therapeutic context, this data indicates that the efficacy of this compound may be further dependent on tissue type and is a factor kept under consideration while completing the assays (Figure 11).

The MTS proliferation assay was conducted in order to evaluate cellular proliferation and the impact of the compound, with a regular time point of every 24 hours, over a period of 96 hours. Each cell line was standardized in the cell number and treated with 5 and 10μM of IACS-13743, which falls both above and below the ranges of the IC$_{50}$ values in the screened cell lines. This was done to both to validate whether the IC$_{50}$ value that was evaluated was within range and accurately collected, and also to have a more comprehensive assessment of the timeline through which there is impact of the compound.

As shown in the subsequent figures, most of the cell lines began indicating significant impact to proliferation between 24 and 48 hours after administration of the compound. The 10μM dose of the compound induced a significant decrease in proliferation in all cell lines beginning at 48 hours of treatment, while a few of the cell lines began yielding differences at 24 hours (Figure 12). This is consistent with their dose-response data; for the cell lines with lower IC$_{50}$ values, their proliferation is impacted at earlier time points and the cells undergo apoptosis sooner due to the sensistivity to the compound. In our data, this is shown in two of our cell lines, indicating that lower doses may be needed to more accurately determine the timeline of impact. However, the majority of the cell lines saw impact after 48 hours of treatment administration.

Coupled with the experimental IC_{50} data, 48 hours post-treatment was thereby confirmed as the time point for further *in vitro* experiments. The results of this proliferation experiment also confirm that the compound IACS-13743 is indeed effective against tumor cells from multiple tissue types with higher levels of miR-10b expression at concentrations that are promising for therapeutic purposes. Moreover, there is a temporal component that needs to be taken into consideration – it is not an immediate acting agent, and requires approximately two days to induce tumor cell death. This effect is also persistent, and the cell counts do not appear to recover given our data up to 96 hours, with the higher dose.
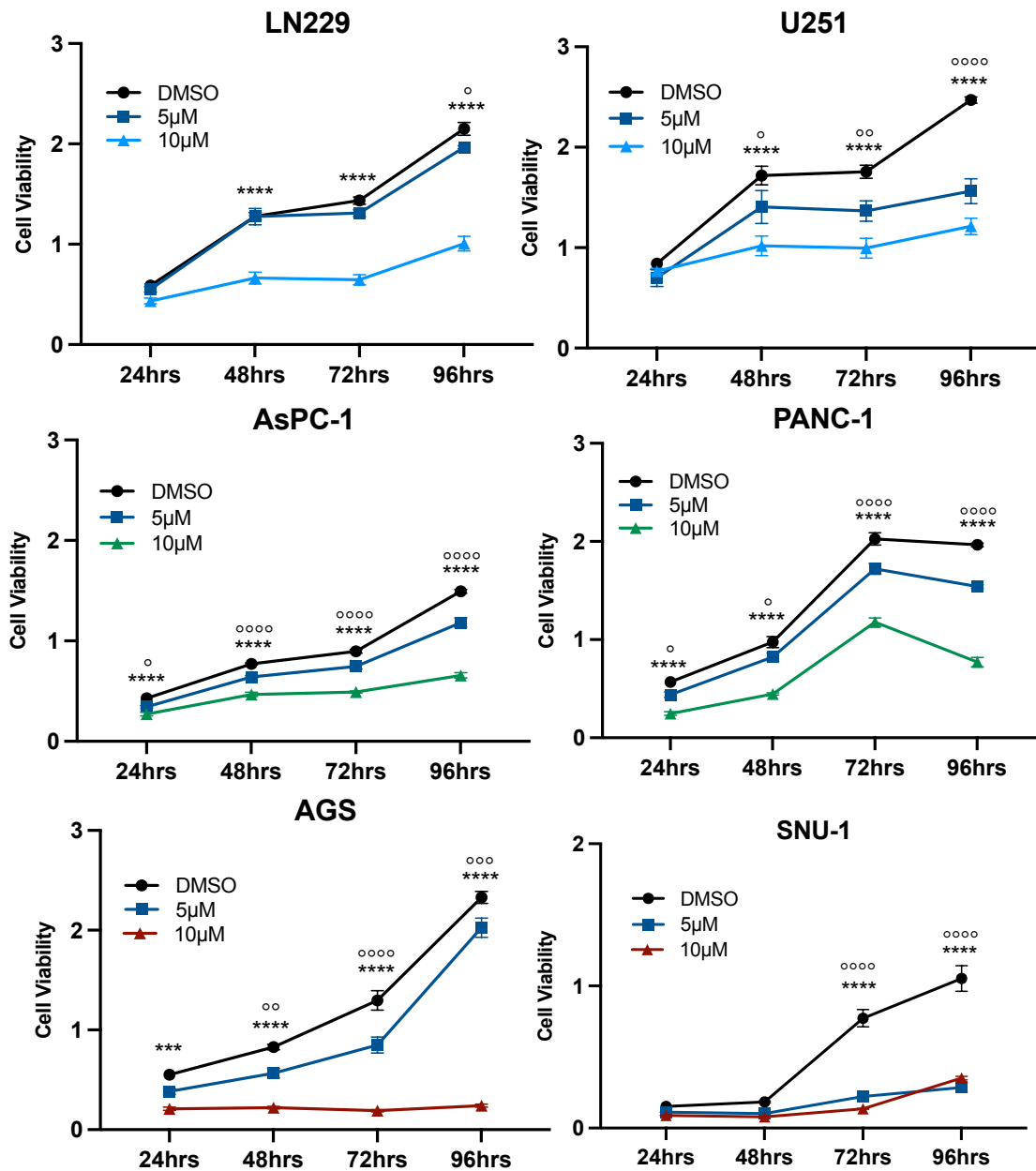
Figure 12. Proliferation assay conducted on six cell lines, treated with control, 5μM or 10μM of IACS-13743. Symbols signify the group compared to the DMSO control, with ° representing DMSO vs. 5μM and * representing DMSO vs. 10μM. One symbol indicates $p < 0.05$, two indicate $p < 0.01$, three indicate $p < 0.001$ and four indicate $p < 0.0001$.

For a more qualitative assessment of the effect of the compound on the two brain cancer cell lines, the morphology of the cells was evaluated for LN229 and U251, shown in Figure 13. Equal amounts of cells were plated in 6 well plates and were allowed to reach 70-80% confluence. At this point, the compound was administered at 10μM, and images were taken using a standard microscope at both 24 hours and 48 hours after treatment.

Our previous *in vitro* experiments had indicated that the effect of the compound became more potent at the 48-hour time point. As shown in the images, at 24 hours after treatment, the cells appeared unaffected and still remained attached to the well and relatively confluent. At that time point, there were no visible indications of the impact from the compound as of yet. By 48 hours after treatment however, qualitatively many of the cells were floating within the wells, indicating they had undergone apoptosis, and as shown in the image, much less amounts remained adherent to the floor of the wells and the morphology had changed to more circular than tubular, the latter of which is characteristic of these two brain cancer cell lines, indicating the cells had been impacted.

LN229

24 hours

48 hours

DMSO   IACS-13743

U251

24 hours

48 hours
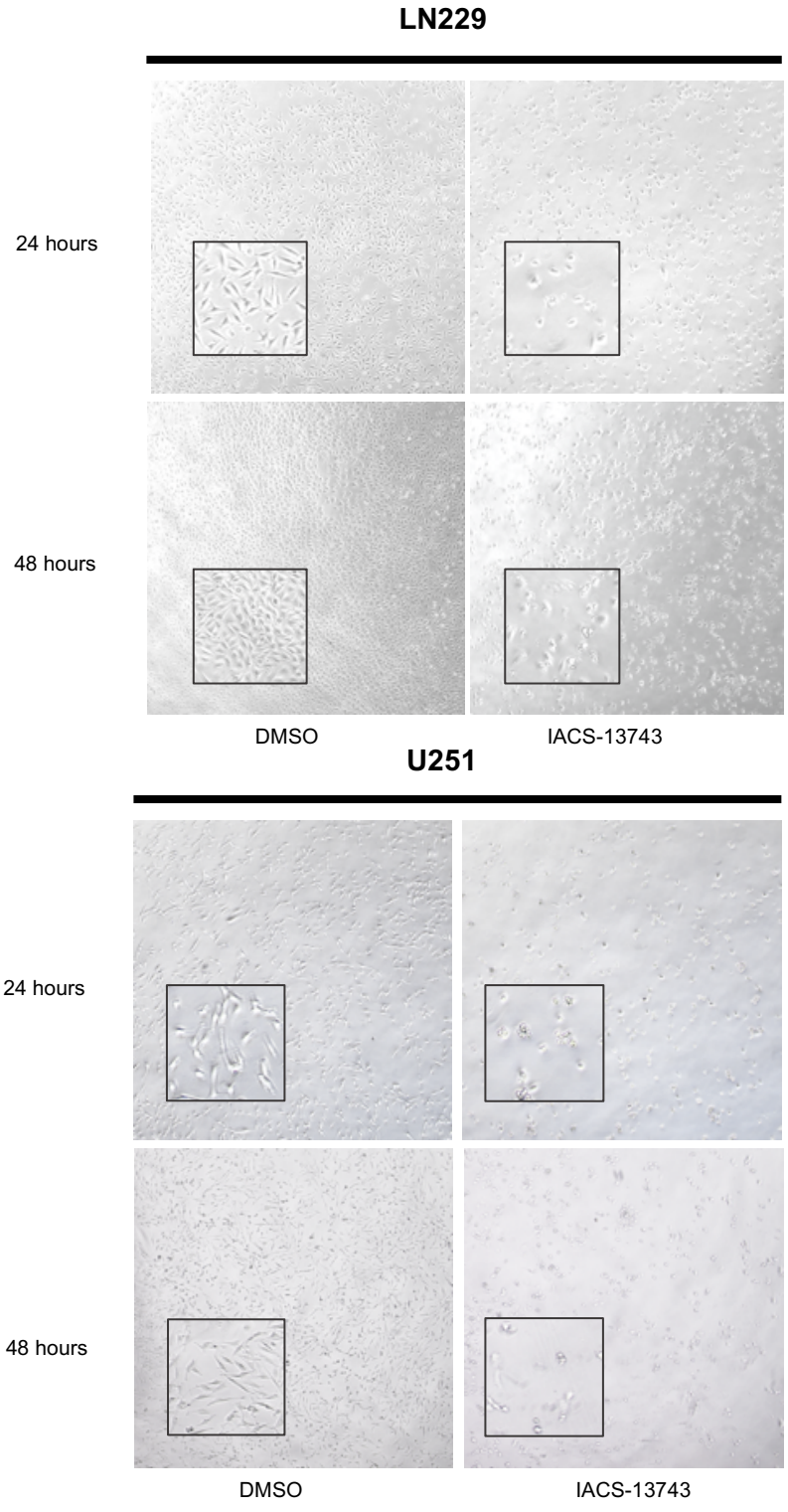
DMSO   IACS-13743

Figure 13: Cellular morphology of the brain cancer cell lines at control and 10μM of IACS-13743 over 24 and 48 hours. Images taken at 20X magnification.

The inhibition of miR-10b expression by IACS-13743 was evaluated via quantitative real-time polymerase chain reaction or qRT-PCR. It is presented as the fold change normalized to internal control U6 in the U251 brain cancer cell line. It indicates a significant downregulation of the expression of the miRNA after treatment with the compound (Figure 14A). To test the compound specificity for miR-10b and to ensure that it does not specifically target other miRNAs, qRT-PCR was conducted to test the compound against a miRNA with a very similar nucleotide sequence to assess whether it also binds and impacts expression level. The miRNA miR-10a is the other member of the miR-10 family and its sequence differs from miR-10b by only one nucleotide. In theory, given the sequence similarity, if the IACS-13743 compound is not very specific, it should also target this miRNA similarly and downregulate its expression. However, when evaluating both miRNAs with their respective control groups, it was found that the compound significantly targeted miR-10b expression level and not miR-10a, solidifying the hypothesis that IACS-13743 specifically targets oncogenic miR-10b (Figure 14B)
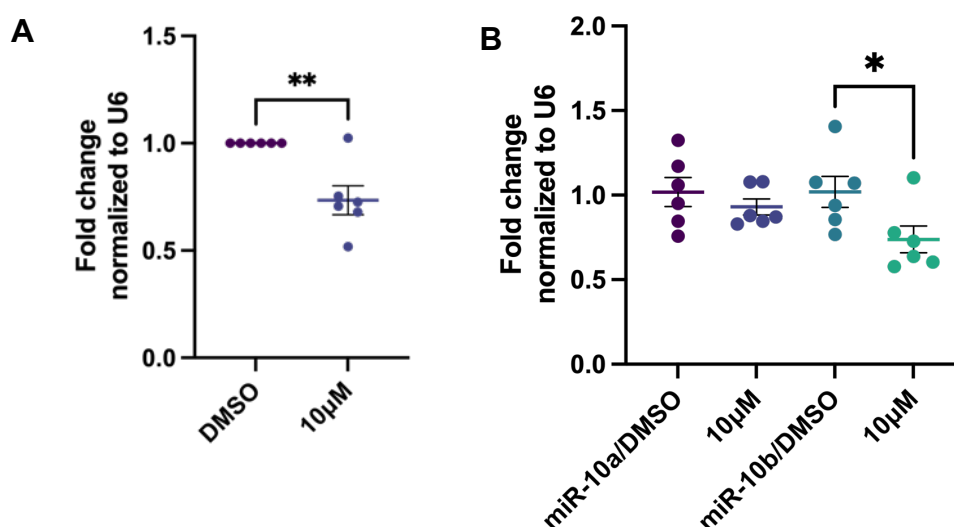
Figure 14. A. qRT-PCR evaluating miR-10b expression in U251 with and without treatment with IACS-13743. B. qRT-PCR evaluating expression of miR-10a and miR-10b

A clonogenic assay was conducted to investigate the formation of colonies after treatment with IACS-13743; data is shown for the U251 brain cancer cell line, the cell line with the highest expression level of miR-10b in the study. As shown in Figure 15A, there is a clear decrease in the growth and proliferation of the cancer cells in a dose-dependent manner, beginning at 1μM up to 5μM, where no colonies are detected, clearly demonstrating the impact of the compound.

Next, the degree of apoptosis was assessed via flow cytometry, using the Annexin V/PI FITC model. As shown in Figure 15A, it was found that at 5μM, there was a clear increase of approximately 4.5 times in total apoptotic cells, as compared to the control group in the U251 brain cancer cell line. In this analysis, total apoptotic cells are defined as the sum of the early apoptotic and late apoptotic cells. Necrosis, or accidental cell death, was not accounted for in this value, as apoptosis and necrosis ultimately indicate different cell death mechanisms[82]. When evaluated at a dose level of 10μM, the cell amounts were approximately the same in this cell line, indicating that the rate of apoptosis plateaus after a certain threshold is met (Figure 15C, left). In order to investigate whether this effect was tissue specific, this analysis was also conducted in the AGS cell line, which has a lower IC_{50} value using the compound of interest than U251 (3.722μM to 7.686μM). It was found that while there was a significant increase in apoptotic cells at 5μM compared to control, the sharp increase occurred by 10μM, with nearly 60% of cells found to have undergone apoptosis (Figure 15C, right). This confirms that this gastric cell line is more sensitive to the compound, as shown by its IC_{50} value. It remains to be shown to what degree this is a tissue specific effect.

Lastly, cell cycle analysis via flow cytometry was conducted. In the U251 brain cancer cell line, while other cellular checkpoints remained approximately the same, a significant increase was shown at the G2/M phase, indicating cell cycle arrest. Cell cycle arrest at this stage is an indicator of potential induction of apoptosis, which is found to be consistent with the ongoing *in vitro* results (Figure 15D).
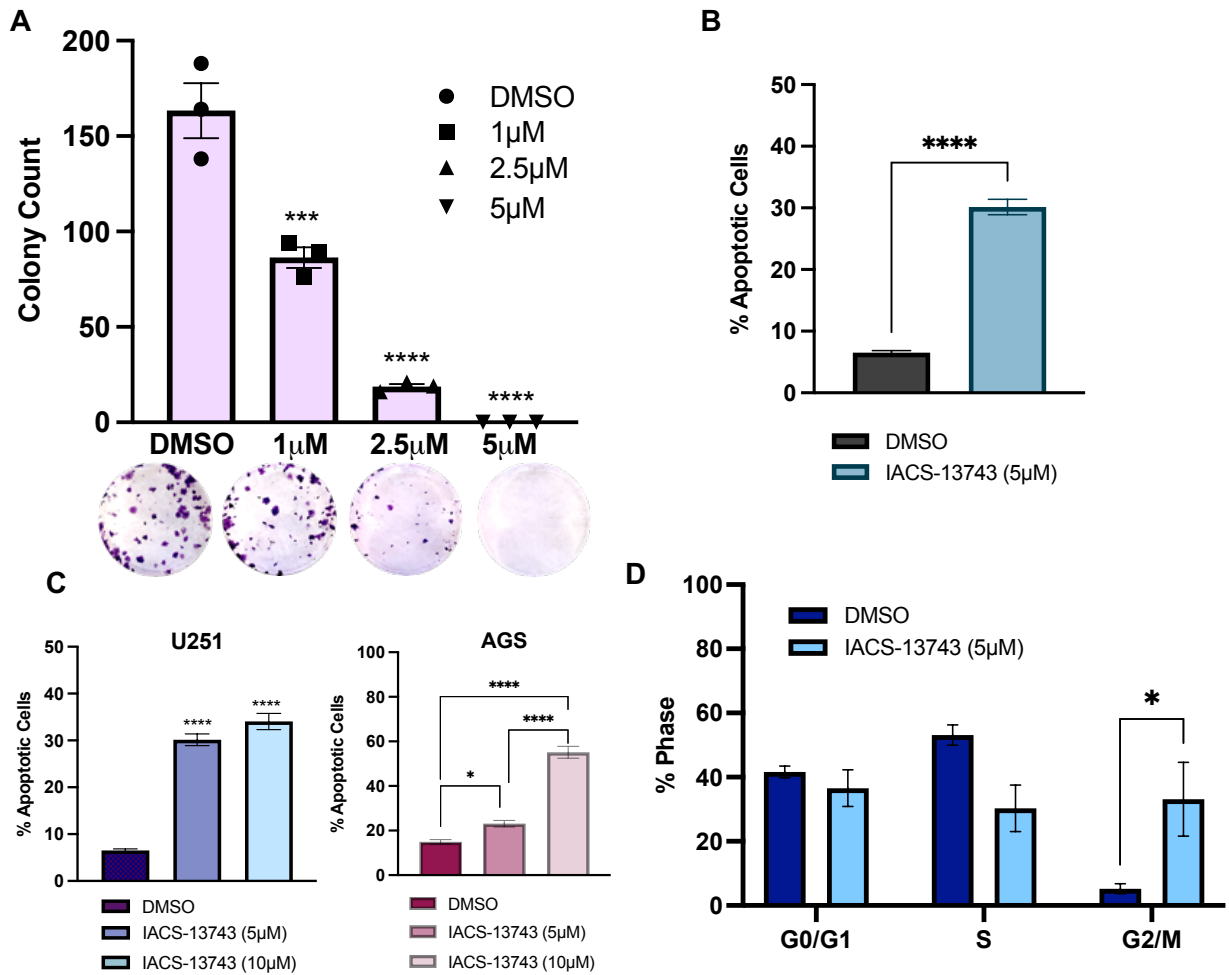
Figure 15. Panel of *in vitro* experiments.
A. Clonogenic assay in the U251 brain cancer cell line indicating significant decrease in colony formation in a dose-dependent manner.
B. Apoptotic assay done via Annexin V/PI FITC flow cytometry analysis indicating a 4.5x change in early and late apoptotic cells after treatment with 5µM of IACS-13743
C. Comparison of degree of apoptosis at two doses between U251 brain cancer and AGS gastric cell line.
D. Cell cycle analysis done via flow cytometry indicating cell cycle arrest at the G2/M phase. For all figures, * represents $p < 0.05$, ** indicates $p < 0.01$, *** indicates $p < 0.001$ and **** indicates $p < 0.0001$.

IACS-13743 directly binds to the precursor transcript of miR-10b. Ligand and target detected NMR experiments were used to assess whether IACS-13743 directly binds the apical loop structure common to both the primary-and precursor miR-10b transcripts (Figure 16). This apical loop region is critical for key enzymatic processing steps of the miRNA biogenesis pathway including nuclear processing by Drosha (primary) and cytoplasmic processing by Dicer cleavage (precursor). Identifying compounds that bind this apical loop region may provide dual inhibition of both enzymatic steps, thereby reducing the overexpression of mature miR-10b. To detect direct binding, the ligand detected 1D-1H line broadening approach was used to confirm a direct interaction with the RNA (Figure 16)[68, 83]. In this experiment, the free ligand is held at a constant 100μM concentration, then slowly titrated with the target RNA. The height of the ligand chemical shift resonance signals are measured at each titration point and the decrease in ligand signal upon addition of RNA target is proportional to the affinity (K_D) and size of the RNA target.[68, 83] This approach detects a wide dynamic range of binding affinities between low nM to mid mM K_D.[68] Non-binding compounds show no change in chemical shift or peak height; therefore, this approach can be used in a binary fashion to confirm binding. For IACS-13743, a large decrease in peak signal was found (Figure 16A) between the free (black) and bound ligand samples, particularly the methyl protons (starred) which is indicative of direct binding of the two components.

To confirm the direct binding using ligand detected NMR methods, target detect NMR methods, which monitor changes of the RNA upon titration of the ligand using the 2D ^{1}H-^{1}H TOCSY NMR experiment, were also conducted (Figure 16B). In

this experiment, 50μM of pre-miR-10b sequence was titrated with 100μM of IACS-13743. After resonance assignment of the pre-miR-10b apical loop, a binding site for IACS-13743 was able to be identified. This approach has been used in previous work to map binding sites of small molecules and macrocyclic ligands.[83-85] The pyrimidines which showed the largest chemical shift in the 2D-1H-1H TOCSY experiment were identified as follows: (U6, U7, U8, U26, C27, C29 and U33). There were also weaker shifts noted in the remaining dsRNA stem region, however, no chemical shift change was seen in the upper loop region (C18, C19, U21, or U23). From these NMR results, the binding site location of IACS-13743 can be approximated onto the pre-miR-10b structure (Figure 16C). Here, the chemical shift changes are mapped on to the NMR derived secondary structure and a 3D model of pre-miR-10b is generated. The 3D model of pre-miR10b was created using the NMR derived secondary structure and proton chemical shifts as structure restraints for the FARFAR2 method.[86] Identifying compounds that bind in this region, the junction between the apical loop and apical stem, may be particularly interesting as this region correlates to the Dicer cleavage site of pre-miR-10b (5' Dicer cut site U12, 3' Dicer cut site C27). These data strongly support that IACS-13743 directly binds to the hairpin structure of precursor miR-10b. In addition, this finding allows for more precise approximation of how and where the molecule is specifically binding, and will provide valuable insight into further modifications of this molecule if a tertiary compound library is pursued, or for novel compounds during development for therapeutic purposes.
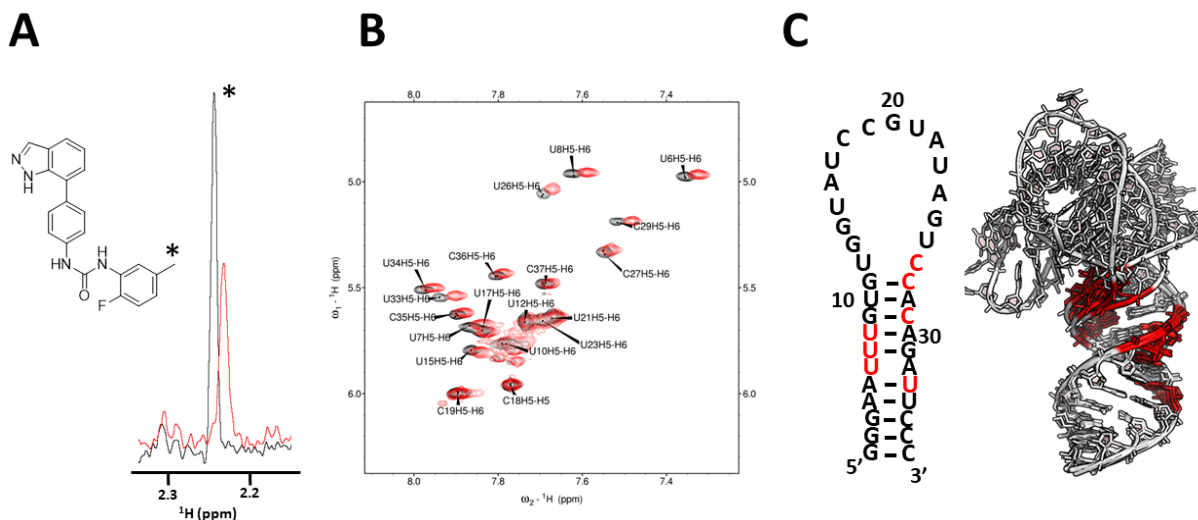
Figure 16. Confirmation of direct interaction between IACS-13743 and miR-10b using NMR: A.) Methyl protons (starred) of IACS-13743 resonate at a chemical shift of 2.23ppm. Ligand detect, line broadening experiments show significant line broadening upon addition of pre-miR-10b. Here, the free ligand was maintained at constant at 100mM (black). To measure a binding event, 10mM of pre-miR-10b sequence was added to the free ligand sample (red) and data were collected identically. The decrease in peak signal is indicative of direct binding interaction B.) To confirm binding and identify the ligand binding site on the RNA, we conducted a target detect NMR experiment which monitors changes in chemical shift of pyrimidine H5-H6 protons; 2D TOCSY. The free 50uM of pre-miR10b sequence (black) was titrated with 100uM IACS-13743 (red). Overlaying the two NMR spectra show which pyrimidine residues are most likely near the ligand. C.) The pyrimidine peaks that show largest chemical shift change are mapped onto the NMR derived secondary structure of miR-10b with bases perturbed in the presence of IACS-13743, colored in red. A model of the pre-miR-10b 3D-structure was generated with FARFAR2 and the results from B also mapped on to this structure. Given many of the largest chemical shift changes occur in a localized region near the Dicer cleave site, suggests this compound could inhibit processing of pre-miR10b.

The same direct binding experiments were conducted in the parent compound linifanib for comparison and to identify whether the same effects were seen as those in IACS-13743. Due to the insolubility of the molecule, however, direct binding of the target RNA and linifanib were unable to be confirmed. As shown in Figure 17, there is no decrease in peak signal, as in the one shown in IACS-13743 and there is no line broadening portrayed in the spectra, indicating that it cannot be concluded either way that linifanib directly binds miR-10b, as it can be for IACS-13743. (Figure 17). This is encouraging data, as since linifanib advanced to clinical trials, it possesses the capability to be therapeutically used in humans. With further testing of IACS-13743, and with this data on the direct binding, this increases its potential to be used in a clinical setting in indications that have miR-10b overexpression.
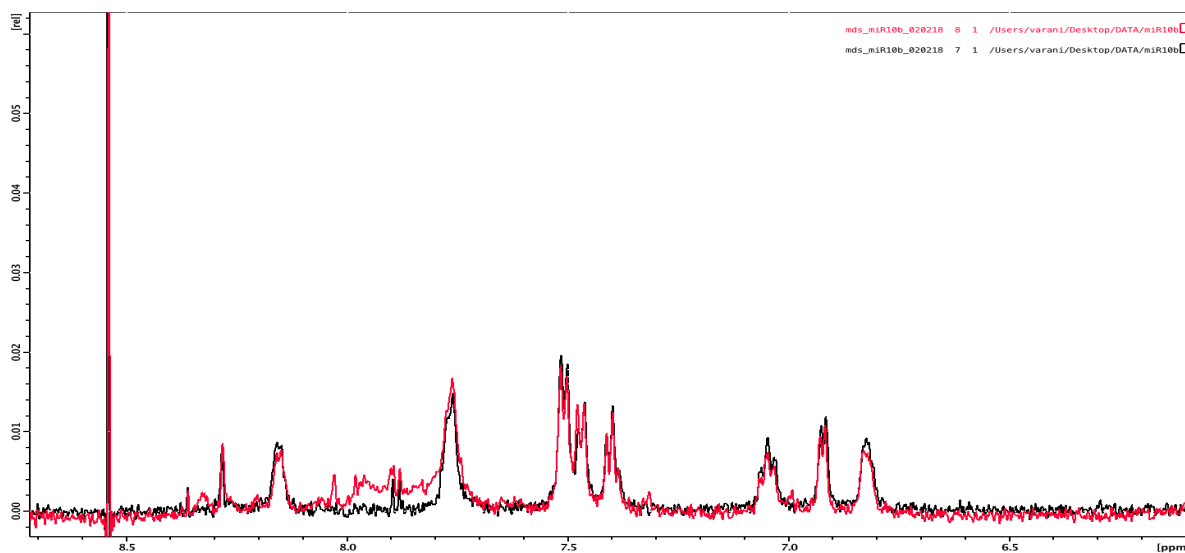
Figure 17. Direct binding experiment for linifanib via NMR. No line broadening detected and there was no decrease in peak signal, as found in the derivative compound, indicating that direct binding could not be confirmed

IACS-13743 functions via miR-10b and the kinase pathway. To confirm that the mechanism of IACS-13743 operates via the miR-10b pathway and not via the target kinases, an in-house kinase assay was conducted to measure the enzymatic activity of the compound as it compares to the parent compound linifanib. The ADPGlo Kinase Assay was used for this experiment, which is an established and highly sensitive biochemical approach[87] to kinase screening and profiling of molecular agonists and antagonists. The kinase of interest for this experiment was PDGFRβ, which is one of the primary targets of the parent compound linifanib, the other being VEGF. The IC_{50} value of the novel compound and parent compound was sought as they relate to this kinase; IC_{50} in this context is a measure of chemical potency and differs from the IC_{50} values derived from cellular *in vitro* studies, as this is a biochemical assay comparing the activity of the inhibitors, with no consideration of cell or cancer type. According to the literature, linifanib has a biochemical IC_{50} of approximately 66nM in PDGFRβ cell-free kinase assays, which shows a high degree of efficacy through that kinase pathway[88]. The expectation for this assay is that IACS-13743 would have a greater IC_{50} than that of linifanib, because it would provide evidence that the effects that are seen are not through the interaction with the kinases or going through a kinase pathway, but that it is also operating through the direct binding and inhibition of the oncogenic miRNA. Therefore, it would have less affinity to the kinases and would require a larger amount to yield efficacy. The experimental results generated in the laboratory have supported this effect, as detected by a luminometer and reported via relative luminescence units (RLU). An IC_{50} of 251.9nM for IACS-13743 and 81.74nM for linifanib is reported against the kinase PDGFβ.

As this was a preliminary evaluation of one specific kinase done in-house, it requires external validation by an established institution with biochemical expertise and preferably a host of kinases can be evaluated in kind. In a preliminary result from collaborators at IACS, a panel of kinases that linifanib is known to act through was evaluated. It was found that while IACS-13743 had low nanomolar activity towards the same kinases, indicating that there is activity upon these kinases, the values were all higher than the activity of linifanib. This indicates that it requires more of the small molecule compound to be active towards these kinases, and since we were able to detect direct binding towards miR-10b, it provides evidence for a potential dual mechanism, wherein it is mechanistically operating on both pathways. This could be beneficial from a therapeutic standpoint, as simply stated, if there is treatment resistance via one oncogenic mechanism, the compound could work through the other.

Aim 2: To validate findings in cerebral organoid studies

Cerebral organoids are a model of brain cancer growth. The brain cancer cell lines U251 and LN229 were evaluated in a model of cerebral organoids, derived from human induced pluripotent stem cells (iPSCs). The brain was chosen to be modeled out of the three cancer types in this study, as within The Cancer Genome Atlas (TCGA)[89] it was shown that the brain had the greatest upregulation of miR-10b in cancer between normal and glioblastoma multiforme cohorts as compared to the normal and tumor cohorts found in pancreas and stomach (Figure 18A).

To determine this expression level difference of miR-10b among normal and tumor tissues of these three different cancer types, a Shapiro-Wilk test was first employed to determine whether or not the data followed a normal distribution. It verified that the available data did not follow a normal distribution, thus the non-parametric Mann–Whitney test was applied to assess the relationship between mRNA expression and tissue type in the data from the TCGA.   A point plot along with color key was used to display fold changes and p-values for the comparisons performed (Figure 18A). A box-and-whisker plot, with the box representing first (lower bound) and third (upper bound) quartiles, and the whiskers representing 1.5 times the interquartile range, was used to visualize the distribution of the miRNA data that was available for the glioblastoma cohort, as compared to the data available for the normal brain tissue (Figure 18B). All tests were two-sided and considered statistically significant at the 0.05 level. As shown, it was found that between brain, pancreas and

stomach, the expression of miR-10b was clearly significantly upregulated as compared to normal only in the context of brain cancer (Figure 18A).

As glioblastoma multiforme was the first cancer type for which data was collected in the The Cancer Genome Atlas (TCGA), the majority of available samples have been analyzed and encoded via the Agilent microarray technology, as opposed to the newer miRNAseq techniques that were employed for the stomach and pancreas tissues and the more innovative manner that the datasets have been processed through. While the sample sizes are shown to be unbalanced, this effect provides a trending direction through which the levels of this microRNA can be assessed in multiple tissue types and can be further investigated in alternate models. In addition, the brain cancer cell lines have consistent expression of miR-10b within the panel of cell lines and represent a potential robust model to first test the efficacy in IACS-3743 in organoids.
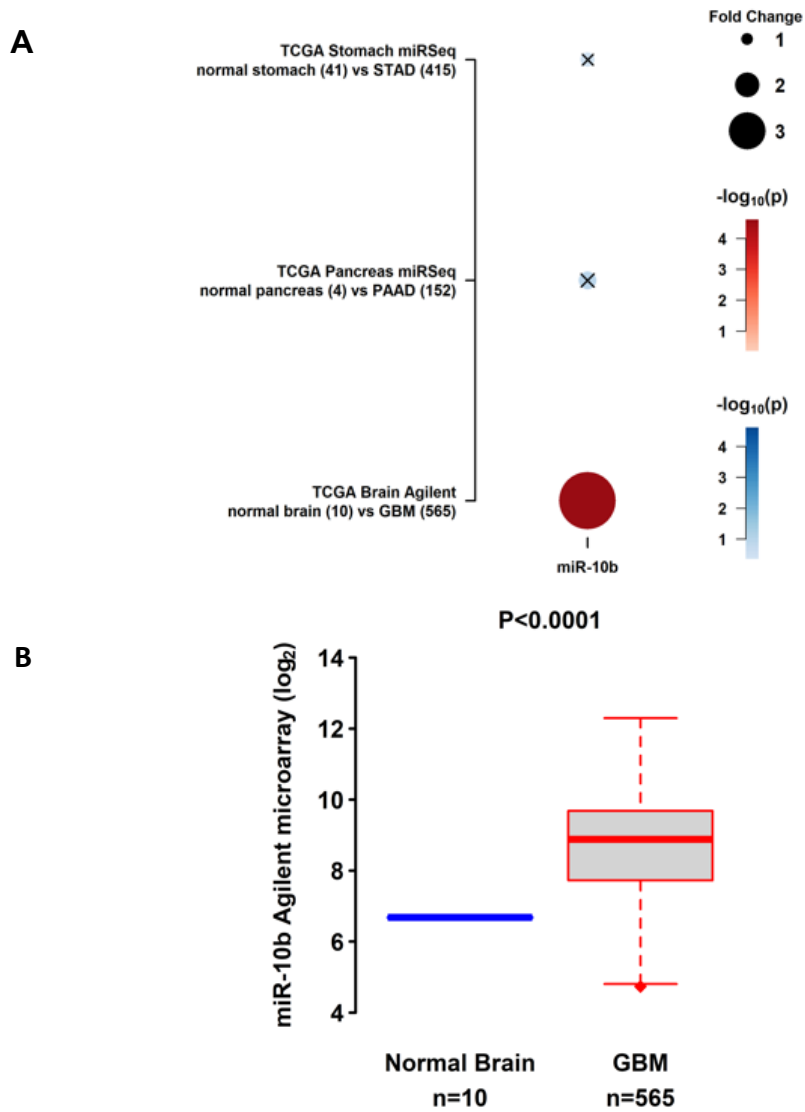
Figure 18. miR-10b expression in The Cancer Genome Atlas (TCGA). A. Comparison between normal and tumor cohorts in expression of miR-10b in three cancer types of interest. B. miR-10b expression in normal vs tumor cohorts in glioblastoma multiforme.

Cerebral organoids are an innovative method in cancer research to study the expression of cancer stem cells and cell lines in conjunction with drug development and therapeutics approaches with novel compounds (Figure 19). It is becoming more common in biomedical science to introduce models that are derived from patient cells to mimic the human tumor microenvironment, and more directly test the effects of therapeutics and develop more personalized intervention methods. Cerebral organoids, as previously mentioned, are unique in that they are often developed from patient-derived cells, and can also serve as a robust model to further study brain malignancies on the pathway from *in vitro* and *in vivo* to the clinic.

In this work, this innovative cerebral model was used to answer three main questions. The first objective was to determine whether a stable model could be developed using these iPSC-derived cerebral organoids in culture with brain cancer cell lines with significant levels of miR-10b expression; previously, only glioma stem cells have been stably and successfully co-cultured within this particular model. The second objective was to establish and validate the upregulation of miR-10b that has been established in the literature in a brain tumor context in this cerebral model. Third, to determine whether this compound is able to decrease the expression levels of the oncogenic miRNA in this model.
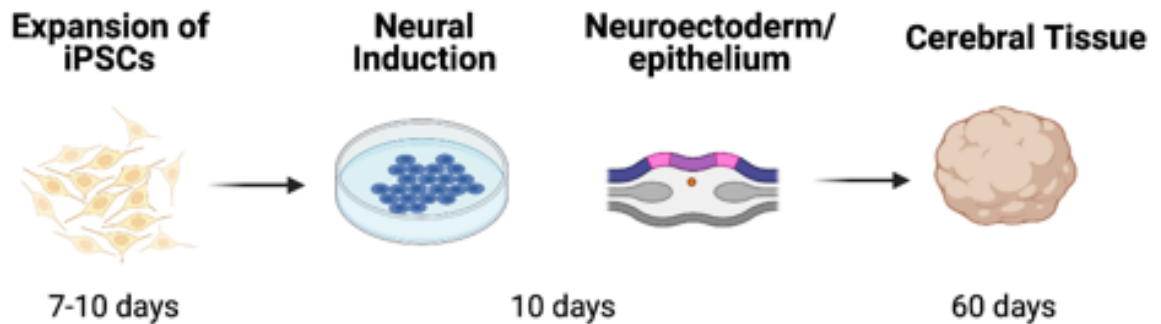
Figure 19. Diagram of the process used to generate the iPSC-derived cerebral organoids.

To address these questions sequentially, control organoids with no tumor involvement that had reached steady state of growth were initially analyzed via qRT-PCR, to obtain a baseline level of miR-10b expression. The expectation would be that the levels of expression are low to undetectable, per the past research that has been conducted wherein expression of this miRNA is not found to be high in normal, non-cancerous brain tissue[13, 18-20]. Given that all major cell types are meant to be represented[51], the idea would be that the organoids are modeling what occurs endogenously in human brain development. Prior to co-culturing, both cancer cell lines were individually tagged with RFP, in order to fluoresce under the microscope and to detect where the cells would be end up. After tagging, cell lines were expanded to increase the number of cells, and then sorted twice via flow cytometry, to ensure that all cells would be RFP-positive when placed in with the organoids. The organoids were then co-cultured individually, with either brain cancer cell line LN229 or U251. Shown in Figure 20A are the co-cultured organoids shown under the fluorescent

microscope at approximately 48 hours and 2 weeks post co-culture. All tumorigenic cells were tagged with red fluorescent protein (RFP) and are easily seen at 48 hours, as at that point they were still on the surface of the organoid and had not yet invaded into the tissue microenvironment. Over the course of one to two weeks, as migration and proliferation occurred throughout the tissue, what can be seen is enhanced bright red areas within and throughout the organoid, but not isolated and circumscribed foci as before. The signal is more diffuse and the cells appear to have aggregated as they moved throughout the organoid. This indicates that the cells had migrated inwards and had begun proliferating, showing that the brain cancer cells were successfully co-cultured in the organoids. Expression of the miRNA was then measured via qRT-PCR and the effect was confirmed as shown by the data showing a significant increase in miR-10b expression in the co-cultured organoids with LN229 and a trending increase with U251 (Figure 20B).
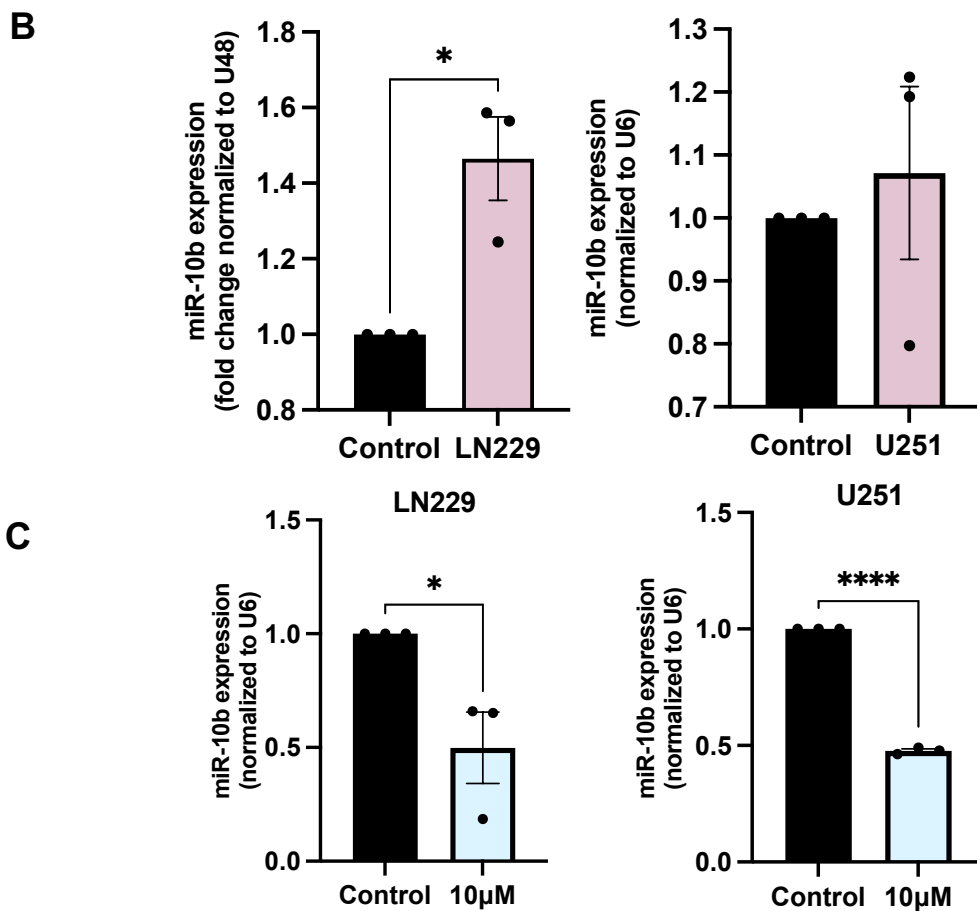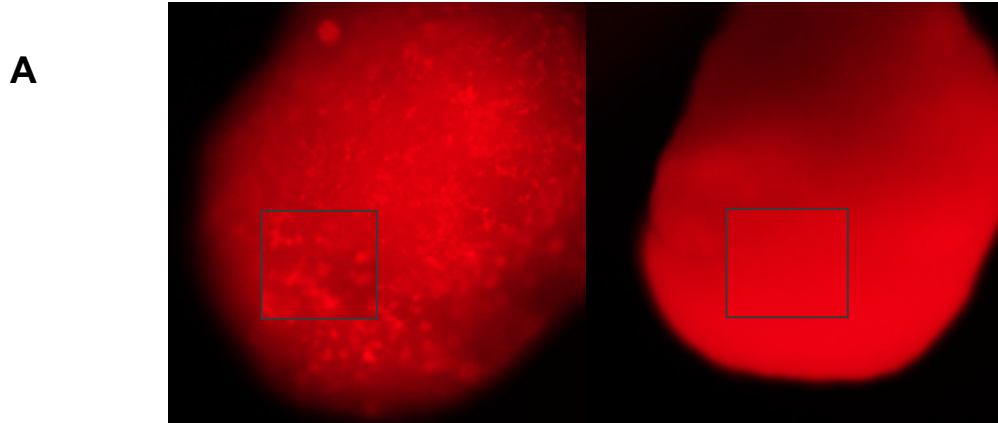
Figure 20: Cerebral organoid studies. A. (left) Cerebral organoid co-cultured with LN229 brain cancer cell line. (right) Cerebral organoid shown at 2 weeks post-co-culture. B. qRT-PCR confirming significant upregulation of miR-10b in the LN229 brain cancer co-cultured cerebral organoid model and a trending upregulation in the U251 brain cancer cell line model. C. miR-10b expression levels in cerebral organoids after treatment with IACS-13743. Both cell lines showed significant downregulation of expression.

Importantly, up until this point, these iPSC-derived cerebral organoids have only been successfully co-cultured with glioma stem cells (GSCs), which are cells that possess the capability of differentiation and self-renewal, characteristic of cancer stem cells and are thought to be more resistant to therapy[90]. They differ from traditional cancer cell lines in how they are maintained and grown for these reasons. In this work, two established brain cancer cell lines were used, which were conditioned over time with specialized neural-based media and nutrients that are compatible with the growth of the organoid, and the study was able to prove increased expression of this oncogenic biomarker.

To further confirm that IACS-13743 yields an impact in this more advanced *in vitro* model, the co-cultured organoids were treated with varying doses of the compound and levels were evaluated using qRT-PCR. Significant downregulation of miR-10b with 10μM of treatment with the compound after 48 hours was detected in both brain cancer cell lines (Figure 20C). This supports the *in vitro* data well wherein at 5μM there was not a detectable change in expression, whereas after the IC$_{50}$ amount for LN229 (7.395μM) and for U251 (7.686μM), there was a significant decrease in the expression of miR-10b. An *in-situ* hybridization experiment was conducted to qualitatively confirm the effect of this compound treatment on miR-10b expression at the two doses in the two cell lines, with U6 serving as the positive control and scramble miRNA as the negative control. Control in this context represents cerebral organoids that have no tumor cells, whereas the DMSO group represents vehicle treatment. Qualitatively, miR-10b is clearly expressed in the tumor co-cultured organoids as compared to the control organoids. (Figure 20). This

confirms that the compound has the potential to work in more models than just biochemical and *in vitro*, and can potentially be used downstream in higher order models.

	Control	LN229			U251		
		DMSO	5µM	10µM	DMSO	5µM	10µM
miR-10b							
U6							
Scramble							
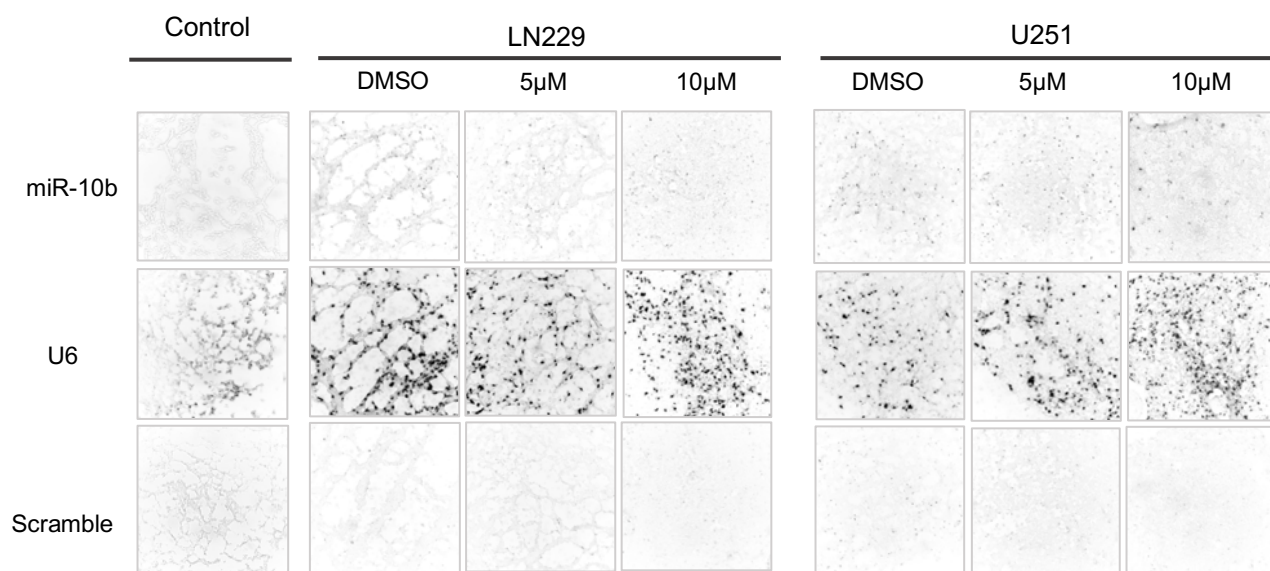
Figure 20. Representative *in situ* hybridization images of U251 and LN229 cerebral organoid model with IACS-13743 compound treatment, with U6 serving as positive control and scramble miRNA as negative control.

Aim 3: To identify oncogenic pathways implicated in the effects of IACS-13743

Targets of miR-10b and the mechanism of action of IACS-13743. When evaluating the impact of oncogenic miRNAs, the traditional approach is looking at the proposed targets of the overexpressed miRNA. In the initial hypotheses into this project, datasets of predicted and validated targets of miR-10b were investigated to determine potential molecular targets to provide potential insight into the mechanism of action of this microRNA. Using publicly available datasets, namely target prediction and validation software in conjunction with comprehensive databases such as Oncomine[91] and TCGA[89], a series of experimentally validated targets were proposed using the sequence of miR-10b, by complementarily matching them with the sequences of potential targets. When a miRNA interacts with mRNA, it binds the complementary nucleotide sequence, which is called a "canonical" interaction. Non-canonical interactions are when miRNA sequences are similar enough to still bind the mRNA, but function via other cellular processes and normal mRNA levels and functionality are not affected.

Using the dataset of experimentally validated targets derived from TargetScan, which lists sequences collects references of studies that experimentally test the relationships between microRNAs and genes, and cross-referencing them with Oncomine, a preliminary list of miR-10b targets were analyzed for the three cancer types. All available and complete datasets were analyzed, which included six datasets for malignant brain cancer, three datasets for pancreatic cancer, and two datasets for gastric cancer. The targets identified were filtered to only those with

experimental validation in the established miRNA datasets in miRPathDB[92], which was integrated from data with miRTarbase[93], TargetScan[94] and miRanda[95], other comprehensive miRNA datasets that include target information. Only one gene, PTEN, was shown to be common across the three cancer types (Figure 21). PTEN was an experimentally validated target of miR-10b that was shared between these three cancer types, which indicates a potentially more global mechanism of oncogenic progression and thus PTEN was proposed as an initial tumor suppressor gene of interest. This was the first indication of involvement from the PI3K/AKT pathway.
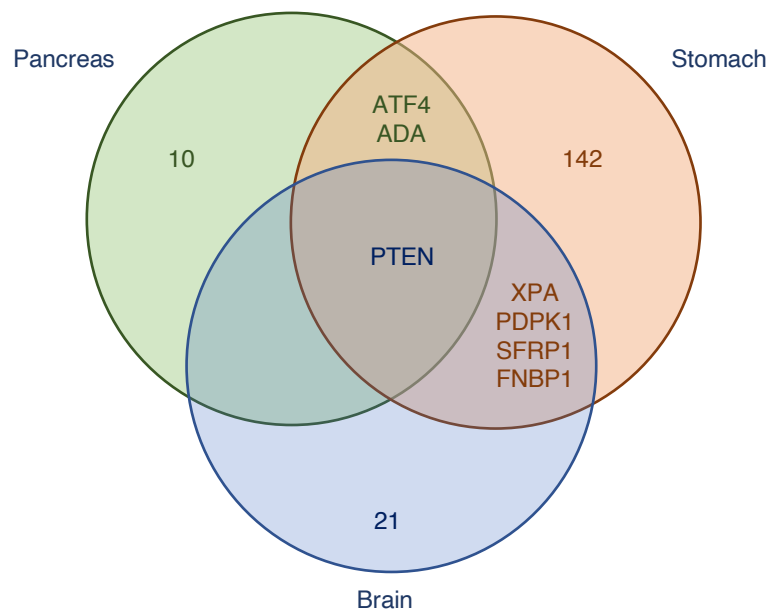
Figure 21: Venn diagram shown overlap of experimentally derived targets of miR-10b-5p from multiple datasets within Oncomine

Reverse Phase Protein Array (RPPA) analysis was conducted on a subset of the panel of cell lines, with one cell line per cancer type. RPPA is a high-throughput analysis evaluating the levels of a panel of antibodies on protein expression in control and intervention groups. In this context, control and IACS-13743 treated cell lines were submitted for analysis to evaluate the impacts of the compound at the protein level. The cell lines used were the U251 brain cancer cell line, AsPC-1 pancreatic cancer cell line, and the AGS gastric cell line. Control and treatment samples were done in triplicate and were stained for 486 unique antibodies, which were analyzed by Array-Pro Analyzer 6.3 then by SuperCurve_1.5.0 via SuperCurveGUI_2.1.1. The results from this analysis were first displayed volcano plots, to evaluate differentially expressed genes and the degree to which they differed via fold change (Figure 22).
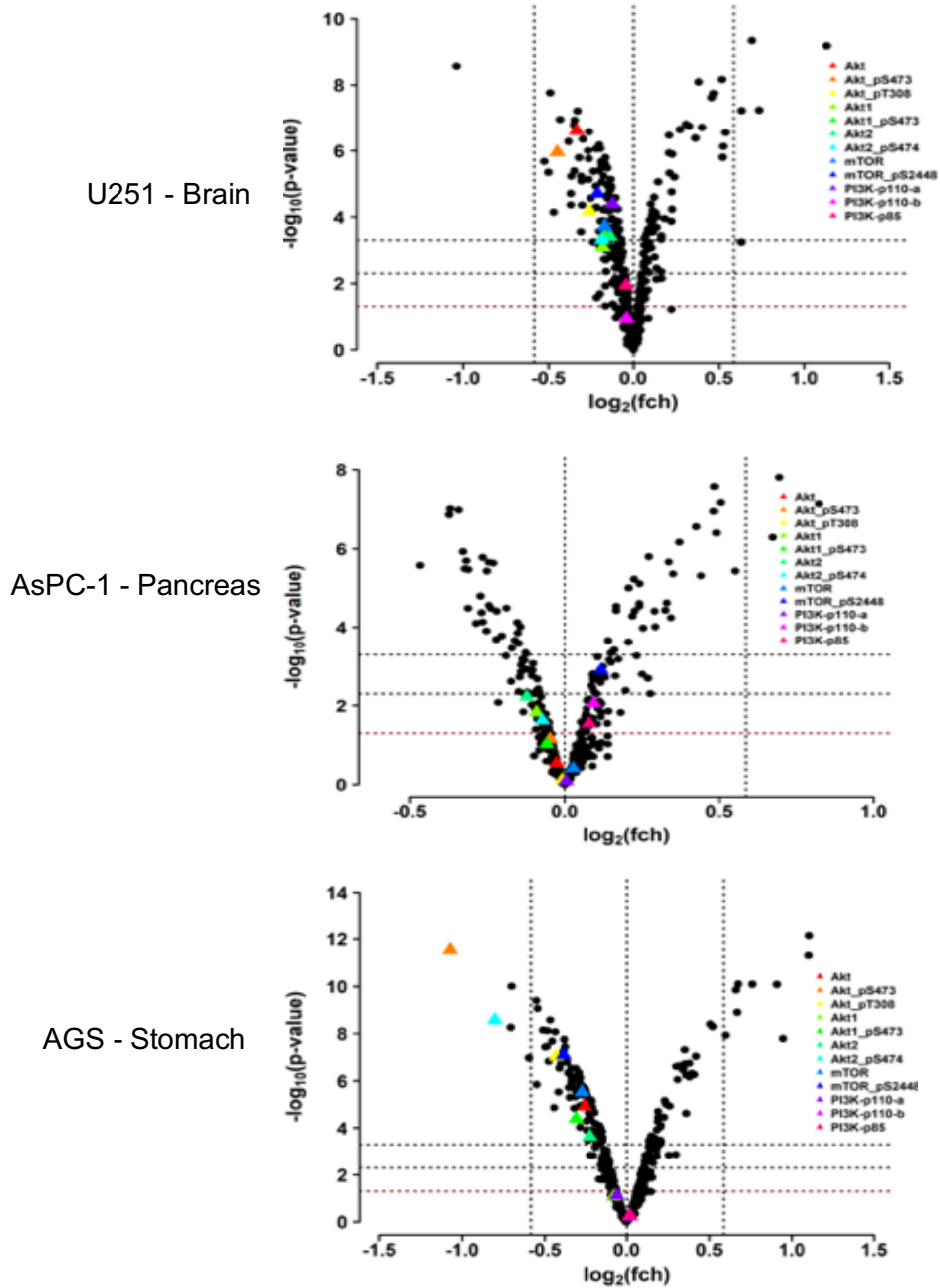
Figure 22. Volcano plots displaying proteomics data from Reverse Phase Protein Array (RPPA) for the U251 brain cancer cell line. Horizontal red line is statistical significance at –log10(.05), -log10(.005), -log10(.0005). Vertical lines indicate fold change: FCH=-1.5 and FCH=1.5, so +/-log2(1.5) = +/-0.58496.

Upon further analysis and ranking of the fold changes in the differentially expressed genes according to the adjusted p-value, many of the proteins on the PI3K/AKT pathway were significantly dysregulated in the tested cell lines (Figure 23); most notably, all of the relevant antibodies targeting proteins on this pathway were downregulated in the U251 brain cancer cell line, with ten of the twelve proteins showing significant downregulation at $p < 0.01$ (Figure 23A).

When evaluating the tumor types, AKT2 was the only protein found to be significantly downregulated in brain cancer, gastric cancer and pancreatic cancer, after treatment with IACS-13743, indicating a potential direction of further research. Differential expression was seen for almost all other proteins tested along this pathway among the three cancer types.
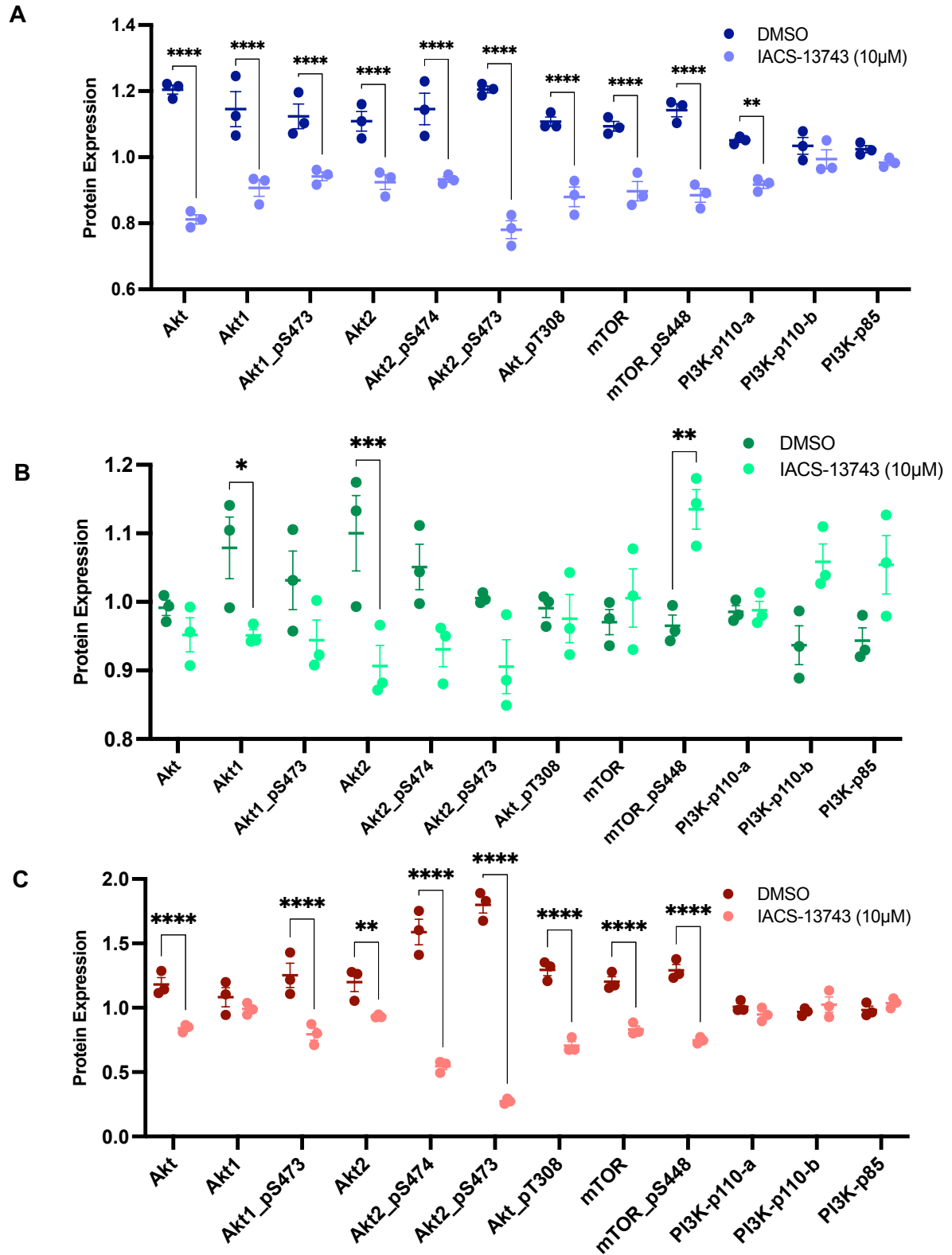
Figure 23. Proteins on the PI3K/AKT pathway and the degree of dysregulation according to cancer type. A. U251 brain cancer cell line. B. AsPC-1 pancreatic cancer cell line. C. AGS gastric cancer cell line. * indicates p < 0.05, ** indicates p < 0.01, *** indicates p < 0.001 and *** indicates p < 0.0001.

The PI3K/AKT pathway is known to be one of the most oncogenic, and operates in a complex and dynamic way. PI3K is upstream of AKT, which is upstream of mTOR, so intervention at any phase of this pathway will yield varying outcomes (Figure 24). Looking at the data, there is significant dysregulation seen at one of the phosphorylated forms of PI3K, which could yield all of the effects that are seen in this data downstream. Interestingly, with gastric cancer, none of the forms of PI3K are dysregulated and appear to not have been affected by the treatment, though impacts on AKT and mTOR are seen, so for this cancer type it is possible the effect is PI3K-independent and occurs further downstream on the pathway than that of brain cancer. With pancreatic cancer, there is a different relationship overall, as not only is there

not downregulation at the PI3K point, there is upregulation. A number of the AKT forms show downregulation, but there's no discernable relationship between the downregulation of AKT and the upregulation of mTOR, indicating that while this form of pancreatic cancer does yield dysregulation in this pathway, it may do so supplemented by another mechanism.
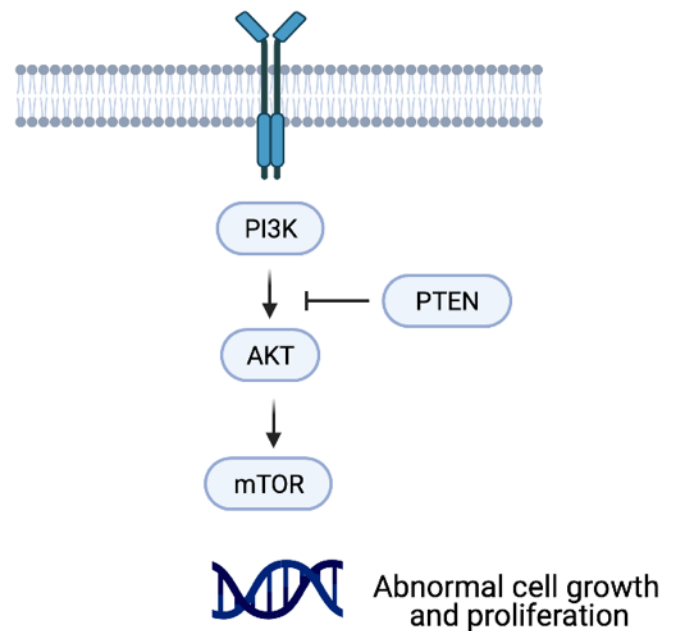
Figure 24: Schematic of PI3K/AKT pathway

As an additional interesting finding, the proteomics results found PTEN expressed differentially across the cancer types as a result of IACS-13743 (Figure 25). As it is an experimentally validated target of miR-10b, the expectation would be that when oncomiR-10b is overexpressed, it binds the tumor suppressor gene, causing it to be downregulated and impacting its regular function, leading to an oncogenic outcome. Administration of the therapeutic compound would then lead to increased binding to the overexpressed oncogenic miRNA of interest, leading to restored mechanism of action of the target gene, bringing back its function. However, this effect only appeared to be the case in the brain tumor cell lines that were tested (LN229 and U251). A significant increase was seen, providing evidence indicating that this compound had inhibited the oncogenic miRNA, restoring the function of the tumor suppressor gene and thereby supporting the PI3K/AKT pathway suppression data from the RPPA analysis. There are several reasons why this effect is not seen throughout the screened cell line panel, primarily that the pathway through which miR-10b and IACS-13743 interact through the AKT pathway could be PTEN-dependent in some cancer tissue types and not others, as in this study, in the gastric cancer cell line and in the pancreatic cancer cell line. This is supported through the literature where there are mechanisms linking miR-10b to AKT via other pathways[17, 27]
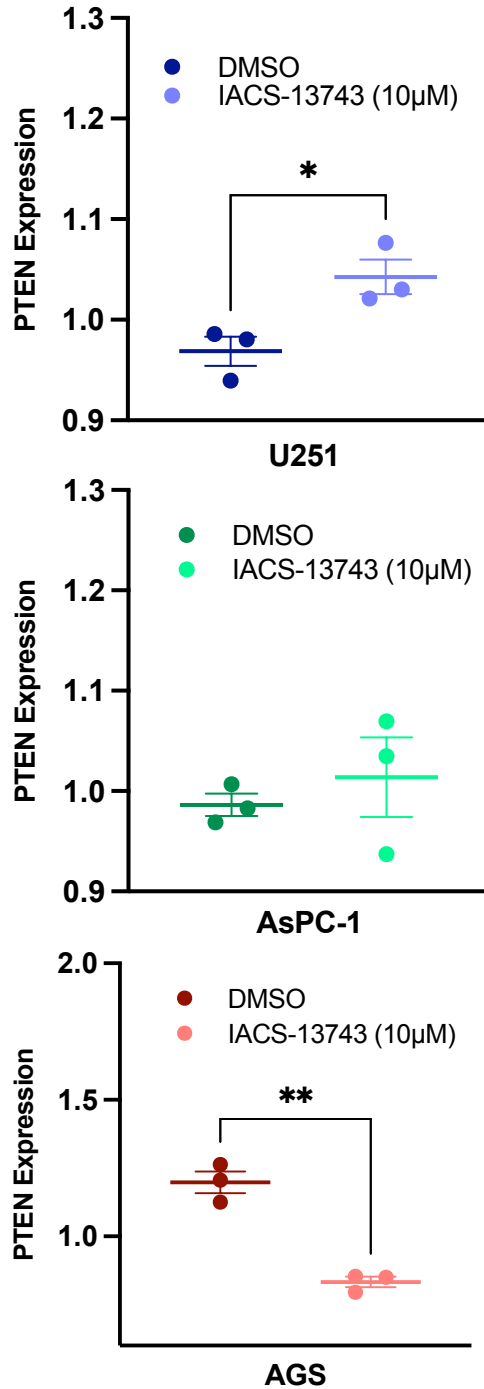
Figure 25: PTEN expression in the three cancer types. This data indicates a cell-type dependent response to IACS-13743 and the further direction of finding tissue-specific targets in these cancer types. * indicates $p < 0.05$, ** indicates $p < 0.01$.

Western blot experiments were conducted to investigate these effects on identified target genes in our two brain cancer cell lines (Figure 26). As expected, the results were found to be consistent with what was found within the proteomics analysis. As they are found to be the primary targets in the mechanistic pathway of the parent compound linifanib, the protein expression of VEGF and PDGF were evaluated after treatment with IACS-13743 via Western blot to determine their levels as shown in Figure 26. In U251 and LN229, there seems to be little to no impact of the compound on the expression level of these two targets, indicating that for these cell lines, it leads credence to the theory that the drug is operating via the miRNA and not necessarily via the kinases, or at the very least, it is working via a combination of the two. Further investigation and validation would need to be conducted via kinome screening to confirm with more certainty whether or not the kinases activated when using this compound, and if so, whether this effect is cell or context-specific.
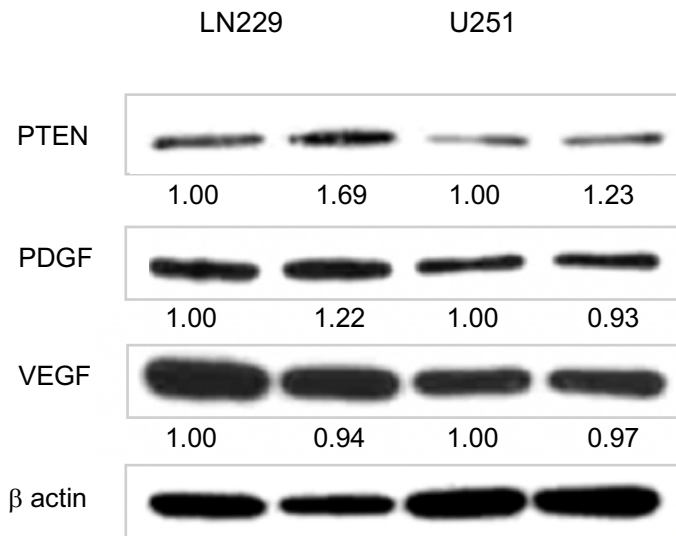
Figure 26. A. Western blot of PTEN expression, a validated target of miR-10b, and VEGF and PDGF expression, the target kinases of the parent compound.

As the PI3K/AKT pathway has long been established to be oncogenic[96-98], the findings indicate a potential mechanistic link between the inhibition of miR-10b and the downstream genes in this pathway. This mechanism remains to be elucidated and would require further analysis, as the two have a direct relationship, whereas miRNAs operate via targeting, which would require an inverse relationship. One approach is to computationally interrogate the pathways to determine which genes appear to play important roles in this relationship. When preparing the data for analysis, the $\log_2$ fold change of the data was calculated and the adjusted p-value was used for analysis. Gene symbols were converted using the DAVID bioinformatics resource[99, 100] and the clusterProfiler data visualization and analysis package was also used[74]. Pathway enrichment analysis was conducted on the significantly

dysregulated genes in the U251 brain cancer cell line, the line in the cancer cell panel with the greatest expression of miR-10b, and using the Hallmark gene set, it was found that "Apoptosis" was the pathway most implicated in this change, along with involvement of the "PI3K-AKT-MTOR1 signaling" pathway (Figure 27). The "G2M checkpoint" was also implicated, which supports the cell cycle analysis *in vitro* data presented earlier, although further investigation into the specific genes and potential feedback mechanisms yielding this effect is needed. In addition, the "MTORC1 signaling" pathway is found to be negatively enriched, which is consistent with what is expected given these findings. Investigating functional enrichment via Gene Ontology yielded similar results, with "regulation of apoptotic signaling" as one of the primary responses when evaluating the Biological Processes dataset (Figure 27B). The results in the U251 brain cancer cell line were compared with those taken from the AGS gastric cancer cell line (Figure 28), and from the Gene Ontology results it is seen that apoptosis continues to be a primary hit, with "regulation of apoptotic pathway" and "intrinsic apoptotic signaling pathway" within the top five results when investigating the Biological Processes dataset, which a high level of significance (Figure 26B). When interrogating the Hallmark gene set, "Apoptosis" was also the top hit, along with involvement of the "PI3K-AKT-MTOR1 signaling" pathway, indicating that while there are tissue and/or cancer specific effects of this compound on eventual gene expression, ultimately both cancer types are implicating similar mechanistic pathways.
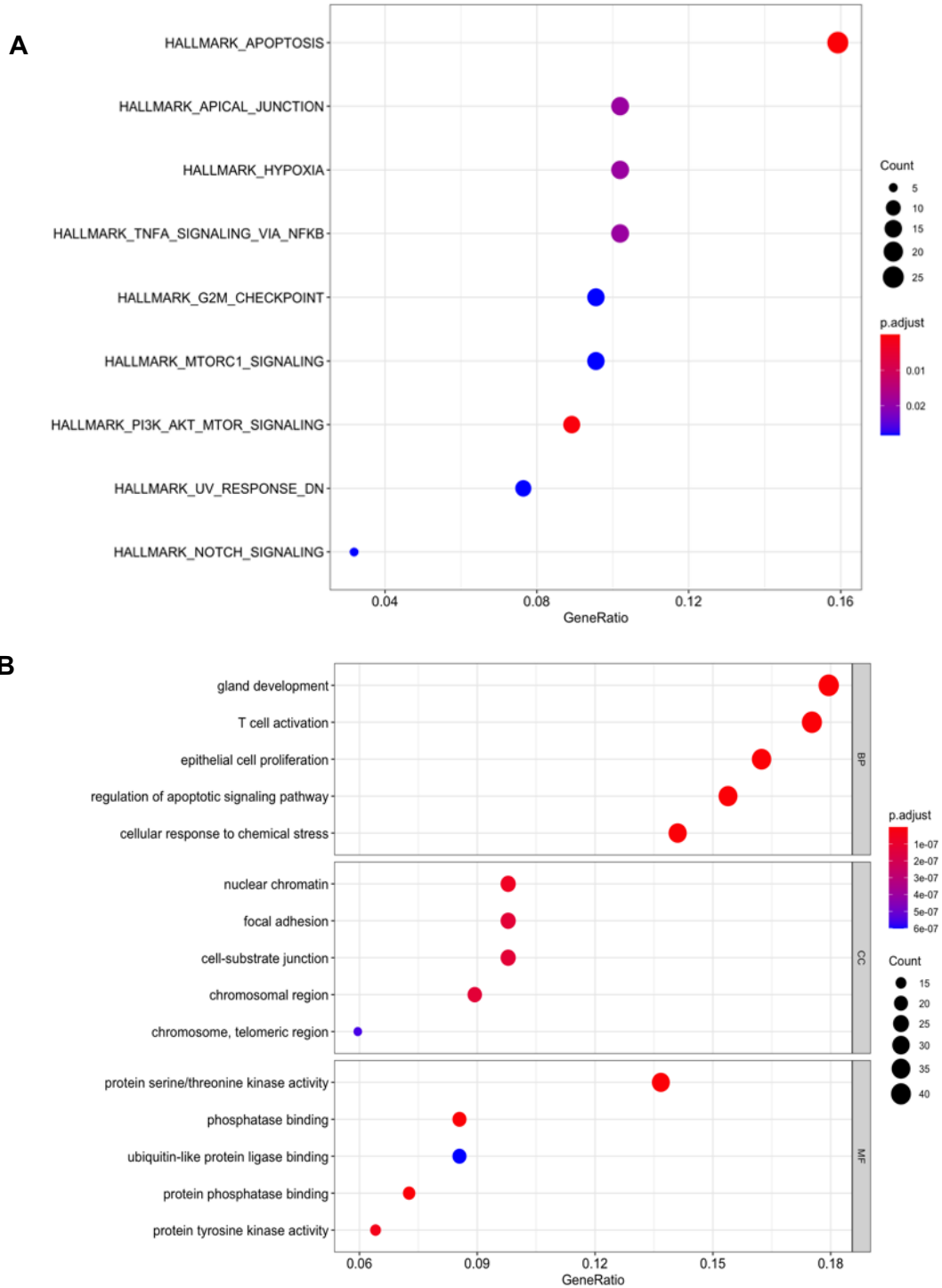
Figure 27: Pathway enrichment analysis of differentially expressed genes after Reverse Phase Protein Array (RPPA) in the U251 brain cancer cell line. A. Gene Set Enrichment Analysis from the MSigDB database. B. Pathway enrichment analysis using Gene Ontology (GO). GeneRatio refers to the ratio of differentially expressed genes and p.adjust refers to p-values adjusted for the false discovery rate (FDR) using the Benjamin-Hochberg correction
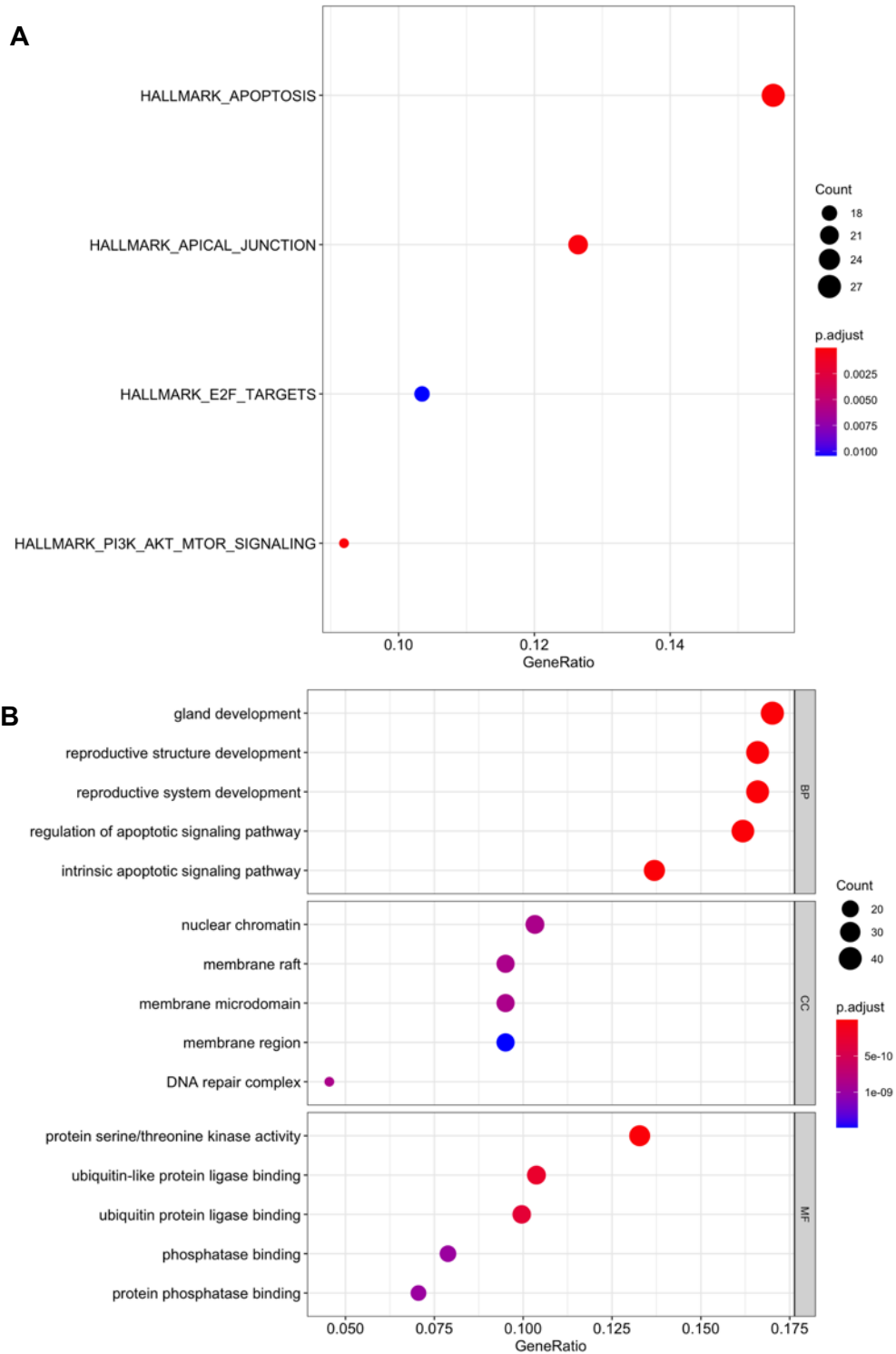
Figure 28: Pathway enrichment analysis of differentially expressed genes after Reverse Phase Protein Array (RPPA) in the AGS gastric cancer cell line. A. Gene Set Enrichment Analysis from the MSigDB database from the Broad Institute. B. Pathway enrichment analysis using Gene Ontology (GO). GeneRatio refers to the ratio of differentially expressed genes and p.adjust refers to p-values adjusted for the false discovery rate (FDR) using the Benjamin-Hochberg correction

Chapter 4. Discussion

Cancer continues to lead as one of the most prevalent health problems globally. While advances have been made, it is becoming increasingly clear that there are no cure-all forms of therapy and that successful treatment of these malignancies will require more tailored and personalized approaches. To that end, in this work, a novel small molecule is characterized against a unique oncogenic driver of cancer, miRNA-10b. This compound has been found both to directly bind and inhibit this miRNA, along with yielding potent anti-tumor effects.

While it is has long established that miR-10b functions in an oncogenic manner, there have been varied proposed mechanisms as to how it operates in recent years. Early studies implicated miR-10b in the promotion of cell migration, invasion, and angiogenesis when it is overexpressed[14, 19]. However, other studies have considered the dysregulation of the mechanisms of cellular apoptosis and cell cycle arrests[13], which ultimately the data supports. Six cancer cell lines from three malignant cancer cell types with varying expression levels of miR-10b were used for the *in vitro* analyses of this work, namely cancer cell lines from brain, pancreas and stomach. Advanced cancers from these tissues are known to generally be resistant to common treatment modalities and alternative approaches to target oncogenic biomarkers are critically needed[101-103].

Brain cancer was used as the cell line of interest in the cerebral organoid model, as it has been established in the literature that in the context of the brain microenvironment, while a baseline expression of miR-10b has generally not been found in amounts in normal brain cells, miR-10b has been found to be highly

overexpressed in several malignant primary brain tumor types[3, 18-20]. Therefore, adding this cancer cell type to this more advanced *in vitro* model more closely recapitulates what occurs in a clinical setting.

The data has confirmed that the compound IACS-13743 directly inhibits miR-10b and yields anti-tumor effects through apoptosis and cell cycle arrest at the G2/M phase in a brain tumor cell line model. Apoptosis is established as the mechanism for programmed cell death and is a known hallmark of cancer, where cancer cells are able to evade apoptotic mechanisms to continue proliferating abnormally[104]. The discovery and development of clinical agents that are able to modulate apoptosis are integral to the treatment of cancer as they would allow for the abnormal cells to undergo appropriate cell death, be highly effective and allow for the cancer to be treated in a mechanistic way by the cells. The G2/M phase is a cell cycle checkpoint that operates via modulating whether sustained DNA damage is significant enough to delay the process in order to undergo DNA repair, or if the damage is too severe and must induce apoptosis[105]. The results suggest that cell cycle arrest is found at G2/M, indicating that there is a degree of DNA damage induced by IACS-13743 that is insurmountable against the tumor cells, leading the cells to continue to apoptosis. This is further supported by the proteomics results using high-throughput Reverse-Phase Protein Array (RPPA) and computational pathway enrichment analysis, where in two databases, the Hallmark Gene Set in GSEA and Gene Ontology, apoptosis was detected as one of the top hits of the pathways implicated by this compound in two of the cancer cell types. Additionally, the RPPA results revealed downregulation after IACS-13743 treatment in many of the key proteins implicated in the PI3K/AKT

pathway. As this pathway has long been established to be oncogenic and an attractive target for cancer drug discovery due to its predisposition to aberration in cancer[96-98], this provides an interesting future direction for further investigation. More specifically, given the data, the isoform AKT2 is significantly downregulated in all three of the cancer types from three varied tissues, which provides a potential biomarker for further investigation and therapeutic targeting. Overall, these results of this study support a mechanistic link between miR-10b and the genes of this pathway, the exact link of which remains to be elucidated.

A common challenge within miRNA research is that direct binding of the sequence and target can be challenging to confirm for a number of reasons. These reasons can be the size of the sequence, which for miRNAs is known to be very short, on the order of 18-22 nucleotides, or the overall solubility of the compound. For the compound linifanib, the parent compound found in a screening of a small molecule library to target miR-10b in the first phase of this study[56], its efficacy was established *in vitro* and *in vivo*, but due to the lack of thorough solubility of the molecule in solution, there was no ability to confirm whether there was direct binding between the miRNA and the compound. Therefore, any conclusions as to the effect of the compound on tumor cells can only be correlations, with no confirmation of causation.

However, in this work, direct binding of IACS-13743 and miR-10b was confirmed via robust NMR studies. When overlaying the NMR spectra generated when combining the novel compound and the sequence of the miRNA, a decrease in the NMR peak signal was shown and line broadening was seen, which is indicative of direct binding of the two elements. The proposed region on the molecule where

binding occurs has also been computationally modeled, shown as a 3D reconstruction in Figure 16C, providing information that will be instrumental for further structural derivations of this compound and the development of small compounds against other oncogenic miRNAs. As stated earlier, the same experiments yielded no effect in the parent compound.

To additionally validate that this direct binding exists and that the mechanism of this compound is working through the oncogenic miRNA, an in-house kinase assay for detection of enzymatic activity was conducted. The results showed that while IACS-13743 does act at a low nanomolar level towards certain kinases, the values at which it acts is an order of magnitude less potent than that of the parent compound linifanib. This is promising, as this provides evidence that this novel compound doesn't primarily operate via kinase pathway, and could thus be working via inhibition of miR-10b. Alternatively, the decrease in potency with the kinases it could mean the compound is operating via both pathways, kinases and miRNA. Linifanib is a potent kinase inhibitor and low nanomolar activity is expected, however, it is promising that while the derivative compound acts on the same kinases, it acts upon them to a lesser degree. It is known from the direct binding studies that this oncogenic miRNA is being targeted and inhibited via IACS-13743, and that key signaling pathways in cancer are also being activated. This opens the door for the evaluation of whether this compound can remain potent in acting against malignant cells when mechanisms of treatment resistance arise via kinase signaling pathways in specific cancer types. The response to this compound has also been found to be cell type and context dependent, thus if the ratio of how this compound operates towards these distinct oncogenic elements

is evaluated, it may provide more information to stratify its administration to maximize impact to patients who have these cancers, and are identified to have overexpression of this miRNA. While the results are promising, they are preliminary, and a full-scale, high-throughput kinase screening is planned to further and conclusively validate the degree through which the compound is working through the miR-10b pathway and target kinases.

This study is the first of its kind in investigating small molecule inhibitors of miRNAs in organoids. As previously mentioned, organoids are 3D cultures of human-derived cells that are able to develop into tissues that are structurally and phenotypically similar to the origin organ of interest. When cultivated and grown, they can be used in cancer research to bridge the gap between *in vitro*, *in vivo*, and clinical studies in humans and represent the tissue and tumor microenvironment in which tumors are growing and proliferating[49, 53]. Evaluating endogenous levels of miR-10b in the cerebral organoid model has supported what has been reported in the current literature, that the expression of miR-10b is low and nearly undetectable in normal brain tissue. This is further shown in the *in-situ* hybridization experiment that was conducted, where the control group containing organoids with no tumor involvement had very low to no miR-10b expression detected (Figure 20). Co-culturing with brain cancer cell lines known to contain high levels of miR-10b increased the expression level of this oncogenic miRNA as detected by qRT-PCR, establishing that the cancer cell lines successfully invaded the organoid and thereby providing a solid therapeutic model through which this, or any other therapeutic downstream, can be tested. The novel compound IACS-13743 was then evaluated on both cell lines co-cultured with

the organoids using two doses and it was found that there was a significant decrease of the expression of miR-10b at $10\mu M$, indicating that even in a more advanced model, the results of the *in vitro* studies as to the efficacy of the compound are confirmed. One aspect to consider with the evaluation of these results is that the organoids are a system that do not contain a vasculature, so while the compound mechanism and function is valuable information to assess, the cerebral organoids do not have an inherent blood-brain barrier, so further research will need to be conducted to ensure that it does operate and permeate well throughout the BBB in a functional *in vivo* context and later in a clinical context. Nevertheless, these results are promising as to the establishment of this model, through which to date only glioma stem cells (GSCs) have been successful in developing, and using well-designed therapeutics to evaluate effects down the line. This work has validated existing knowledge that endogenous neural tissue expresses low miR-10b, and that in a cancer context, the level of miR-10b in the brain increases due to the presence of tumor. It has also introduced confirmatory data that this small molecule yields significant anti-tumor effects in this model.

These findings provide evidence for using a small molecule inhibitor of an oncogenic miRNA in an *in vitro* and cerebral organoid context. Furthermore, anti-tumor effects in these models have been characterized against a panel of cancer cell lines and have further confirmed the oncogenic role of this miRNA in various tumor types. While a potential mechanistic link between miR-10b and dysregulation of the PI3K/AKT pathway has been proposed, the role of miR-10b has been found to be both cell type and context dependent, and ultimately the anti-tumor effects that are

reported will depend on a multitude of factors and require even further rigorous characterization when evaluated in individual cancer types. While there is optimism about further downstream analyses, it is kept in mind that cancer is a highly dynamic and complex disease, and while this compound isn't proposed as a sole cure for these cancer types, the goal is to present a methodology in drug design and development that can take what has been established and apply it in innovative ways, that can target oncogenic mechanisms. These drugs can then either be used independently or in conjunction with existing therapeutic modalities and to target malignancies with unique biomarkers in patients that may be more receptive to these treatments. Moving forward with this compound or other therapeutic approaches will necessitate needing to keep these aspects in mind.

To conclude, it has become more important to move towards more personalized therapeutic approaches as more is learned about the compositions of malignant and heterogeneous cancers. Using existing compound libraries that have already been FDA-approved and tested for human safety to identify clinical agents that target oncogenic miRNAs presents the opportunity for identification of novel biomarkers and directions of study, along with the development of innovative therapeutic approaches that significantly lessen the bench-to-bedside process and allow for more robust and expedient development of therapeutics for patients. The findings in this study highlight the IACS-13743 as an inhibitor of oncogenic miR-10b via the PI3K/AKT pathway in multiple malignant cancer types.

Chapter 5. Future Directions

The long-term goal of this work is to further develop a novel therapeutic compound derived from an established FDA-approved and clinically tested agent, that was found to inhibit the oncogenic driver miR-10b and can move forward to clinical applicability. This work provides a foundational step from the perspectives of medicinal chemistry, structural biology, molecular biology and cancer therapeutics. While these results have been encouraging, more research is needed to further optimize the design and development of this clinical agent with the potency and efficacy to yield significant therapeutic benefit to patients with cancer. Ultimately, this may require analysis and development of a tertiary chemical library with structures that have increased specificity, affinity and sensitivity to the target of interest, in this case, miR-10b. These modifications will further strengthen the relationship between the compound and miRNA direct binding that was found in this work. Now that direct binding yielding miRNA inhibition was established, it provides evidence and solid backing for the anti-tumor effects that were shown. In a more generalizable manner, this study provides a framework through which future compound libraries can be interrogated in order to test compounds and their affinities for known oncogenic drivers. There is still much to learn about the interplay of cancer elements, but with the identification of miRNAs that can impact gene expression pre and post-transcriptionally yielding oncogenic outcomes, this opens the door to utilizing more molecules to target these aberrant elements and ultimately design more specific and impactful targeted therapeutics. The compounds can not only stand alone, but work with our existing therapeutics to yield greater impact.

Combination therapies have been found to yield greater efficacy in many contexts, particularly in cancer therapy[106, 107], where there is such heterogeneity of tumor and tissue types that it becomes apparent that there are no true standard treatment regimens. A potential therapeutic direction moving forward is the introduction of small molecule compounds as adjuvant agents to be administered with conventional therapies such as chemotherapy and radiation. Given their chemical and physical properties when it comes to size and permeability, these agents may not only operate in isolation, but further enhance response of these existing modalities. For instance, in the work by Zhen et al., the authors found overexpressed miR-10b to be associated with increased treatment resistance to radiation in glioblastoma via the PI3K/AKT pathway[108]. Given the results with IACS-13743, there is the high applicability and potential for further research and advances in that domain to applying an anti-miR-10b therapeutic in conjunction with radiation therapy for a subset of patients. Additionally, there has been work from the systems biology perspective investigating the concept of cooperative miRNAs, where miRNAs work together to operate through the targeting of a similar pathway, as a supplemental therapeutic avenue for combination therapy[109].

Another potential opportunity for exploration is investigating closely related miRNAs. As previously mentioned, this specific microRNA is part of the highly conserved miR-10 family, composed of both miR-10a and miR-10b. For these two miRNAs, their respective nucleotide sequences differ by only one nucleotide base. Theoretically, given their sequences, these two miRNAs should yield very similar, if not identical, targets given how close they are structurally[110]. However, while miR-

10b has consistently been found to be dysregulated and most commonly upregulated in a number of cancer types, there is some inconsistency as to how miR-10a presents in cancer, where miR-10a does not tend to yield the same oncogenic outcomes, at the very least not in the same cancer types. Given their near similarity, it would be enlightening to investigate further, especially from the therapeutic perspective, to assess the differences in the binding to their target genes, and how molecules bind their sequences, to determine whether this work may yield any additional benefit to indications and conditions where miR-10a is dysregulated.

As another potential research direction, there are various limitations in the lack of reliable biomarkers that allow for accurate diagnosis and treatment response to current therapeutic modalities. Earlier, the use of biomedical imaging was discussed and its powerful impact on evaluating morphology and volumes, along with treatment response of established tumors. In terms of early detection and longitudinal assessment, while imaging is a powerful tool, it is not always the most accessible and feasible to conduct.

As oncogenic miRNAs are becoming more established as biomarkers for cancer, determining novel and alternative methods to measure miRNA levels in the human body could be useful for early diagnosis and prognostics. For instance, in the work by Huang et al. (2016), they identified a panel of miRNAs, with miR-10b included, as a diagnostic signature for gastric cancer using serum from patients[111]. Additionally, cerebrospinal fluid (CSF) in the brain is commonly used as a source for diagnosis for a multitude of neurological diseases; its use as a biomarker for circulating miRNAs has a great potential for clinical relevance when differentiating

between primary and metastatic lesions and when access to the tumor is difficult or compromised in the brain, as discussed earlier[112, 113]. In fact, in a study by Teplyuk et al., (2012), the authors linked a series of miRNAs, with miR-10b included, with the presence or primary and metastatic brain tumors[114]. As access to CSF is more readily available than a biopsy, this allows for the opportunity of longitudinal monitoring of levels as an indicator of malignancy, in addition to other modalities such as advanced non-invasive imaging.

Overall, this study serves as a fundamental step forward in characterizing a novel small molecule compound that can inhibit a known oncogenic biomarker in multiple cancer types. As more is learned about the complexity of cancer, it is important to continue to tailor therapeutic advances. Taking from sources in the form of FDA-approved molecules and established chemical libraries and applying them in varied oncogenic contexts will save cost, time and inevitably the lives of many as the work is advanced with new and current knowledge to ultimately help end cancer.

References

1.   Siegel, R. L.; Miller, K. D.; Fuchs, H. E.; Jemal, A., Cancer Statistics, 2021. *CA Cancer J Clin* **2021,** *71* (1), 7-33.

2.   Padma, V. V., An overview of targeted cancer therapy. *Biomedicine (Taipei)* **2015,** *5* (4), 19.

3.   Fauman, E. B.; Rai, B. K.; Huang, E. S., Structure-based druggability assessment--identifying suitable targets for small molecule therapeutics. *Curr Opin Chem Biol* **2011,** *15* (4), 463-8.

4.   Warner, K. D.; Hajdin, C. E.; Weeks, K. M., Principles for targeting RNA with drug-like small molecules. *Nat Rev Drug Discov* **2018,** *17* (8), 547-558.

5.   Santos, R.; Ursu, O.; Gaulton, A.; Bento, A. P.; Donadi, R. S.; Bologa, C. G.; Karlsson, A.; Al-Lazikani, B.; Hersey, A.; Oprea, T. I.; Overington, J. P., A comprehensive map of molecular drug targets. *Nat Rev Drug Discov* **2017,** *16* (1), 19-34.

6.   Hubé, F.; Francastel, C., Coding and Non-coding RNAs, the Frontier Has Never Been So Blurred. *Front Genet* **2018,** *9*, 140.

7.   Shah, M. Y.; Calin, G. A., MicroRNAs as therapeutic targets in human cancers. *Wiley Interdiscip Rev RNA* **2014,** *5* (4), 537-48.

8.   Mishra, P. J., The miRNA-drug resistance connection: a new era of personalized medicine using noncoding RNA begins. *Pharmacogenomics* **2012,** *13* (12), 1321-4.

9.   Yoshida, T.; Naito, Y.; Yasuhara, H.; Sasaki, K.; Kawaji, H.; Kawai, J.; Naito, M.; Okuda, H.; Obika, S.; Inoue, T., Evaluation of off-target effects of gapmer antisense oligonucleotides using human cells. *Genes Cells* **2019,** *24* (12), 827-835.

10.   Zhang, S.; Chen, L.; Jung, E. J.; Calin, G. A., Targeting microRNAs with small molecules: from dream to reality. *Clin Pharmacol Ther* **2010,** *87* (6), 754-8.

11.   Chen, L.; Calin, G. A.; Zhang, S., Novel insights of structure-based modeling for RNA-targeted drug discovery. *J Chem Inf Model* **2012,** *52* (10), 2741-53.

12.   Monroig, P. e. C.; Chen, L.; Zhang, S.; Calin, G. A., Small molecule compounds targeting miRNAs for cancer therapy. *Adv Drug Deliv Rev* **2015,** *81*, 104-16.

13.   Gabriely, G.; Yi, M.; Narayan, R. S.; Niers, J. M.; Wurdinger, T.; Imitola, J.; Ligon, K. L.; Kesari, S.; Esau, C.; Stephens, R. M.; Tannous, B. A.; Krichevsky, A. M., Human glioma growth is controlled by microRNA-10b. *Cancer Res* **2011,** *71* (10), 3563-72.

14.   Lin, J.; Teo, S.; Lam, D. H.; Jeyaseelan, K.; Wang, S., MicroRNA-10b pleiotropically regulates invasion, angiogenicity and apoptosis of tumor cells resembling mesenchymal subtype of glioblastoma multiforme. *Cell Death Dis* **2012,** *3*, e398.

15.   Saldanha, G.; Elshaw, S.; Sachs, P.; Alharbi, H.; Shah, P.; Jothi, A.; Pringle, J. H., microRNA-10b is a prognostic biomarker for melanoma. *Mod Pathol* **2016,** *29* (2), 112-21.

16.   Ma, Z.; Chen, Y.; Min, L.; Li, L.; Huang, H.; Li, J.; Yan, Q.; Song, P.; Dai, L.; Yao, X., Augmented miR-10b expression associated with depressed expression of its target gene KLF4 involved in gastric carcinoma. *Int J Clin Exp Pathol* **2015,** *8* (5), 5071-9.

17.   Ouyang, H.; Gore, J.; Deitz, S.; Korc, M., microRNA-10b enhances pancreatic cancer cell invasion by suppressing TIP30 expression and promoting EGF and TGF-β actions. *Oncogene* **2017,** *36* (34), 4952.

18.   Sasayama, T.; Nishihara, M.; Kondoh, T.; Hosoda, K.; Kohmura, E., MicroRNA-10b is overexpressed in malignant glioma and associated with tumor invasive factors, uPAR and RhoC. *Int J Cancer* **2009,** *125* (6), 1407-13.

19.   Guessous, F.; Alvarado-Velez, M.; Marcinkiewicz, L.; Zhang, Y.; Kim, J.; Heister, S.; Kefas, B.; Godlewski, J.; Schiff, D.; Purow, B.; Abounader, R., Oncogenic effects of miR-10b in glioblastoma stem cells. *J Neurooncol* **2013,** *112* (2), 153-63.

20.   Teplyuk, N. M.; Uhlmann, E. J.; Gabriely, G.; Volfovsky, N.; Wang, Y.; Teng, J.; Karmali, P.; Marcusson, E.; Peter, M.; Mohan, A.; Kraytsberg, Y.; Cialic, R.; Chiocca, E. A.; Godlewski, J.; Tannous, B.; Krichevsky, A. M., Therapeutic potential of targeting microRNA-10b in established intracranial glioblastoma: first steps toward the clinic. *EMBO Mol Med* **2016,** *8* (3), 268-87.

21.   Lavon, I.; Zrihan, D.; Granit, A.; Einstein, O.; Fainstein, N.; Cohen, M. A.; Zelikovitch, B.; Shoshan, Y.; Spektor, S.; Reubinoff, B. E.; Felig, Y.; Gerlitz, O.; Ben-Hur, T.; Smith, Y.; Siegal, T., Gliomas display a microRNA expression profile reminiscent of neural precursor cells. *Neuro Oncol* **2010,** *12* (5), 422-33.

22.   Sun, B.; Zhao, X.; Ming, J.; Liu, X.; Liu, D.; Jiang, C., Stepwise detection and evaluation reveal miR-10b and miR-222 as a remarkable prognostic pair for glioblastoma. *Oncogene* **2019,** *38* (33), 6142-6157.

23.   Ma, C.; Wei, F.; Xia, H.; Liu, H.; Dong, X.; Zhang, Y.; Luo, Q.; Liu, Y.; Li, Y., MicroRNA-10b mediates TGF-β1-regulated glioblastoma proliferation, migration and epithelial-mesenchymal transition. *Int J Oncol* **2017,** *50* (5), 1739-1748.

24.   Sitarz, R.; Skierucha, M.; Mielko, J.; Offerhaus, G. J. A.; Maciejewski, R.; Polkowski, W. P., Gastric cancer: epidemiology, prevention, classification, and treatment. *Cancer Manag Res* **2018,** *10*, 239-248.

25.   Li, X.; Zhang, Y.; Ding, J.; Wu, K.; Fan, D., Survival prediction of gastric cancer by a seven-microRNA signature. *Gut* **2010,** *59* (5), 579-85.

26.   Wang, Y. Y.; Ye, Z. Y.; Zhao, Z. S.; Li, L.; Wang, Y. X.; Tao, H. Q.; Wang, H. J.; He, X. J., Clinicopathologic significance of miR-10b expression in gastric carcinoma. *Hum Pathol* **2013,** *44* (7), 1278-85.

27.   Liu, Z.; Zhu, J.; Cao, H.; Ren, H.; Fang, X., miR-10b promotes cell invasion through RhoC-AKT signaling pathway by   targeting HOXD10 in gastric cancer. *Int J Oncol* **2012,** *40* (5), 1553-60.

28.   Li, Z.; Lei, H.; Luo, M.; Wang, Y.; Dong, L.; Ma, Y.; Liu, C.; Song, W.; Wang, F.; Zhang, J.; Shen, J.; Yu, J., DNA methylation downregulated mir-10b acts as a tumor suppressor in gastric cancer. *Gastric Cancer* **2015,** *18* (1), 43-54.

29.   Nakata, K.; Ohuchida, K.; Mizumoto, K.; Kayashima, T.; Ikenaga, N.; Sakai, H.; Lin, C.; Fujita, H.; Otsuka, T.; Aishima, S.; Nagai, E.; Oda, Y.;

Tanaka, M., MicroRNA-10b is overexpressed in pancreatic cancer, promotes its invasiveness, and correlates with a poor prognosis. *Surgery* **2011,** *150* (5), 916-22.

30.   Preis, M.; Gardner, T. B.; Gordon, S. R.; Pipas, J. M.; Mackenzie, T. A.; Klein, E. E.; Longnecker, D. S.; Gutmann, E. J.; Sempere, L. F.; Korc, M., MicroRNA-10b expression correlates with response to neoadjuvant therapy and survival in pancreatic ductal adenocarcinoma. *Clin Cancer Res* **2011,** *17* (17), 5812-21.

31.   Young, J. S.; Chmura, S. J.; Wainwright, D. A.; Yamini, B.; Peters, K. B.; Lukas, R. V., Management of glioblastoma in elderly patients. *J Neurol Sci* **2017,** *380*, 250-255.

32.   Verhaak, R. G.; Hoadley, K. A.; Purdom, E.; Wang, V.; Qi, Y.; Wilkerson, M. D.; Miller, C. R.; Ding, L.; Golub, T.; Mesirov, J. P.; Alexe, G.; Lawrence, M.; O'Kelly, M.; Tamayo, P.; Weir, B. A.; Gabriel, S.; Winckler, W.; Gupta, S.; Jakkula, L.; Feiler, H. S.; Hodgson, J. G.; James, C. D.; Sarkaria, J. N.; Brennan, C.; Kahn, A.; Spellman, P. T.; Wilson, R. K.; Speed, T. P.; Gray, J. W.; Meyerson, M.; Getz, G.; Perou, C. M.; Hayes, D. N.; Network, C. G. A. R., Integrated genomic analysis identifies clinically relevant subtypes of glioblastoma characterized by abnormalities in PDGFRA, IDH1, EGFR, and NF1. *Cancer Cell* **2010,** *17* (1), 98-110.

33.   Wang, Q.; Hu, B.; Hu, X.; Kim, H.; Squatrito, M.; Scarpace, L.; deCarvalho, A. C.; Lyu, S.; Li, P.; Li, Y.; Barthel, F.; Cho, H. J.; Lin, Y. H.; Satani, N.; Martinez-Ledesma, E.; Zheng, S.; Chang, E.; Sauvé, C. G.; Olar, A.; Lan, Z. D.; Finocchiaro, G.; Phillips, J. J.; Berger, M. S.; Gabrusiewicz, K. R.;

Wang, G.; Eskilsson, E.; Hu, J.; Mikkelsen, T.; DePinho, R. A.; Muller, F.;

Heimberger, A. B.; Sulman, E. P.; Nam, D. H.; Verhaak, R. G. W., Tumor Evolution

of Glioma-Intrinsic Gene Expression Subtypes Associates with Immunological

Changes in the Microenvironment. *Cancer Cell* **2017,** *32* (1), 42-56.e6.

34.   Daneman, R.; Prat, A., The blood-brain barrier. *Cold Spring Harb Perspect*

Biol **2015,** *7* (1), a020412.

35.   Mikitsh, J. L.; Chacko, A. M., Pathways for small molecule delivery to the

central nervous system across the blood-brain barrier. *Perspect Medicin Chem*

2014, *6*, 11-24.

36.   Dong, X., Current Strategies for Brain Drug Delivery. *Theranostics* **2018,** *8*

(6), 1481-1493.

37.   Arvanitis, C. D.; Ferraro, G. B.; Jain, R. K., The blood-brain barrier and

blood-tumour barrier in brain tumours and metastases. *Nat Rev Cancer* **2020,** *20*

(1), 26-41.

38.   Sarkaria, J. N.; Hu, L. S.; Parney, I. F.; Pafundi, D. H.; Brinkmann, D. H.;

Laack, N. N.; Giannini, C.; Burns, T. C.; Kizilbash, S. H.; Laramy, J. K.;

Swanson, K. R.; Kaufmann, T. J.; Brown, P. D.; Agar, N. Y. R.; Galanis, E.;

Buckner, J. C.; Elmquist, W. F., Is the blood-brain barrier really disrupted in all

glioblastomas? A critical assessment of existing clinical data. *Neuro Oncol* **2018,** *20*

(2), 184-191.

39.   Siegal, T.; Charbit, H.; Paldor, I.; Zelikovitch, B.; Canello, T.; Benis, A.;

Wong, M. L.; Morokoff, A. P.; Kaye, A. H.; Lavon, I., Dynamics of circulating

hypoxia-mediated miRNAs and tumor response in patients with high-grade glioma treated with bevacizumab. *J Neurosurg* **2016,** *125* (4), 1008-1015.

40.   Neal, M. T.; Chan, M. D.; Lucas, J. T.; Loganathan, A.; Dillingham, C.; Pan, E.; Stewart, J. H.; Bourland, J. D.; Shaw, E. G.; Tatter, S. B.; Ellis, T. L., Predictors of survival, neurologic death, local failure, and distant failure after gamma knife radiosurgery for melanoma brain metastases. *World Neurosurg* **2014,** *82* (6), 1250-5.

41.   Fedorov, A.; Beichel, R.; Kalpathy-Cramer, J.; Finet, J.; Fillion-Robin, J. C.; Pujol, S.; Bauer, C.; Jennings, D.; Fennessy, F.; Sonka, M.; Buatti, J.; Aylward, S.; Miller, J. V.; Pieper, S.; Kikinis, R., 3D Slicer as an image computing platform for the Quantitative Imaging Network. *Magn Reson Imaging* **2012,** *30* (9), 1323-41.

42.   Titov, A.; Petukhov, A.; Staliarova, A.; Motorin, D.; Bulatov, E.; Shuvalov, O.; Soond, S. M.; Piacentini, M.; Melino, G.; Zaritskey, A.; Barlev, N. A., The biological basis and clinical symptoms of CAR-T therapy-associated toxicites. *Cell Death Dis* **2018,** *9* (9), 897.

43.   Hunter, B. D.; Jacobson, C. A., CAR T-Cell Associated Neurotoxicity: Mechanisms, Clinicopathologic Correlates, and Future Directions. *J Natl Cancer Inst* **2019,** *111* (7), 646-654.

44.   Neelapu, S. S.; Tummala, S.; Kebriaei, P.; Wierda, W.; Gutierrez, C.; Locke, F. L.; Komanduri, K. V.; Lin, Y.; Jain, N.; Daver, N.; Westin, J.; Gulbis, A. M.; Loghin, M. E.; de Groot, J. F.; Adkins, S.; Davis, S. E.; Rezvani, K.; Hwu, P.;

Shpall, E. J., Chimeric antigen receptor T-cell therapy - assessment and management of toxicities. *Nat Rev Clin Oncol* **2018,** *15* (1), 47-62.

45.   Smith, S. M.; Jenkinson, M.; Woolrich, M. W.; Beckmann, C. F.; Behrens, T. E.; Johansen-Berg, H.; Bannister, P. R.; De Luca, M.; Drobnjak, I.; Flitney, D. E.; Niazy, R. K.; Saunders, J.; Vickers, J.; Zhang, Y.; De Stefano, N.; Brady, J. M.; Matthews, P. M., Advances in functional and structural MR image analysis and implementation as FSL. *Neuroimage* **2004,** *23 Suppl 1*, S208-19.

46.   Woolrich, M. W.; Jbabdi, S.; Patenaude, B.; Chappell, M.; Makni, S.; Behrens, T.; Beckmann, C.; Jenkinson, M.; Smith, S. M., Bayesian analysis of neuroimaging data in FSL. *Neuroimage* **2009,** *45* (1 Suppl), S173-86.

47.   Jenkinson, M.; Beckmann, C. F.; Behrens, T. E.; Woolrich, M. W.; Smith, S. M., FSL. *Neuroimage* **2012,** *62* (2), 782-90.

48.   Drost, J.; Clevers, H., Organoids in cancer research. *Nat Rev Cancer* **2018,** *18* (7), 407-418.

49.   Lee, C. T.; Bendriem, R. M.; Wu, W. W.; Shen, R. F., 3D brain Organoids derived from pluripotent stem cells: promising experimental models for brain development and neurodegenerative disorders. *J Biomed Sci* **2017,** *24* (1), 59.

50.   Nagle, P. W.; Plukker, J. T. M.; Muijs, C. T.; van Luijk, P.; Coppes, R. P., Patient-derived tumor organoids for prediction of cancer treatment response. *Semin Cancer Biol* **2018,** *53*, 258-264.

51.   Lancaster, M. A.; Renner, M.; Martin, C. A.; Wenzel, D.; Bicknell, L. S.; Hurles, M. E.; Homfray, T.; Penninger, J. M.; Jackson, A. P.; Knoblich, J. A.,

Cerebral organoids model human brain development and microcephaly. *Nature* **2013,** *501* (7467), 373-9.

52. Kim, J.; Koo, B. K.; Knoblich, J. A., Human organoids: model systems for human biology and medicine. *Nat Rev Mol Cell Biol* **2020,** *21* (10), 571-584.

53. Krieger, T. G.; Tirier, S. M.; Park, J.; Jechow, K.; Eisemann, T.; Peterziel, H.; Angel, P.; Eils, R.; Conrad, C., Modeling glioblastoma invasion using human brain organoids and single-cell transcriptomics. *Neuro Oncol* **2020,** *22* (8), 1138-1149.

54. Linkous, A.; Balamatsias, D.; Snuderl, M.; Edwards, L.; Miyaguchi, K.; Milner, T.; Reich, B.; Cohen-Gould, L.; Storaska, A.; Nakayama, Y.; Schenkein, E.; Singhania, R.; Cirigliano, S.; Magdeldin, T.; Lin, Y.; Nanjangud, G.; Chadalavada, K.; Pisapia, D.; Liston, C.; Fine, H. A., Modeling Patient-Derived Glioblastoma with Cerebral Organoids. *Cell Rep* **2019,** *26* (12), 3203-3211.e5.

55. McCauley, H. A.; Wells, J. M., Pluripotent stem cell-derived organoids: using principles of developmental biology to grow human tissues in a dish. *Development* **2017,** *144* (6), 958-962.

56. Monroig-Bosque, P. D. C.; Shah, M. Y.; Fu, X.; Fuentes-Mattei, E.; Ling, H.; Ivan, C.; Nouraee, N.; Huang, B.; Chen, L.; Pileczki, V.; Redis, R. S.; Jung, E. J.; Zhang, X.; Lehrer, M.; Nagvekar, R.; Mafra, A. C. P.; Monroig-Bosque, M. D. M.; Irimie, A.; Rivera, C.; Dan Dumitru, C.; Berindan-Neagoe, I.; Nikonowicz, E. P.; Zhang, S.; Calin, G. A., OncomiR-10b hijacks the small molecule inhibitor linifanib in human cancers. *Sci Rep* **2018,** *8* (1), 13106.

57.   Chen, J.; Guo, J.; Chen, Z.; Wang, J.; Liu, M.; Pang, X., Linifanib (ABT-869) Potentiates the Efficacy of Chemotherapeutic Agents through the Suppression of Receptor Tyrosine Kinase-Mediated AKT/mTOR Signaling Pathways in Gastric Cancer. *Sci Rep* **2016,** *6*, 29382.

58.   Zhou, J.; Goh, B. C.; Albert, D. H.; Chen, C. S., ABT-869, a promising multi-targeted tyrosine kinase inhibitor: from bench to bedside. *J Hematol Oncol* **2009,** *2*, 33.

59.   Luo, Y.; Jiang, F.; Cole, T. B.; Hradil, V. P.; Reuter, D.; Chakravartty, A.; Albert, D. H.; Davidsen, S. K.; Cox, B. F.; McKeegan, E. M.; Fox, G. B., A novel multi-targeted tyrosine kinase inhibitor, linifanib (ABT-869), produces functional and structural changes in tumor vasculature in an orthotopic rat glioma model. *Cancer Chemother Pharmacol* **2012,** *69* (4), 911-21.

60.   Cainap, C.; Qin, S.; Huang, W. T.; Chung, I. J.; Pan, H.; Cheng, Y.; Kudo, M.; Kang, Y. K.; Chen, P. J.; Toh, H. C.; Gorbunova, V.; Eskens, F. A.; Qian, J.; McKee, M. D.; Ricker, J. L.; Carlson, D. M.; El-Nowiem, S., Linifanib versus Sorafenib in patients with advanced hepatocellular carcinoma: results of a randomized phase III trial. *J Clin Oncol* **2015,** *33* (2), 172-9.

61.   Obach, R. S., Prediction of human clearance of twenty-nine drugs from hepatic microsomal intrinsic clearance data: An examination of in vitro half-life approach and nonspecific binding to microsomes. *Drug Metab Dispos* **1999,** *27* (11), 1350-9.

62.   Bardaro, M. F.; Shajani, Z.; Patora-Komisarska, K.; Robinson, J. A.; Varani, G., How binding of small molecule and peptide ligands to HIV-1 TAR alters the RNA motional landscape. *Nucleic Acids Res* **2009,** *37* (5), 1529-40.

63.   Davidson, A.; Leeper, T. C.; Athanassiou, Z.; Patora-Komisarska, K.; Karn, J.; Robinson, J. A.; Varani, G., Simultaneous recognition of HIV-1 TAR RNA bulge and loop sequences by cyclic peptide mimics of Tat protein. *Proc Natl Acad Sci U S A* **2009,** *106* (29), 11931-6.

64.   Leeper, T. C.; Athanassiou, Z.; Dias, R. L.; Robinson, J. A.; Varani, G., TAR RNA recognition by a cyclic peptidomimetic of Tat protein. *Biochemistry* **2005,** *44* (37), 12362-72.

65.   Abulwerdi, F. A.; Shortridge, M. D.; Sztuba-Solinska, J.; Wilson, R.; Le Grice, S. F.; Varani, G.; Schneekloth, J. S., Development of Small Molecules with a Noncanonical Binding Mode to HIV-1 Trans Activation Response (TAR) RNA. *J Med Chem* **2016,** *59* (24), 11148-11160.

66.   Shortridge, M. D.; Walker, M. J.; Pavelitz, T.; Chen, Y.; Yang, W.; Varani, G., A Macrocyclic Peptide Ligand Binds the Oncogenic MicroRNA-21 Precursor and Suppresses Dicer Processing. *ACS Chem Biol* **2017,** *12* (6), 1611-1620.

67.   Shortridge, M. D.; Wille, P. T.; Jones, A. N.; Davidson, A.; Bogdanovic, J.; Arts, E.; Karn, J.; Robinson, J. A.; Varani, G., An ultra-high affinity ligand of HIV-1 TAR reveals the RNA structure recognized by P-TEFb. *Nucleic Acids Res* **2019,** *47* (3), 1523-1531.

68.   Shortridge, M. D.; Hage, D. S.; Harbison, G. S.; Powers, R., Estimating protein-ligand binding affinity using high-throughput screening by NMR. *J Comb Chem* **2008,** *10* (6), 948-58.

69.   Barretina, J.; Caponigro, G.; Stransky, N.; Venkatesan, K.; Margolin, A. A.; Kim, S.; Wilson, C. J.; Lehár, J.; Kryukov, G. V.; Sonkin, D.; Reddy, A.; Liu, M.; Murray, L.; Berger, M. F.; Monahan, J. E.; Morais, P.; Meltzer, J.; Korejwa, A.; Jané-Valbuena, J.; Mapa, F. A.; Thibault, J.; Bric-Furlong, E.; Raman, P.; Shipway, A.; Engels, I. H.; Cheng, J.; Yu, G. K.; Yu, J.; Aspesi, P.; de Silva, M.; Jagtap, K.; Jones, M. D.; Wang, L.; Hatton, C.; Palescandolo, E.; Gupta, S.; Mahan, S.; Sougnez, C.; Onofrio, R. C.; Liefeld, T.; MacConaill, L.; Winckler, W.; Reich, M.; Li, N.; Mesirov, J. P.; Gabriel, S. B.; Getz, G.; Ardlie, K.; Chan, V.; Myer, V. E.; Weber, B. L.; Porter, J.; Warmuth, M.; Finan, P.; Harris, J. L.; Meyerson, M.; Golub, T. R.; Morrissey, M. P.; Sellers, W. R.; Schlegel, R.; Garraway, L. A., The Cancer Cell Line Encyclopedia enables predictive modelling of anticancer drug sensitivity. *Nature* **2012,** *483* (7391), 603-7.

70.   Network, C. G. A. R., Comprehensive genomic characterization defines human glioblastoma genes and core pathways. *Nature* **2008,** *455* (7216), 1061-8.

71.   Schneider, C. A.; Rasband, W. S.; Eliceiri, K. W., NIH Image to ImageJ: 25 years of image analysis. *Nat Methods* **2012,** *9* (7), 671-5.

72.   Siwak, D. R.; Li, J.; Akbani, R.; Liang, H.; Lu, Y., Analytical Platforms 3: Processing Samples via the RPPA Pipeline to Generate Large-Scale Data for Clinical Studies. *Adv Exp Med Biol* **2019,** *1188*, 113-147.

73.   Ritchie, M. E.; Phipson, B.; Wu, D.; Hu, Y.; Law, C. W.; Shi, W.; Smyth, G. K., limma powers differential expression analyses for RNA-sequencing and microarray studies. *Nucleic Acids Res* **2015,** *43* (7), e47.

74.   Yu, G.; Wang, L. G.; Han, Y.; He, Q. Y., clusterProfiler: an R package for comparing biological themes among gene clusters. *OMICS* **2012,** *16* (5), 284-7.

75.   Liberzon, A.; Birger, C.; Thorvaldsdóttir, H.; Ghandi, M.; Mesirov, J. P.; Tamayo, P., The Molecular Signatures Database (MSigDB) hallmark gene set collection. *Cell Syst* **2015,** *1* (6), 417-425.

76.   Ashburner, M.; Ball, C. A.; Blake, J. A.; Botstein, D.; Butler, H.; Cherry, J. M.; Davis, A. P.; Dolinski, K.; Dwight, S. S.; Eppig, J. T.; Harris, M. A.; Hill, D. P.; Issel-Tarver, L.; Kasarskis, A.; Lewis, S.; Matese, J. C.; Richardson, J. E.; Ringwald, M.; Rubin, G. M.; Sherlock, G., Gene ontology: tool for the unification of biology. The Gene Ontology Consortium. *Nat Genet* **2000,** *25* (1), 25-9.

77.   Consortium, G. O., The Gene Ontology resource: enriching a GOld mine. *Nucleic Acids Res* **2021,** *49* (D1), D325-D334.

78.   Ma, L., Role of miR-10b in breast cancer metastasis. *Breast Cancer Res* **2010,** *12* (5), 210.

79.   Ma, L.; Teruya-Feldstein, J.; Weinberg, R. A., Tumour invasion and metastasis initiated by microRNA-10b in breast cancer. *Nature* **2007,** *449* (7163), 682-8.

80.   Lipinski, C. A.; Lombardo, F.; Dominy, B. W.; Feeney, P. J., Experimental and computational approaches to estimate solubility and permeability in drug discovery and development settings. *Adv Drug Deliv Rev* **2001,** *46* (1-3), 3-26.

81.   Berrouet, C.; Dorilas, N.; Rejniak, K. A.; Tuncer, N., Comparison of Drug Inhibitory Effects ([Formula: see text]) in Monolayer and Spheroid Cultures. *Bull Math Biol* **2020,** *82* (6), 68.

82.   Wlodkowic, D.; Skommer, J.; Darzynkiewicz, Z., Flow cytometry-based apoptosis detection. *Methods Mol Biol* **2009,** *559*, 19-32.

83.   Abulwerdi, F. A.; Shortridge, M. D.; Sztuba-Solinska, J.; Wilson, R.; Le Grice, S. F. J.; Varani, G.; Schneekloth, J. S., Development of Small Molecules with a Noncanonical Binding Mode to HIV-1 Trans Activation Response (TAR) RNA. *Journal of Medicinal Chemistry* **2016,** *59* (24), 11148-11160.

84.   Shortridge, M. D.; Walker, M. J.; Pavelitz, T.; Chen, Y.; Yang, W.; Varani, G., A Macrocyclic Peptide Ligand Binds the Oncogenic MicroRNA-21 Precursor and Suppresses Dicer Processing. *ACS Chemical Biology* **2017**.

85.   Shortridge, M. D.; Wille, P. T.; Jones, A. N.; Davidson, A.; Bogdanovic, J.; Arts, E.; Karn, J.; Robinson, J. A.; Varani, G., An ultra-high affinity ligand of HIV-1 TAR reveals the RNA structure recognized by P-TEFb. *Nucleic Acids Res* **2018**.

86.   Watkins, A. M.; Rangan, R.; Das, R., FARFAR2: Improved De Novo Rosetta Prediction of Complex Global RNA Folds. *Structure* **2020,** *28* (8), 963-976 e6.

87.   Zegzouti, H.; Zdanovskaia, M.; Hsiao, K.; Goueli, S. A., ADP-Glo: A Bioluminescent and homogeneous ADP monitoring assay for kinases. *Assay Drug Dev Technol* **2009,** *7* (6), 560-72.

88.   Albert, D. H.; Tapang, P.; Magoc, T. J.; Pease, L. J.; Reuter, D. R.; Wei, R. Q.; Li, J.; Guo, J.; Bousquet, P. F.; Ghoreishi-Haack, N. S.; Wang, B.; Bukofzer, G. T.; Wang, Y. C.; Stavropoulos, J. A.; Hartandi, K.; Niquette, A. L.;

Soni, N.; Johnson, E. F.; McCall, J. O.; Bouska, J. J.; Luo, Y.; Donawho, C. K.; Dai, Y.; Marcotte, P. A.; Glaser, K. B.; Michaelides, M. R.; Davidsen, S. K., Preclinical activity of ABT-869, a multitargeted receptor tyrosine kinase inhibitor. *Mol Cancer Ther* **2006,** *5* (4), 995-1006.

89.   Weinstein, J. N.; Collisson, E. A.; Mills, G. B.; Shaw, K. R.; Ozenberger, B. A.; Ellrott, K.; Shmulevich, I.; Sander, C.; Stuart, J. M.; Network, C. G. A. R., The Cancer Genome Atlas Pan-Cancer analysis project. *Nat Genet* **2013,** *45* (10), 1113-20.

90.   Liebelt, B. D.; Shingu, T.; Zhou, X.; Ren, J.; Shin, S. A.; Hu, J., Glioma Stem Cells: Signaling, Microenvironment, and Therapy. *Stem Cells Int* **2016,** *2016*, 7849890.

91.   Rhodes, D. R.; Yu, J.; Shanker, K.; Deshpande, N.; Varambally, R.; Ghosh, D.; Barrette, T.; Pandey, A.; Chinnaiyan, A. M., ONCOMINE: a cancer microarray database and integrated data-mining platform. *Neoplasia* **2004,** *6* (1), 1-6.

92.   Kehl, T.; Kern, F.; Backes, C.; Fehlmann, T.; Stöckel, D.; Meese, E.; Lenhof, H. P.; Keller, A., miRPathDB 2.0: a novel release of the miRNA Pathway Dictionary Database. *Nucleic Acids Res* **2020,** *48* (D1), D142-D147.

93.   Huang, H. Y.; Lin, Y. C.; Li, J.; Huang, K. Y.; Shrestha, S.; Hong, H. C.; Tang, Y.; Chen, Y. G.; Jin, C. N.; Yu, Y.; Xu, J. T.; Li, Y. M.; Cai, X. X.; Zhou, Z. Y.; Chen, X. H.; Pei, Y. Y.; Hu, L.; Su, J. J.; Cui, S. D.; Wang, F.; Xie, Y. Y.; Ding, S. Y.; Luo, M. F.; Chou, C. H.; Chang, N. W.; Chen, K. W.; Cheng, Y. H.; Wan, X. H.; Hsu, W. L.; Lee, T. Y.; Wei, F. X.; Huang, H. D., miRTarBase 2020:

updates to the experimentally validated microRNA-target interaction database. *Nucleic Acids Res* **2020,** *48* (D1), D148-D154.

94.   Agarwal, V.; Bell, G. W.; Nam, J. W.; Bartel, D. P., Predicting effective microRNA target sites in mammalian mRNAs. *Elife* **2015,** *4.*

95.   Enright, A. J.; John, B.; Gaul, U.; Tuschl, T.; Sander, C.; Marks, D. S., MicroRNA targets in Drosophila. *Genome Biol* **2003,** *5* (1), R1.

96.   Hennessy, B. T.; Smith, D. L.; Ram, P. T.; Lu, Y.; Mills, G. B., Exploiting the PI3K/AKT pathway for cancer drug discovery. *Nat Rev Drug Discov* **2005,** *4* (12), 988-1004.

97.   Hoxhaj, G.; Manning, B. D., The PI3K-AKT network at the interface of oncogenic signalling and cancer metabolism. *Nat Rev Cancer* **2020,** *20* (2), 74-88.

98.   Cheung, M.; Testa, J. R., Diverse mechanisms of AKT pathway activation in human malignancy. *Curr Cancer Drug Targets* **2013,** *13* (3), 234-44.

99.   Huang, d. W.; Sherman, B. T.; Lempicki, R. A., Systematic and integrative analysis of large gene lists using DAVID bioinformatics resources. *Nat Protoc* **2009,** *4* (1), 44-57.

100.   Huang, d. W.; Sherman, B. T.; Lempicki, R. A., Bioinformatics enrichment tools: paths toward the comprehensive functional analysis of large gene lists. *Nucleic Acids Res* **2009,** *37* (1), 1-13.

101.   Gaianigo, N.; Melisi, D.; Carbone, C., EMT and Treatment Resistance in Pancreatic Cancer. *Cancers (Basel)* **2017,** *9* (9).

102. Grasso, C.; Jansen, G.; Giovannetti, E., Drug resistance in pancreatic cancer: Impact of altered energy metabolism. *Crit Rev Oncol Hematol* **2017,** *114*, 139-152.

103. Holohan, C.; Van Schaeybroeck, S.; Longley, D. B.; Johnston, P. G., Cancer drug resistance: an evolving paradigm. *Nat Rev Cancer* **2013,** *13* (10), 714-26.

104. Pfeffer, C. M.; Singh, A. T. K., Apoptosis: A Target for Anticancer Therapy. *Int J Mol Sci* **2018,** *19* (2).

105. Wang, Y.; Ji, P.; Liu, J.; Broaddus, R. R.; Xue, F.; Zhang, W., Centrosome-associated regulators of the G(2)/M checkpoint as targets for cancer therapy. *Mol Cancer* **2009,** *8*, 8.

106. Bayat Mokhtari, R.; Homayouni, T. S.; Baluch, N.; Morgatskaya, E.; Kumar, S.; Das, B.; Yeger, H., Combination therapy in combating cancer. *Oncotarget* **2017,** *8* (23), 38022-38043.

107. Palmer, A. C.; Sorger, P. K., Combination Cancer Therapy Can Confer Benefit via Patient-to-Patient Variability without Drug Additivity or Synergy. *Cell* **2017,** *171* (7), 1678-1691.e13.

108. Zhen, L.; Li, J.; Zhang, M.; Yang, K., MiR-10b decreases sensitivity of glioblastoma cells to radiation by targeting AKT. *J Biol Res (Thessalon)* **2016,** *23*, 14.

109. Lai, X.; Eberhardt, M.; Schmitz, U.; Vera, J., Systems biology-based investigation of cooperating microRNAs as monotherapy or adjuvant therapy in cancer. *Nucleic Acids Res* **2019,** *47* (15), 7753-7766.

110. Tehler, D.; Høyland-Kroghsbo, N. M.; Lund, A. H., The miR-10 microRNA precursor family. *RNA Biol* **2011,** *8* (5), 728-34.

111. Huang, Z.; Zhu, D.; Wu, L.; He, M.; Zhou, X.; Zhang, L.; Zhang, H.; Wang, W.; Zhu, J.; Cheng, W.; Chen, Y.; Fan, Y.; Qi, L.; Yin, Y.; Zhu, W.; Shu, Y.; Liu, P., Six Serum-Based miRNAs as Potential Diagnostic Biomarkers for Gastric Cancer. *Cancer Epidemiol Biomarkers Prev* **2017,** *26* (2), 188-196.

112. Shalaby, T.; Grotzer, M. A., Tumor-Associated CSF MicroRNAs for the Prediction and Evaluation of CNS Malignancies. *Int J Mol Sci* **2015,** *16* (12), 29103-19.

113. Alsidawi, S.; Malek, E.; Driscoll, J. J., MicroRNAs in brain metastases: potential role as diagnostics and therapeutics. *Int J Mol Sci* **2014,** *15* (6), 10508-26.

114. Teplyuk, N. M.; Mollenhauer, B.; Gabriely, G.; Giese, A.; Kim, E.; Smolsky, M.; Kim, R. Y.; Saria, M. G.; Pastorino, S.; Kesari, S.; Krichevsky, A. M., MicroRNAs in cerebrospinal fluid identify glioblastoma and metastatic brain cancers and reflect disease activity. *Neuro Oncol* **2012,** *14* (6), 689-700.

Vita

Iman Sahnoune was born in Montreal, Quebec. After completing her work at Clear Lake High School in Houston, Texas, she entered the University of Houston where she received the degree of Bachelor of Science with a major in Biochemistry, with minors in Chemistry and Psychology. She then obtained a Master of Arts in Neuroscience, also at the University of Houston with an affiliation at the Baylor College of Medicine, where she completed a thesis investigating the effects of radiation therapy on the developing brain in the context of cancer. From 2015 to 2016, she worked in clinical research at Texas Children's Hospital in the Department of Pediatrics - Hematology and Oncology. In August of 2016, she entered The University of Texas MD Anderson Cancer Center UTHealth Graduate School of Biomedical Sciences.